THE MINISTRY OF SCIENCE AND HIGHER EDUCATION OF THE RUSSIAN FEDERATION

Computing, Telecommunications and Control

Vol. 14, no. 1
2021

Peter the Great St. Petersburg
Polytechnic University
2021

The journal is included in the List of Leading PeerReviewed Scientific Journals and other editions to publish major findings of PhD theses for the research degrees of Doctor of Sciences and Candidate of Sciences.

The journal is indexed by Ulrich's Periodicals Directory, Google Scholar, EBSCO, ProQuest, Index Copernicus, VINITI RAS Abstract Journal (Referativnyi Zhurnal), VINITI RAS Scientific and Technical Literature Collection, Russian Science Citation Index (RSCI) database © Scientific Electronic Library and Math-Net.ru databases.

ISSN 2687-0517

The journal is registered with the Federal Service for Supervision in the Sphere of Telecom, Information Technologies and Mass Communications (ROSKOMNADZOR). Certificate ЭЛ No. ФС77-77378 issued 25.12.2019.

The address: 195251 Polytekhnicheskaya Str. 29,
St. Petersburg, Russia.

МИНИСТЕРСТВО НАУКИ И ВЫСШЕГО ОБРАЗОВАНИЯ РОССИЙСКОЙ ФЕДЕРАЦИИ

Информатика, телекоммуникации и управление

Том 14, № 1
2021

Санкт-Петербургский политехнический
университет Петра Великого
2021

ИНФОРМАТИКА, ТЕЛЕКОММУНИКАЦИИ И УПРАВЛЕНИЕ

Журнал с 2002 года входит в Перечень ведущих рецензируемых научных журналов и изданий, в которых должны быть опубликованы основные результаты диссертаций на соискание ученой степени доктора и кандидата наук.

Сведения о публикациях представлены в Реферативном журнале ВИНИТИ РАН, в международной справочной системе «Ulrich`s Periodical Directory», в базах данных Российский индекс научного цитирования (РИНЦ), Google Scholar, EBSCO, Math-Net.Ru, ProQuest, Index Copernicus

ISSN 2687-0517

Журнал зарегистрирован Федеральной службой по надзору в сфере информационных технологий и массовых коммуникаций (Роскомнадзор). Свидетельство о регистрации ЭЛ № ФС77-77378 от 25.12.2019.

При перепечатке материалов ссылка на журнал обязательна.

Точка зрения редакции может не совпадать с мнением авторов статей.

Адрес редакции: Россия, 195251, Санкт-Петербург, ул. Политехническая, д. 29.

Тел. редакции (812) 552-62-16.

Contents

Содержание

DOI: 10.18721/JCSTCS.14101
УДК 004.056

IMAGE ENCRYPTION ALGORITHM BASED ON CONTROLLED CHAOTIC MAPS

V.N. Shashikhin, A.V. Turulin, S.V. Budnik

Peter the Great St. Petersburg Polytechnic University,
St. Petersburg, Russian Federation

The article reviews the problem of ensuring the security of storage, processing, and transmission of images based on a cryptographic method using chaotic maps. The encryption algorithm is based on a three-dimensional mapping. The encryption algorithm strength when using systems with chaotic dynamics depends on the value of the largest (positive) Lyapunov characteristic exponent. Therefore, the problem of increasing resistance to various kinds of attacks is reduced to determining the control parameters, at which the leading Lyapunov characteristic exponent increases. The authors propose a procedure for changing the chaotic map characteristics (entropy and Lyapunov characteristic exponents) based on introducing feedback into the system. The procedure is developed using the modal control method based on reducing the system to the canonical Frobenius form. The use of the proposed algorithm is considered on the example of the Rössler system. The test results confirmed an increase in the strength of the proposed encryption algorithm against statistical and differential analysis due to an increase in the Lyapunov characteristic exponent.

Keywords: Image encryption, chaotic maps, control of the spectrum of Lyapunov characteristic exponents, modal control, canonical Frobenius form.

Citation: Shashikhin V.N., Turulin A.V., Budnik S.V. Image encryption algorithm based on controlled chaotic maps. Computing, Telecommunications and Control, 2021, Vol. 14, No. 1, Pp. 7–21. DOI: 10.18721/JCSTCS.14101

АЛГОРИТМ ШИФРОВАНИЯ ИЗОБРАЖЕНИЙ НА ОСНОВЕ УПРАВЛЯЕМЫХ ХАОТИЧЕСКИХ ОТОБРАЖЕНИЙ

В.Н. Шашихин, А.В. Турулин, С.В. Будник

Санкт-Петербургский политехнический университет Петра Великого,
Санкт-Петербург, Российская Федерация

Рассмотрена задача обеспечения безопасности хранения, обработки и передачи изображений на основе криптографического метода с использованием хаотических отображений. Алгоритм шифрования построен на базе трехмерного отображения. Стойкость алгоритма шифрования при использовании систем с хаотической динамикой зависит от величины старшего (положительного) характеристического показателя Ляпунова. Поэтому задача повышения стойкости к различного рода атакам сводится к определению параметров управления, при котором старший характеристический показатель Ляпунова увеличивается. Предложена процедура изменения свойств хаотического отображения (энтропии и характеристических показателей Ляпунова) на основе введения в систему обратной связи. Процедура построена на использовании метода модального управления на основе приведения системы к канонической форме Фробениуса. Рассмотрено применение предлагаемого алгоритма шифрования для системы Рёсслера. Результаты тестирования подтвердили увеличение стойкости предложенного алгоритма шифрования к статистиче-

скому и дифференциальному анализу за счет увеличения старшего характеристического показателя Ляпунова.

Ключевые слова: шифрование изображений, хаотические отображения, управление спектром характеристических показателей Ляпунова, модальное управление, каноническая форма Фробениуса.

Ссылка при цитировании: Shashikhin V.N., Turulin A.V., Budnic S.V. Image encryption algorithm based on controlled chaotic maps // Computing, Telecommunications and Control. 2021. Vol. 14. No. 1. Pp. 7–21. DOI: 10.18721/JCSTCS.14101

Introduction

The problem of ensuring the security of image transmission is currently becoming more and more urgent in connection with the increasing flow of information transmitted over open communication lines. Reliable encryption methods for storing and transmitting digital images are required in various fields: medical information systems, confidential video conferencing, government and military communications systems.

Cryptographic methods stand out among various methods of protecting information and ensuring its integrity. However, traditional encryption algorithms, for example, AES and DES, were developed without taking into account the specific requirements for image encryption [1, 13] (a large amount of memory occupied, limited processing and transmission time) [2]. Therefore, it became necessary to create new encryption algorithms based on the use of nonlinear functions [3, 14].

One of the promising directions in modern cryptography is the development and research of data encryption algorithms based on dynamic chaos [4–7, 15, 16]. Such properties of chaotic systems as the exponential divergence of trajectories, ergodicity, and randomization are useful in the development of encryption schemes for digital images [8, 17–20]. Modern approaches to encryption use various chaotic maps and algorithms based on the composition of two maps that implement the operation of randomization and entanglement [9, 21, 22].

The paper considers an image encryption algorithm based on a chaotic mapping, which simultaneously implements the operation of randomizing and confusion. To improve the cryptographic stability of the algorithm, a procedure is proposed for changing the chaotic map characteristics (entropy and Lyapunov characteristic exponents) based on introducing feedback into the system. A procedure for changing the spectrum of Lyapunov characteristic exponents of a chaotic map is developed using the modal control method based on reducing the system to the canonical Frobenius form.

Image encryption problem statement

Mathematical model of the image. Let the raster model of the original rectangular image be represented by the following map:

$$I:[a,b]\times[c,d]\to L\left(R^{N\times M}\right), \tag{1}$$

where $L\left(R^{N\times M}\right)$ is the space of numerical dimension matrices of $N\times M$ size.

The N, M values are related to the dimensions of the pixel grid:

$$\Delta^{WH}=\left\{(i,j):i=\overline{1,N}=[W],j=\overline{1,M}=[H]\right\}, \tag{2}$$

where [*] is the integer part of the number.

With the help of digitalization and quantization operations, the description of digital images is reduced to a set of samples, which can be represented in the form of a matrix:

$$\mathrm{I} = \left(I_{ij}\right)_{i,j=1}^{N,M} \in L\left(R^{N\times M}\right), \tag{3}$$

whose elements are realizations on a discrete grid of continuous functions of two variables $\mathrm{I}:\left(0,W\right)\otimes\left(0,H\right)\to R$. The elements of these matrices take integer values from the [0; 255] interval when coding the pixel intensity with an eight-bit code.

Mathematical model of a system with chaotic dynamics. A nonlinear differential equation with a given initial state is considered as an evolutionary operator for the implementation of the encryption algorithm:

$$\dot{x}\left(t\right) = F\left(x\left(t\right)\right),\ x\left(t_0\right) = x_0, \tag{4}$$

where $x\left(t\right)\in \mathrm{P}\subseteq \mathrm{R}^n$ is the phase vector of the system; region P – phase space of the system; t – time function, $F:\mathrm{R}^n\to\mathrm{R}^n$ – vector function with $f_i\left(x\left(t\right)\right), i=\overline{1,n}$ components.

Among the set of nonlinear dynamical systems $S=\left\{\mathrm{P},F\right\}$, we will consider systems with a chaotic mapping for which the following conditions are satisfied.

1. The f map has an essential dependence on the initial data or it is sensitive (if there is such a number $\delta > 0$, that for any $\varepsilon > 0$ and any $x'\in X$ point there is a $x''\in X$ and the $m\in M$ number such that $\rho\left(x',x''\right)<\varepsilon$, but $\rho\left(f^{(m)}\left(x''\right)-f^{(m)}\left(x'\right)\right)\geq\delta$).

2. The f map p is transitive (for any U, V pair of open sets there is $m\geq 0$, that $f^{(m)}\left(U\right)\bigcap V\neq \mathrm{O}$).

The problem of controlling the spectrum of Lyapunov characteristic exponents. The mathematical model of a chaotic system in the synthesis of an encryption algorithm is a heterogeneous differential equation with a control

$$\dot{x}\left(t\right) = F\left(x\left(t\right)\right) + Bu\left(t\right),\ x\left(t_0\right) = x_0. \tag{5}$$

Lyapunov spectrum of the original nonlinear system (4)

$$\sigma\left(F\right) = \left\{\chi_i\left(F\right), i=\overline{1,n}\right\}$$

consists of n various Lyapunov characteristic exponents $\chi_1\left(F\right)\geq\chi_2\left(F\right)\geq\ldots\geq\chi_n\left(F\right)$ in descending order.

The problem of controlling the Lyapunov spectrum is to determine the feedback from the phase vector of the nonlinear system:

$$u\left(t\right) = K^*x\left(t\right) \tag{6}$$

such that the closed nonlinear system

$$\dot{x}\left(t\right) = F\left(x\left(t\right)\right) + BK^*x\left(t\right),\ x\left(t_0\right) = x_0 \tag{7}$$

had the following spectrum

$$\sigma\left(F+BK^*\right) = \left\{\chi_i\left(F+BK^*\right), i=\overline{1,n}\right\}, \tag{8}$$

equal to the required spectrum

$$\sigma(G)=\left\{\chi_i(G), i=\overline{1,n}\right\}. \quad (9)$$

The encryption algorithm strength when using systems with chaotic dynamics depends on the value of the largest (positive) Lyapunov characteristic exponent. Therefore, the problem of increasing resistance to various kinds of attacks is reduced to determining the control parameters (6), at which the leading Lyapunov characteristic exponent (9) increases in the closed-loop system (7). Besides, the feedback factor will expand the "keyspace" of the encryption algorithm.

Evaluation of the encryption algorithm strength. It is necessary to build a grayscale image encryption algorithm based on a chaotic map and to carry out a comparative assessment of the algorithm's strength with and without control action.

As a result of statistical cryptanalysis, it is necessary:

- to assess the uniformity of the distribution of pixels by brightness values, construct a histogram of this distribution;
- to calculate the pairwise correlation between two adjacent pixels horizontally, vertically, and diagonally;
- to calculate informational entropy.

To assess the strength of the algorithm to differential analysis, calculate:

- the percentage of pixels that changed the brightness value;
- the average change in gray intensity.

Encryption algorithm based on a 3D chaotic map

Chaotic map and its properties. In the process of image encryption, a three-dimensional chaotic Rössler map is used as a model of a nonlinear system (4)

$$\begin{cases} \dot{x}_1 = -(x_2 + x_3); \\ \dot{x}_2 = x_1 + ax_2; \\ \dot{x}_3 = b + x_3(x_1 - c). \end{cases} \quad (10)$$

For $a = 0.2$, $b = 0.2$, $c = 5.7$ values of the parameters, this map has a spectrum of Lyapunov characteristic exponents equal to

$$\sigma(F)=\left\{\chi_1(F)=0.1016; \chi_2(F)=0.0922; \chi_3(F)=-5.6953\right\}, \quad (11)$$

and a trajectory in three-dimensional phase space, which has the form shown in Fig. 1.

The spectrum of Lyapunov characteristic exponents and a strange attractor indicate the presence of chaotic dynamics in system (10).

Encryption algorithm. The grayscale image encryption algorithm of $N \times M$ size using nonlinear map (10) has the following steps in one round of encryption.

Step 1. Based on the original image, a raster model of the original image (1) with a matrix of the form (3) is formed:

$$\mathrm{I}=\left(I_{ij}\right)_{i,j=1}^{N,M} \in L\left(\mathrm{R}^{N\times M}\right),$$

where i is the number of pixel in the vertical row; j – the number of pixel in the horizontal row; $I_{i,j}$ – pixel with the i, j number brightness value; N – number of rows, and M – number of columns of the pixel matrix determined by the grid size (2).

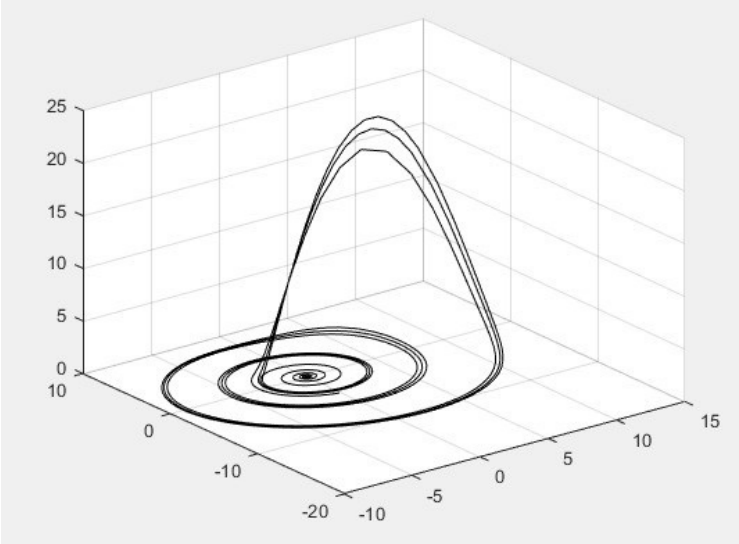

Fig. 1. Trajectory of the Rössler system

Step 2. For some initial state $x(0)=(x_1(0), x_2(0), x_3(0))$, determined by the point of exit of the chaotic system trajectory (10) to a strange attractor, three sequences are generated:

$$\begin{aligned} X_1 &= \{x_1(t_1), \dots x_1(t_k), \dots x_1(t_s)\}; \\ X_2 &= \{x_2(t_1), \dots x_2(t_k), \dots x_2(t_s)\}, \quad s = N \times M; \\ X_3 &= \{x_3(t_1), \dots x_3(t_k), \dots x_3(t_s)\}. \end{aligned} \tag{12}$$

Sequences X_1 and X_2 define the randomization of pixels, and the X_3 sequence defines the scattering (brightness changes) of pixels.

Here, the elements of sequences (12) are formed according to the rule:

$$\begin{aligned} \dot{x}_1(t) &= f_1[x(t)], \\ \dot{x}_2(t) &= f_2[x(t)], \Leftrightarrow \dot{x}(t) = F[x(t)], \\ \dot{x}_3(t) &= f_3[x(t)], \end{aligned} \tag{13}$$

where $F[x(t)] = \left(f_1\left(x(t), f_2\left(x(t), f_3\left(x(t)\right)\right)\right)\right)^T$ is a vector function whose components are the functions on the right-hand side of equations (10).

Step 3. A chaotic matrix of the encrypted image of the first round is formed using the third equation (13):

$$E^{(1)} = \begin{bmatrix} e_{1,1}^{(1)} & e_{1,2}^{(1)} & \dots & e_{1,M}^{(1)} \\ e_{2,1}^{(1)} & e_{2,2}^{(1)} & \dots & e_{2,M}^{(1)} \\ \dots & \dots & \dots & \dots \\ e_{N,1}^{(1)} & e_{N,2}^{(1)} & \dots & e_{N,M}^{(1)} \end{bmatrix} \in \mathrm{R}^{N \times M}, \tag{14}$$

where $e_{i,j}^{(1)} = \left[x_3(t) \bmod 255 \right]$ is the intensity of gray pixel with the $i = \left[x_1(t) \bmod M \right]$ row number and the $j = \left[x_2(t) \bmod N \right]$ column number; [*] is the integer part of number.

Further, repeating steps 2–3 for the image (14) for p rounds, we get an encrypted image $\hat{E}^{(p)}$ of the following form:

$$\hat{E}^{(1)} = \left(\hat{e}_{i,j}^{(1)} \right)_{i,j}^{N,M} \in \mathrm{R}^{N \times M}. \tag{15}$$

The number of rounds is determined by the required cipher strength indicators.

Cryptanalysis of the encryption algorithm. The assessment of the algorithm strength is carried out using statistical and differential cryptanalysis [2]. The 512 × 512 gray-scale Lena photo is used as the source image.

To determine the distribution of pixels of the encrypted image $\hat{E}^{(p)}$ (15) in grayscale, the following probability is calculated:

$$P(m_s) = \frac{m_s}{N \times M}, \tag{16}$$

where m_s is the number of pixels e_{ij}, for the gray intensity takes on $s \in [0; 255]$ values. The distribution of pixels by gray intensity values for the original image is shown in Fig. 2, and for the encrypted image – in Fig. 3.

Pairwise correlation between two adjacent pixels horizontally, vertically and diagonally of the original and encrypted images is calculated by the formula:

$$\rho(u_i, v_{i+1}) = \frac{\dfrac{\sum_{i=1}^{N \times M} (u_i - \bar{U})(v_{i+1} - \bar{V})}{N \times M}}{\sqrt{\dfrac{\sum_{i=1}^{N \times M} (u_i - U)^2}{N \times M}} \sqrt{\dfrac{\sum_{i=1}^{N \times M} (v_{i+1} - V)^2}{N \times M}}}, \tag{17}$$

$$\bar{U} = \frac{\sum_{i=1}^{N \times M} u_i}{N \times M}, \ \bar{V} = \frac{\sum_{i=1}^{N \times M} v_i}{N \times M},$$

where u_i, v_{i+1} – the intensity of the i^{th} gray pixel and the pixel adjacent to it, $U = \{u_1, u_2, \ldots u_i, \ldots u_{N \times M}\}$, $V = \{v_1, v_2, \ldots v_i, \ldots v_{N \times M}\}$ – a series of gray intensity values of pixels in the image and a series of gray intensity values of neighboring pixels.

Information entropy is determined by the expression:

$$H(m_s) = \sum_{s=0}^{2^n - 1} P(m_s) \log_2 \left(1 / P(m_s) \right), \tag{18}$$

where $P(m_s)$ is the probability of the gray intensity belonging to the $s \in [0; 255]$ level.

To assess the strength of the algorithm against the differential analysis, the following are calculated:

- number of changing pixel rate (NPCR):

$$\Pi(I_1, I_2) = \frac{\sum_{i=1}^{N} \sum_{j=1}^{M} D(i, j)}{N \times M} \times 100\%, \tag{19}$$

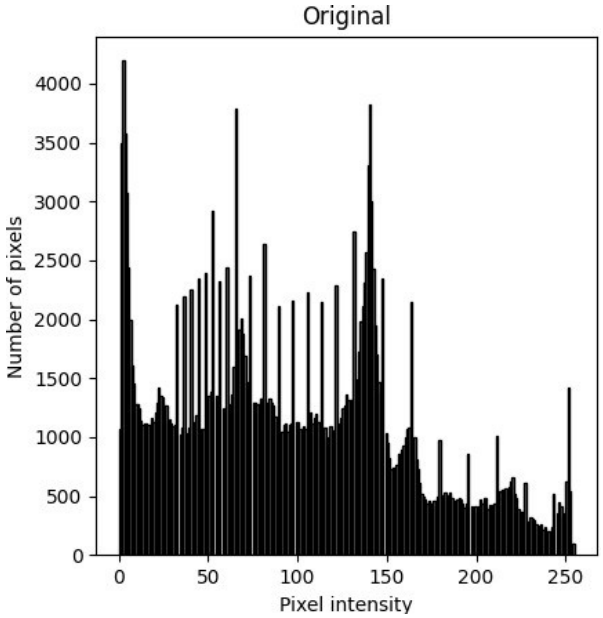

Fig. 2. Original image histogram

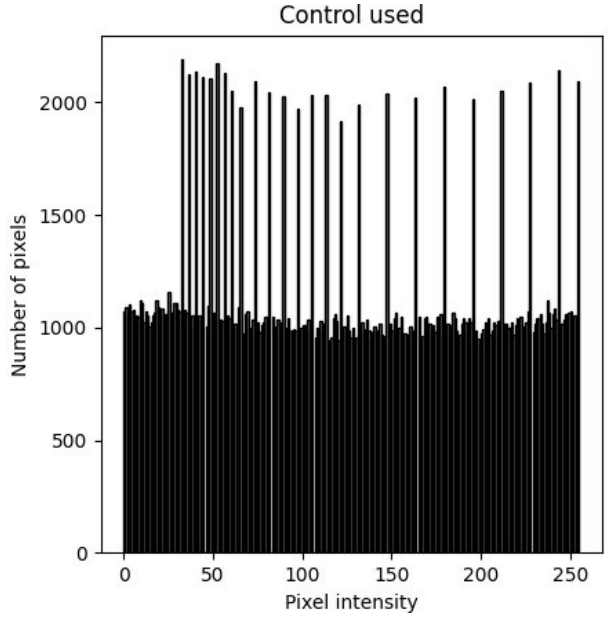

Fig. 3. Encrypted image histogram

where

$$D(i,j)=\begin{cases}1, & if \quad e_1(i,j)=e_2(i,j)\\ 0, & if \quad e_1(i,j)\neq e_2(i,j)\end{cases} \quad \forall i=\overline{1,N}, \quad \forall j=\overline{1,M},$$

I_1 – the original image, I_2 – the original image with the gray level of one pixel being changed;

$\hat{E}_1^{(p)} \cdot \hat{E}_2^{(p)}$ – the encrypted images corresponding to the I_1, I_2 original images;

$\hat{e}_1^{(p)}(i, j), \hat{e}_2^{(p)}(i, j)$ – the value of the gray level for the pixel with the (i, j) number in the $\hat{E}_1^{(p)}$ and $\hat{E}_2^{(p)}$ images;

- unified averaged changed intensity (UACI)

$$C(E_1, E_2) = \frac{1}{N \times M} \sum_{i=1,\, j=1}^{N,\, M} \frac{\left| e_1(i, j) - e_2(i, j) \right|}{255} \times 100\,\%. \tag{20}$$

The results of calculating the strength criteria after two rounds of encryption using the chaotic map with and without control are shown in Table 1.

Table 1

Encryption algorithm strength criteria

Chaotic map	Largest LCE	Image	Correlation coefficient			Entropy	NPCR, %	UACI, %
			Horizontal	Vertical	Diagonal			
–	–	original	0.0293	0.0263	0.0653	7.55	–	–
No control	0.1016	encrypted	0.000175	0.000192	0.000380	7.76	99.54	33.42
With control	0.2862	encrypted	0.000101	0.000186	0.000117	7.96	99.55	33.45

Control of Lyapunov characteristic exponent of chaotic map

To increase the strength of the proposed image encryption algorithm, a control action is introduced into a system with chaotic dynamics to increase the positive Lyapunov characteristic exponent and information entropy. Control is sought in the form of linear feedback in phase coordinates.

The solution to the problem of changing the spectrum of characteristic exponents of a nonlinear system is based on the Grobman-Hartman theorem [11]. Any system in a neighborhood of a hyperbolic singular point is locally topologically equivalent to its linear approximation. Thus, the behavior of a nonlinear system in the neighborhood of a hyperbolic singular point is similar to the behavior of a linearized system. A singular point is hyperbolic if the Jacobi matrix has no eigenvalues in it on the imaginary axis. A change in the characteristic exponents of a linearized system, which coincides with the real part of the eigenvalues of the Jacobi matrix, entails a change in the characteristic exponents of a nonlinear system.

Synthesis of linearized system control. It is possible to provide the desired eigenvalues of the Jacobi matrix of the linearized system using the method of synthesis of a modal controller based on a reduction to the canonical Frobenius form [12].

Let the equations of state of the linearized system have the form:

$$\dot{y}(t) = Ay(t) + bu(t), \;\; y(t_0) = y_0, \tag{21}$$

where $y(t) \in R^n$ is the vector of state coordinates; $u(t) \in R^1$ – the control action; $A \in R^{n \times n}$ – the Jacobi matrix of the nonlinear system (10) at the hyperbolic singular point.

It is required to determine the $k = (k_1, k_2, \ldots k_n)^T$ parameters of the linear feedback control law $u(t) = kx(t)$ providing the given eigenvalues $\overline{v}_i, \; i = 1, \ldots, n$ of the matrix of the closed system $A_c = A + bk$. From the expression for the matrix of the $A_c = A + bk^T$ closed system, it is impossible to directly obtain

the values of the feedback coefficient, since the matrix is unknown. Therefore, such a change of variables $y = Q\tilde{y}$ is used that the mathematical model of the transformed system $\dot{\tilde{y}} = \left(\tilde{A} + \tilde{b}\tilde{k}^T\right)\tilde{y}$ has the canonical Frobenius form with the A matrix and the b vector of the following form:

$$A_f = \begin{bmatrix} 0 & 1 & \dots & 0 \\ \dots & \dots & \dots & \dots \\ 0 & 0 & \dots & 1 \\ -a_n & -a_{n-1} & \dots & -a_1 \end{bmatrix}, \; b_f = \begin{bmatrix} 0 \\ 0 \\ 0 \\ 1 \end{bmatrix},$$

where a_i are the coefficients of the characteristic polynomial of the matrices A and A_f.

To bring the matrix of the system to the canonical form, the matrix T formed from the coefficients of the characteristic polynomial of the matrix A is used as follows:

$$T = \begin{bmatrix} a_{n-1} & a_{n-2} & \dots & 1 \\ a_{n-2} & a_{n-3} & \dots & 0 \\ a_{n-3} & 1 & \dots & 0 \\ 1 & 0 & \dots & 0 \end{bmatrix}.$$

The similarity transformation $y = Q\tilde{y}$ uses the matrix $Q = S_y T$, where S_y is the system controllability matrix. If this similarity transformation is performed in system (21):

$$\dot{\tilde{y}} = Q^{-1}AQ\tilde{y} + Q^{-1}bk^TQ\tilde{y}$$

and the following notation is introduced

$$\tilde{k} = Q^T k, \; \tilde{b} = Q^{-1}b, \; \tilde{A} = Q^{-1}AQ,$$

then the system model will take the following form:

$$\dot{\tilde{y}} = \left(\tilde{A} + \tilde{b}\tilde{k}^T\right)\tilde{y}.$$

Considering the peculiarities of constructing the Q matrix, the matrix of the system will have the Frobenius matrix form, and the b vector will be reduced to the simplest form:

$$\tilde{A} = I_n^{(1)} - e_n a^T, \; \tilde{b} = e_n,$$

where $I_n^{(1)}$ is a matrix of $n \times n$ size, having unities over the main diagonal, and the remaining elements being zero; e_n is a unit vector of n, the n^{th} coordinate of which is equal to unity, and the rest are equal to zero; $a = (a_n, a_{n-1}, ..., a_1)^T$.

The closed-loop matrix will take the form:

$$\tilde{A}_c = \tilde{A} + \tilde{b}\tilde{k}^T = I_n^{(1)} - e_n\left(a - \tilde{k}\right)^T.$$

For this matrix to have the required eigenvalues, the coefficients of its characteristic equation must correspond to the $a_{est} = \left(a_n^{est}, a_{n-1}^{est}, ..., a_1^{est}\right)^T$ vector, where a_i^{est} are the coefficients of the characteristic

polynomial of the matrices A_c and $\tilde{A}_c$. Then $a_{est} = a - \tilde{k},$ and the coefficients of the controller for linearized system (21) are determined by the relation:

$$k = \left(Q^T\right)^{-1}\left(a - a_{est}\right). \tag{22}$$

Synthesis of a nonlinear system control. Let the Jacobian matrix equal J^* at the singular point x^* of system (4) in the absence of control, and the vector of its eigenvalues is equal to v^*. Let us set the vector of the desired eigenvalues $\overline{v}^*$ of the Jacobian $\overline{J}^*$ of the nonlinear system (5) in the form:

$$\overline{v}_i^* = v_i^* + \alpha \operatorname{Re}\left(v_i^*\right), \tag{23}$$

where α is the coefficient selected according to the graph in Fig. 4.

For the Jacobian $\overline{J}^*$ of system (21) to have given eigenvalues, we choose a control in the form:

$$u(t) = kx(t), \tag{24}$$

then the Jacobian of system (21) with control (24) will be equal to

$$\overline{J}^* = J^* + Bk, \tag{25}$$

where $k \in R^{1\times n}$ is the feedback coefficient, which is found by the method of synthesis of modal control according to formula (22).

The largest Lyapunov characteristic exponent of system (5) with control (24) will differ from the largest Lyapunov characteristic exponent of uncontrolled nonlinear system (4). It is necessary to increase the largest Lyapunov characteristic exponent to increase chaos in the system, which is achieved by the appropriate choice of the α coefficient in formula (23).

A graph of the dependence of the largest characteristic exponent of the nonlinear system with control from the α coefficient is built to select the α (see Fig. 4). Based on this graph, the α* coefficient is selected that satisfies the desired value of the largest characteristic exponent of the nonlinear system.

After choosing the α* coefficient, the corresponding feedback coefficient k^* is substituted into formula (24) instead of k.

We will illustrate the control synthesis technique for the Rössler system, the model of which in dimensionless variables and parameters has the following form:

$$\begin{cases} \dot{x}_1 = -\left(x_2 + x_3\right) \\ \dot{x}_2 = x_1 + ax_2 \\ \dot{x}_3 = b + x_3\left(x_1 - c\right) \end{cases} \Leftrightarrow \dot{x}(t) = F\left(x(t)\right).$$

The Rössler system, with the $a = 0.2$, $b = 0.2$, $c = 5.7$ values of the parameters, has two singular points:

$$x1^* = \left(0.0070 \quad -0.0351 \quad 0.0351\right),$$
$$x2^* = \left(5.6930 \quad -28.4649 \quad 28.4649\right),$$

and the Jacobi matrix equals:

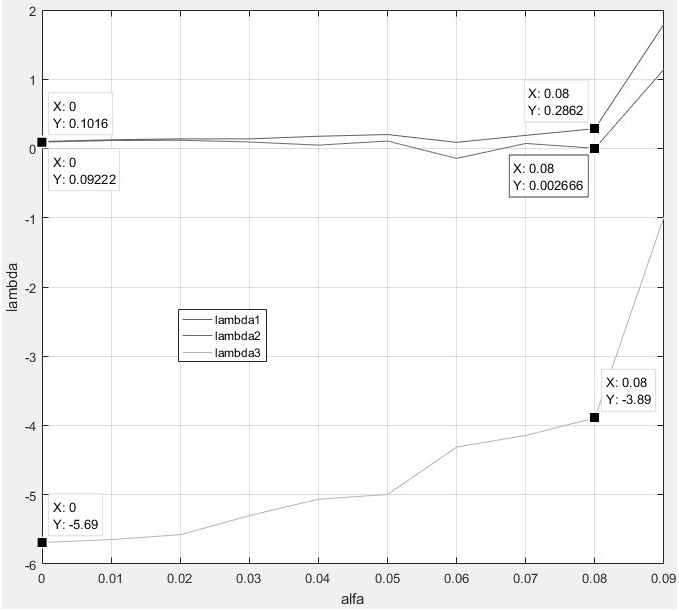

Fig. 4. Dependence of the largest Lyapunov characteristic exponent χ_1 on α

$$J = \begin{bmatrix} 0 & -1 & -1 \\ 1 & a & 0 \\ x_3 & 0 & x_1 - c \end{bmatrix}.$$

Eigenvalues of the Jacobi matrix calculated at singular points are:

$$v\left(J\left(x1^*\right)\right) = \begin{cases} v_1 = 0.0970 + 0.9952i \\ v_2 = 0.0970 - 0.9952i, \\ v_3 = -5.6870 \end{cases}$$

$$v\left(J\left(x2^*\right)\right) = \begin{cases} v_1 = 5.4280i \\ v_2 = -5.4280i. \\ v_3 = 0.1930 \end{cases}$$

We will change the eigenvalues of the Jacobian at the hyperbolic singular point $x1^*$. The desired eigenvalues of the Jacobian (25) of the closed system calculated at $x1^*$ point are determined by equality (23). Fig. 4 shows the graph of the dependence of the largest Lyapunov characteristic exponent of the nonlinear system (7) on α.

According to the graph shown in Fig. 4, we select the $a^* = 0.08$ value of the coefficient at which the condition $\chi_1^* > \chi_1\left(F\right)$ is fulfilled. Using the selected $a^* = 0.08$ value, we calculate the required eigenvalue of the Jacobian, and using formula (22) we calculate the feedback coefficient in the nonlinear system:

$$k^* = \left(1.0426 \quad -0.4943 \quad -22.8945\right).$$

Spectrum (8) of a nonlinear system (7) with synthesized control is equal to:

$$\sigma\left(F + bk^*\right) = \left\{\chi_1 = 0.2862; \chi_2 = 0.0026; \chi_3 = -3.8931\right\}.$$

The largest indicator of a closed system is 2.82 times higher than the largest indicator of the original system, which indicates an increase in chaos in the system.

Properties of an encryption algorithm based on controlled chaos

The strength of the encryption algorithm based on a chaotic feedback system is estimated according to the same criteria of statistical and differential cryptanalysis that were used when testing the algorithm with no control, namely: the probability of gray intensity distribution was calculated by formula (16); correlation coefficients – according to formulas (17); information entropy – according to formula (18), and the percentage of changed pixels and average change in gray color intensity – according to formulas (19) and (20), respectively. The results of testing the encryption algorithm with control are shown in Table 1.

It follows from the above test results that all the compared cryptographic strength criteria are improved when using an encryption algorithm with the control in comparison with an algorithm with no control.

Conclusion

An algorithm for encrypting a grayscale image based on the use of a three-dimensional chaotic map, which implements simultaneous randomization and scattering, is presented. To increase the cryptographic strength of the algorithm, a method for synthesizing feedback on the phase vector of a nonlinear system is proposed, which ensures an increase in the largest Lyapunov characteristic exponent responsible for the degree of chaos. The synthesis technique is based on the modal control method using the canonical Frobenius form, which is extended to nonlinear chaotic systems.

The use of the proposed algorithm is considered using the example of the Rössler system. The test results confirmed an increase in the strength of the proposed encryption algorithm against statistical and differential analysis due to an increase in the Lyapunov characteristic exponent, which is achieved by introducing feedback into the chaotic system used for encryption.

REFERENCES

1. **Sidorenko A.V., Shakinko I.V., Sidorenko Yu.V.** Algoritm shifrovaniya izobrazheniy s ispolzovaniyem dvumernykh khaoticheskikh otobrazheniy [Image encryption algorithm using two-dimensional chaotic maps]. *Sistemnyy analiz i prikladnaya informatika* [*System analysis and applied information science*], 2016, No. 2, Pp. 44–49. (rus)

2. **Sidorenko A.S., Shishko M.S.** Shifrovaniye izobrazheniy na osnove khaoticheskikh otobrazheniy s ispolzovaniyem parallelnykh vychisleniy [Encryption of images on the basis of chaotic mapping and parallel computing]. *Informatika* [*Informatics*], 2017, No. 4(56), Pp. 78–88. (rus)

3. **Novitskiy V.V., Tsvetkov V.Yu.** Szhatiye polutonovykh izobrazheniy na osnove klasterizatsii i progressivnogo vlozhennogo kodirovaniya veyvlet-koeffitsiyentov [Halftone image compression based on clustering and progressive nested encoding of wavelet coefficients]. *Telekommunikatsii: Seti i Tekhnologii, Algebraicheskoye Kodirovaniye i Bezopasnost Dannykh, Materialy nauchno-tekhnicheskogo seminara* [*Materials of the Scientific and Technical Seminar on Telecommunications: Networks and Technologies, Algebraic Coding and Data Security*], Minsk, BGUIR, 2015, Pp. 45–51. (rus)

4. **Sidorenko A.V., Mulyarchuk K.S.** Shifrovaniye dannykh s ispolzovaniyem khaoticheskoy dinamiki v sensornoy seti [ATA encryption using the chaotic dynamics in wireless sensor networks]. *Doklady BGUIR*, 2015, Vol. 92, No. 6, Pp. 41–47. (rus)

5. **Sidorenko A.V., Mulyarchuk K.S.** Shifrovaniye dannykh na osnove diskretnykh khaoticheskikh sistem i otobrazheniy [The data encryption based on discrete chaotic systems and maps]. *Doklady BGUIR*, 2013, Vol. 71, No. 1, Pp. 62–67. (rus)

6. **Burkin I.M.** Ob odnoy sisteme tretyego poryadka s 3-D reshetkoy khaoticheskikh attraktorov [On a third-order system with a 3-D lattice of chaotic attractors]. *Vestnik YeGU. Differentsialnyye uravneniya i prikladnyye zadachi* [*TSU Bulletin. Differential equations and applied problems*], 2020, No. 1, Pp. 3–8. (rus)

7. **Gulyayev Yu.V., Belyayev R.V., Vorontsov G.M., et al.** Informatsionnyye tekhnologii na osnove khaoticheskoy dinamiki dlya peredachi, obrabotki, khraneniya i zashchity informatiki [Dynamic-chaos information technologies for data transmission, storage, and protection]. *Informatsionnyye tekhnologii, RENSIT* [*Information technology, RENSIT*], 2018, Vol. 10, No. 2, Pp. 279–312. (rus). DOI: 10.17725/rensit.2018.10.279

8. **Ten T.A., Beysenbi M.A., Kogay G.D.** *Kriptograficheskiye sistemy po upravleniyu khaosom: Monografiya* [*Cryptographic systems for managing deterministic chaos*]. Gamburg: LAP LAMBERT Academic Publishing, 2014. 228 p. (rus)

9. **Sidorenko A.S., Shishko M.S.** Shifrovaniye izobrazheniy na osnove khaoticheskoy dinamiki s elementami geneticheskogo algoritma [The image encryption based on chaotic dynamics and genetic algorithm elements]. *Informatika* [*Informatics*], 2018, Vol. 29, No. 1, Pp. 95–100. (rus)

10. **Shashikhin V.N., Budnik S.V.** *Upravleniye krupnomasshtabnymi dinamicheskimi sistemami* [*Managing large-scale dynamic systems*]. St. Petersburg: POLITEKhPRESS, 2020. 308 p. (rus)

11. **Grobman D.** Gomeomorfizm sistem differentsialnykh uravneniy [Homeomorphism of systems of differential equations]. *DAN SSSR*, 1959, Vol. 128, No. 5, Pp. 880–881. (rus)

12. **Budnik S.V., Shashikhin V.N.** Upravleniye khaoticheskoy dinamikoy nelineynykh sistem [Control of chaotic dynamics of nonlinear systems]. *XXIII Mezhdunarodnaya nauchnaya uchebno-prakticheskaya konferentsiya "Sistemnyy analiz v proyektirovanii i upravlenii"* [*XXIII International Scientific Educational and Practical Conference on System Analysis in Design and Management*], St. Petersburg, 2019, Pp. 12–19. (rus)

13. **Chen P.** A fast image encryption based on chaotic map and lookup table. *Nonlinear Dynamics*, 2015, Vol. 79, No. 3, Pp. 2121–2131.

14. **Seyedzadeh S.M., Norouzi B., Mirzakuchaki S.** RGB image encryption algorithm based on choquet fuzzy integral. *The Journal of Systems and Software*, 2014, Vol. 97, No. 11, Pp. 128–139.

15. **Faraoun K.M.** A parallel block-based encryption schema for digital images using reversible cellular automata. *Engineering Science*, 2014, Vol. 17, Pp. 85–94.

16. **Behnia S., Akhshani A., Mahmodi H.** Applications of tripled chaotic maps in cryptography. *Chaos, Solitons & Fractals*, 2009, Vol. 40, No. 1, Pp. 505–519.

17. **Li C., Luo G., Qim K.** An image encryption scheme based on chaotic map. *Nonlinear Dynamics*, 2017, Vol. 87, No. 3, Pp. 127–136.

18. **Jaryal S., Marwaha C.** Comparative analysis of various image encryption techniques. *International Journal of Computational Intelligence Research*, 2017, Vol. 13, No. 2, Pp. 273–286.

19. **Xu L., Li Z., Li J.** A novel bit-level image encryption based on chaotic map. *Optics and Lasers in Engineering*, 2016, Vol. 78, No. 3, Pp. 17–25.

20. **Kanso A., Ghebleh M.** A robust chaotic algorithm for digital image. *Communications in Nonlinear Science and Numerical Simulation*, 2014, Vol. 19, No. 6, Pp. 1898–1907.

21. **Xiuli C., Xiaoyu Z., Zhihua G.** An image encryption algorithm based on chaotic system and compressive sensing. *Signal Processing*, 2018, Vol. 148, No. 7, Pp. 124–144.

22. **Kaur M., Singh D., Sun K.** Color image encryption using non-dominated sorting generated algorithm with local chaotic search based 5D chaotic map. *Future Generation Computer Systems*, 2020, Vol. 107, No. 6, Pp. 333–350.

23. **Rossler O.E.** An equation for continuous chaos. *Physics letters*, 1976, Vol. 57, No. 5. Pp. 397–398.

Received 14.02.2021.

СПИСОК ЛИТЕРАТУРЫ

1. **Сидоренко А.В., Шакинко И.В., Сидоренко Ю.В.** Алгоритм шифрования изображений с использованием двумерных хаотических отображений // Системный анализ и прикладная информатика. 2016. № 2. С. 44–49.

2. **Сидоренко А.С., Шишко М.С.** Шифрование изображений на основе хаотических отображений с использованием параллельных вычислений // Информатика. 2017. № 4(56). С. 78–88.

3. **Новицкий В.В., Цветков В.Ю.** Сжатие полутоновых изображений на основе кластеризации и прогрессивного вложенного кодирования вейвлет-коэффициентов // Телекоммуникации: сети и технологии, алгебраическое кодирование и безопасность данных: Матер. науч.-техн. Семинара. Минск, БГУИР, 2015. С. 45–51.

4. **Сидоренко А.В., Мулярчук К.С.** Шифрование данных с использованием хаотической динамики в сенсорной сети // Доклады БГУИР. 2015. Т. 92. № 6. С. 41–47.

5. **Сидоренко А.В., Мулярчук К.С.** Шифрование данных на основе дискретных хаотических систем и отображений // Доклады БГУИР. 2013. Т. 71. № 1. С. 62–67.

6. **Буркин И.М.** Об одной системе третьего порядка с 3-D решеткой хаотических аттракторов // Вестник ЕГУ. Дифференциальные уравнения и прикладные задачи. 2020. № 1. С. 3–8.

7. **Гуляев Ю.В., Беляев Р.В. Воронцов Г.М. и др.** Информационные технологии на основе хаотической динамики для передачи, обработки, хранения и защиты информатики // Информационные технологии. РЭНСИТ. 2018. Т. 10. № 2. С. 279–312.

8. **Тен Т.А., Бейсенби М.А., Когай Г.Д.** Криптографические системы по управлению хаосом: Монография. Гамбург: LAP LAMBERT Academic Publishing, 2014. 228 с.

9. **Сидоренко А.С., Шишко М.С.** Шифрование изображений на основе хаотической динамики с элементами генетического алгоритма // Информатика. 2018. Т. 29. № 1. С. 95–100.

10. **Шашихин В.Н., Будник С.В.** Управление крупномасштабными динамическими системами. СПб.: ПОЛИТЕХПРЕСС, 2020. 308 с.

11. **Гробман Д.** Гомеоморфизм систем дифференциальных уравнений // ДАН СССР. 1959. Т. 128. № 5. С. 880–881.

12. **Будник С.В., Шашихин В.Н.** Управление хаотической динамикой нелинейных систем // XXIII Междунар. науч. учеб.-практич. конф. «Системный анализ в проектировании и управлении». Санкт-Петербург, 10-11 июня 2019. С. 12–19.

13. **Chen P.** A fast image encryption based on chaotic map and lookup table // Nonlinear Dynamics. 2015. Vol. 79. No. 3. Pp. 2121–2131.

14. **Seyedzadeh S.M., Norouzi B., Mirzakuchaki S.** RGB image encryption algorithm based on choquet fuzzy integral // The J. of Systems and Software. 2014. Vol. 97. No. 11. Pp. 128–139.

15. **Faraoun K.M.** A parallel block-based encryption schema for digital images using reversible cellular automata // Engineering Science. 2014. Vol. 17. Pp. 85–94.

16. **Behnia S., Akhshani A., Mahmodi H.** Applications of tripled chaotic maps in cryptography // Chaos, Solitons & Fractals. 2009. Vol. 40. No. 1. Pp. 505–519.

17. **Li C., Luo G., Qim K.** An image encryption scheme based on chaotic map // Nonlinear Dynamics. 2017. Vol. 87. No. 3. Pp. 127–136.

18. **Jaryal S., Marwaha C.** Comparative analysis of various image encryption techniques // Internat. J. of Computational Intelligence Research. 2017. Vol. 13. No. 2. Pp. 273–286.

19. **Xu L., Li Z., Li J.** A novel bit-level image encryption based on chaotic map // Optics and Lasers in Engineering. 2016. Vol. 78. No. 3. Pp. 17–25.

20. **Kanso A., Ghebleh M.** A robust chaotic algorithm for digital image // Communications in Nonlinear Science and Numerical Simulation. 2014. Vol. 19. No. 6. Pp. 1898–1907.

21. **Xiuli C., Xiaoyu Z., Zhihua G.** An image encryption algorithm based on chaotic system and compressive sensing // Signal Processing. 2018. Vol. 148. No. 7. Pp. 124–144.

22. **Kaur M., Singh D., Sun K.** Color image encryption using non-dominated sorting generated algorithm with local chaotic search based 5D chaotic map // Future Generation Computer Systems. 2020. Vol. 107. No. 6. Pp. 333–350.

23. **Rossler O.E.** An equation for continuous chaos // Physics letters. 1976. Vol. 57. No. 5. Pp. 397–398.

Статья поступила в редакцию 14.02.2021.

THE AUTHORS / СВЕДЕНИЯ ОБ АВТОРАХ

Shashikhin Vladimir N.
Шашихин Владимир Николаевич
E-mail: shashihin@bk.ru

Turulin Aleksandr V.
Турулин Александр Владимирович
E-mail: sanya.turulin.98@list.ru

Budnik Svetlana V.
Будник Светлана Владимировна
E-mail: budnik.sveta@mail.ru

DOI: 10.18721/JCSTCS.14102
УДК 621.372

CMOS INDUCTOR DESIGN FEATURES FOR LTE DEVICES

E.Yu. Kotlyarov[1,2], V.Yu. Mikhailov[1,2], I.A. Zubov[1], A.V. Nuykin[1], A.F. Iljin[2], M.G. Putrya[2]

[1] Molecular Electronics Research Institute, Moscow, Russian Federation;

[2] National Research University of Electronic Technology, Moscow, Russian Federation

This work is devoted to some aspects of the development of planar elements of the microwave path, which are used in the design of low-noise LTE range amplifiers, namely inductors, for further employment as part of the NB-IoT transceiver. General theoretical calculations on the design of high-frequency inductors are given. By the example of a multilayer CMOS 90 nm inductor with a nominal value of 7 nH, we demonstrated the influence of the structure thickness obtained by replicating layers used to get the required skin layer thickness and to achieve the best quality factor in the LTE frequency range from 0.5 to 3.5 GHz by means of electromagnetic (EM) models. For a better understanding of the inductor operation, the models obtained as a result of the EM simulation for different values of the substrate conductivity are compared. The obtained data partially refute the need of increasing the maximum thickness of the inductors by a set of upper metals combined using multiple TSV arrays for silicon process stacks. Due to the increasing of the capacitive influence of the substrate on the lower metal layers of the inductor, the highest values of Q-factor and self-resonance frequencies are achieved by the structures with a minimum number of metal layers, despite the negative influence of the skin effect for low frequencies.

Keywords: LTE, NB-IoT, inductance coil, 3D inductor, CMOS, EM analysis.

Citation: Kotlyarov E.Yu., Mikhailov V.Yu., Zubov I.A., Nuykin A.V., Iljin A.F., Putrya M.G. CMOS inductor design features for LTE devices. Computing, Telecommunications and Control, 2021, Vol. 14, No. 1, Pp. 22–32. DOI: 10.18721/JCSTCS.14102

ОСОБЕННОСТИ ПРОЕКТИРОВАНИЯ КМОП КАТУШЕК ИНДУКТИВНОСТИ ДЛЯ УСТРОЙСТВ LTE ДИАПАЗОНОВ ЧАСТОТ

Е.Ю. Котляров[1,2], В.Ю. Михайлов[1,2], И.А. Зубов[1], А.В. Нуйкин[1], А.Ф. Ильин[2], М.Г. Путря[2]

[1] Научно-исследовательский институт молекулярной электроники, Москва, Российская Федерация;

[2] Национальный исследовательский университет «Московский институт электронной техники», Москва, Российская Федерация

Статья посвящена некоторым аспектам разработки планарных элементов СВЧ-тракта, которые используются при проектировании малошумящих усилителей LTE диапазона, а именно катушкам индуктивности, для дальнейшего применения в составе приемопередатчика NB-IoT. Даны общие теоретические выкладки по проектированию высокочастот-

ных катушек индуктивности. На примере многослойной КМОП 90 нм катушки номиналом 7 нГн, при помощи электромагнитных (ЭМ) моделей, продемонстрировано влияние толщины структуры, полученной при помощи реплицирования слоев, для набора требуемой толщины скин-слоя и достижения наилучших показателей добротности в частотном диапазоне LTE от 0,5 до 3,5 ГГц. Для наиболее полного представления о работе катушки проведено сравнение моделей, полученных в результате ЭМ симуляции для разных значений проводимости подложки. Полученные данные частично опровергают необходимость наращивания максимальных толщин интегральных катушек индуктивности путем набора верхних металлов, объединенных при помощи множественных массивов TSV, для стеков кремниевых процессов. Из-за увеличения емкостного влияния подложки по отношению к нижним слоям металлизации катушки индуктивности, наибольшие значения добротности и частот собственного резонанса достигаются на конструкциях с минимальным числом слоев металлизации вопреки негативному влиянию скин-эффекта для малых частот.

Ключевые слова: LTE, NB-IoT, катушка индуктивности, 3D-индуктор, КМОП, ЭМ анализ.

Ссылка при цитировании: Kotlyarov E.Yu., Mikhailov V.Yu., Zubov I.A., Nuykin A.V., Iljin A.F., Putrya M.G. CMOS inductor design features for LTE devices // Computing, Telecommunications and Control. 2021. Vol. 14. No. 1. Pp. 22–32. DOI: 10.18721/JCSTCS.14102

Introduction

The rapid growth of the telecommunications industry under the auspices of the announced 5G (and 6G in the future) communication networks has led to the new frequency bands development. At the same time, within the already known frequency ranges, new communication standards and protocols are emerging, forming new areas of application of microelectronic devices in telecommunication systems, such as the Internet-of-Things represented in 3GPP: LTE-M, EC-GSM-IoT, NB-IoT [1] for example.

To provide a competitive position in the mass segment of the telecommunications market, the proposed device must be cheap and technologically advanced. Currently, when designing integrated circuits (IC) for telecommunications, the most widely used silicon technologies are CMOS and SiGe [2], which allow us to provide the required parameters of the element base [3]. At a relatively low cost, silicon technologies allow the implementation of both digital and analog system nodes and systems for the “mixed signals” processing.

This work is devoted to some aspects of RFIC passive planar elements design used in the low-noise amplifiers of the LTE frequency bands range, namely inductance coils or inductors.

Figure 1 shows a functional diagram of a proposed NB-IoT transceiver. A homodyne receiver is used as a receiver.

The building blocks of the receiving (RX) channel of the transceiver device include a bandpass filter of the preselector (BPF), a low-noise amplifier (LNA), a quadrature demodulator (based on mixers with a shift of 90 degrees), automatic gain control systems (AGC-VGA) and low-pass filters (LPF). The LNA is one of the key circuit nodes. In terms of signal conversion and processing, the LNA is responsible for the sensitivity of the receiver and its dynamic range.

The transmitting (TX) channel consists of low-pass filters (LPF), buffer amplifiers (BA), a quadrature modulator, a high-frequency amplifier (HFA), a bandpass filter (BPF), and a power amplifier (PA). As shown in the Fig. 1, the antenna bandpass filters of the receiver and transmitter, and the PA_{TX} are discrete, while the rest of the elements are integrated.

Depending on the type of transceiver (for broadband devices or devices with multiple operating ranges), the LNA can determine the receiver bandwidth by providing uniform gain flatness over the operating range and reverse loss values. Another important thing is that in the transceiver RX channel (usually for communication systems), the LNA [4] is the first device that interacts with the antenna. As the result, the LNA input impedance is a required to match the antenna and minimize insertion loss and distortion.

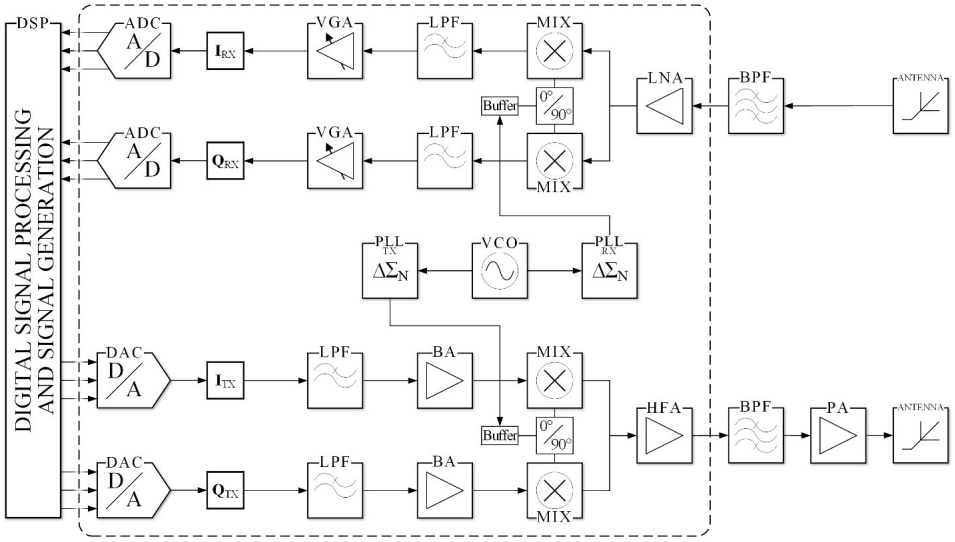

Fig. 1. Functional diagram of the NB-IoT transceiver

One of the simplest ways to design a low noise amplifier is a cascode amplifier circuit. Works [5–7] present the calculated data of the noise figure and the gain of the cascoded LNA models in the frequency domain depending on the various parameters of the inductor – the quality factor and the nominal inductance. These dependencies clearly illustrate the contribution of the coil to the final parameters of the LNA device. Thus, one of the fundamental tasks is to ensure the maximum Q-factor of the inductor cell. Another one is to ensure the required level of the quality factor throughout the entire operating frequency range [8]. These tasks are familiar to all developers of inductors and capacitors, regardless of their design (integral or lumped), but silicon processes introduce some specifics into the development of these elements.

Research and design of RF multilayer inductors

The equations calculating the inductance of flat planar inductors (1, 2 – example for octagonal inductance coil) were formulated by Greenhouse [9, 10] more than 40 years ago and are relevant to date:

$$L = \frac{\mu n^2 d_{avg} C_1}{2}\left(\ln\left(\frac{C_2}{\rho}\right) + C_3\rho + C_4\rho^2\right), \quad (1)$$

$$L = \frac{1.07\mu n^2 d_{avg}}{2}\left(\ln\left(\frac{2.29}{\rho}\right) + 0.19\rho^2\right), \quad (2)$$

where $C_1 ... C_4$ are layout dependent coefficients from Table 1 (based on face spiral number), n is the number of turns, μ is conductor permeability, d_{avg} is the average diameter determined as $d_{avg} = 0.5(d_{OUT} + d_{IN})$, ρ is special outer versus inner diameter ratio, which is determined as $\rho = (d_{OUT} - d_{IN})/(d_{OUT} + d_{IN})$.

The integrated resonant structures are used as RLC models (Fig. 2*a*), as well as their adaptations for high-frequency circuits, "π-models" (pi-models) [11] (Fig. 2*b*), which describe inductors using the coefficients of admittance matrices.

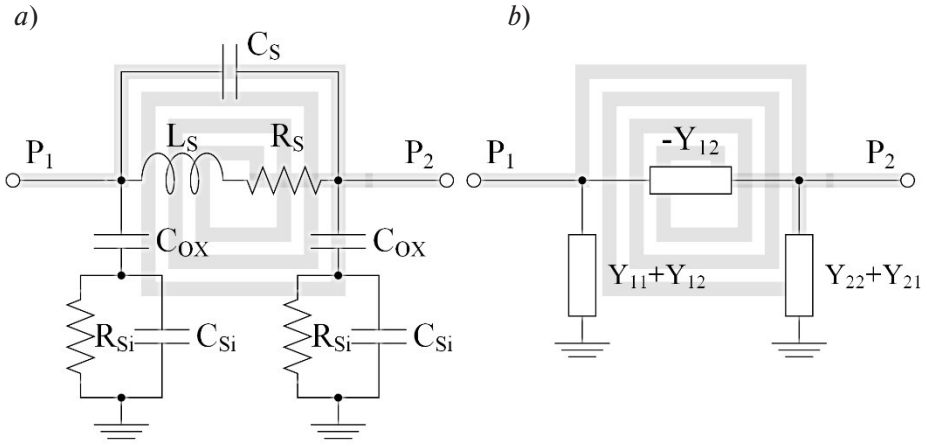

Fig. 2. IC inductor: *a* – lumped circuit; *b* – pi-model

Table 1

Spiral inductor layout coefficients

Layout	C_1	C_2	C_3	C_4
Square	1.27	2.07	0.18	0.13
Hexagonal	1.09	2.23	0.00	0.17
Octagonal	1.07	2.29	0.00	0.19
Circle	1.00	2.46	0.00	0.20

The equations for calculating the quality factor (Q) and inductance (L) are presented below (3, 4):

$$L = \frac{Im\left(\frac{1}{Y_{11}}\right)}{\omega} = \frac{Im\left(\frac{1}{Y_{11}}\right)}{2\pi f}, \tag{3}$$

$$Q = \frac{Im\left(\frac{1}{Y_{11}}\right)}{Re\left(\frac{1}{Y_{11}}\right)} = -\left(\frac{Im(Y_{11})}{Re(Y_{11})}\right), \tag{4}$$

where Y_{11} is the input admittance from Y-parameter matrix, ω is the angular frequency given by $\omega = 2\pi f$, $Re(X)$ and $Im(X)$ are the real and imaginary parts of the complex value X in the parentheses.

While developing integrated inductors and capacitors based on Si CMOS and SiGe BiCMOS technologies, the designer faces some fundamental problems. The first one is the thickness of the skin layer [12, 13], which determines the depth of alternating current flow in the conductor surface, depending on the thickness and material of the conductor. Silicon processes in general are characterized by a large number (6 or more) of metal layers with small thickness (usually less than 1 micron). Some factories provide special options (so-called RF options) that expand the number of metallization layers by adding one or more up-

per layers of "thick metals" with thicknesses of 1 μm or more. Without these additions, the developer may face difficulties when designing devices in the sub-GHz domain [14]. At frequencies of about 500 MHz (typical for the lower bands of the LTE standard), the thickness of the skin layer is about 3.5 microns which will directly affect the quality factor of the entire structure. Unable to achieve the required thickness in the upper stack of metallization layers, the developers use the replication of the inductor layers [15] in several metal layers located below. These layers are connected with arrays of transition holes (through-silicon vias – TSV arrays), like a solid metal layer conductor, thereby increasing the thickness to the desired values.

The second problem is the proximity of the self-resonant frequency (SRF) – the point in the frequency domain that marks the transition from the inductive to the capacitive region of the impedance (or capacitive to inductive in the case of a capacitor design). When approaching the frequency of self resonance, the inductance of the RF inductor begins to grow to a peak value, after which there is a sharp fall in the characteristic and a transition to the opposite impedance region. The higher the value of the inductor, the more difficult it is to achieve high self-resonance frequencies. In some cases, designers can increase the SRF frequency by using special patterns of slotted screens (patterned ground shield, PGS) [16] to "tune" the magnetic field of the inductor.

In this work, it is proposed to consider a model of a symmetrical inductor. Geometry and area are calculated in advance using variations of the parameters mentioned in the formulas above (1, 2). Table 2 presents a diagram of the topology and main parameters of the inductor.

To overcome the negative effects caused by the skin-depth at low frequencies, we used a repetition of several upper metal layers with TSV / via-arrays. Such a constructive solution should allow reaching the maximum Q-factor values for a given inductor structure within a common 90 nm CMOS process. The operating frequency range of the device, in which the inductor cell is supposed to be used, is determined by the frequency bands of the NB-IoT transmitter operating in the LTE frequency range.

The specified working bandwidth of the inductor lies within 0.5 ... 3.5 GHz, therefore the most significant parameters (L, Q) must correspond to the calculated values over the entire operating range.

Computer EM simulation using the extraction of electromagnetic parameters is an extremely costly operation, depending on the required time and the workstation calculating power. To optimize the development process, approximations of via-arrays (thousands of individual holes were replaced by solid polygons) and cell boundary conditions (protective ring elements were replaced by ideal conductors at plane boundaries) were used.

Table 2

The main planar parameters of the inductor

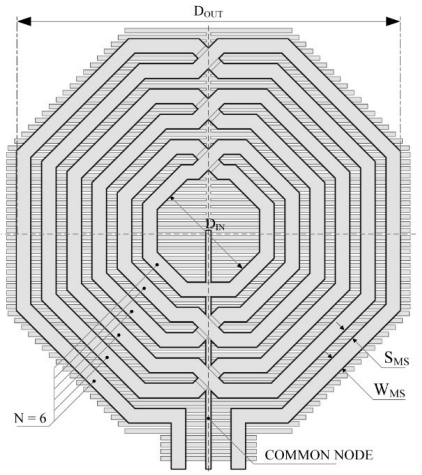

Parameter	Designation	Value
Number of turns	N	6
Microstrip width, um	W_{MS}	12
Microstrip spacing, μm	S_{MS}	10
Outer diameter, μm	D_{OUT}	334
Inner diameter, μm	D_{IN}	90
Calculated inductance value, nH	L	6.9 ... 7.2

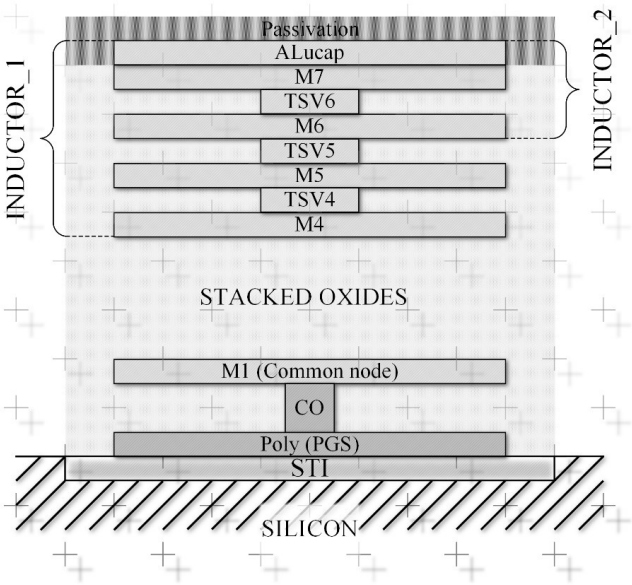

Fig. 3. Layer stack profile of the inductor based on CMOS 90 nm technology

As a computer research, it is proposed to simulate and compare the inductor with different metallization thicknesses due to the different compositions of the layers involved in the structure (Fig. 3). This approach gives a qualitative idea of the parameters of the inductor at metallization thicknesses of ≈4.63 microns for "Inductor_1" and ≈2.1 microns for "Inductor_2".

In addition, EM simulation was carried out on different silicon substrates based on different conductivities of Si-substrate: high-resistance (HR) and low-resistance (LR) silicon. The finite element method (FEM) was used as a mathematical solver mechanic.

The computer modeling results form S-parameters data extraction using Eqs. 3 and 4 presented in Fig. 4, 5 and 6 show the following matrices: the initial matrix of S-parameters obtained as a result of EM analysis and the matrix of Y-parameters derived from the initial S-parameters.

The triangular marker indicates the characteristics of the inductance coil with a large number of metal layers (Fig. 3, Inductor_1), and, accordingly, the round marker is attached to the thin structure (Inductor_2). Different types of lines indicate results for substrates with different conductivity values: continuous for low resistance (LR) and dashed for high resistance (HR) values. A marker with a square denotes the model parameters based on SPICE simulation for a structure with a large number of layers (Inductor_1). It should be noted that the analysis of small-sized structures using the FEM is time-consuming and extremely demanding on the workstation computing power, especially on the RAM.

Figure 4 shows the S- and Y-parameters on the Smith chart of complex characteristics. The S-parameters on the left give an idea of the consistency of all the structures presented. It is shown that upon approaching the mutual resonance frequencies and after them, the structures are mismatched. In the Y diagram (admittance parameters), we can observe that the structures have a clearly defined "inductive" behavior range and that they are ideally symmetrical (superimposed on each other and completely repeated) concerning the first and second ports, i.e. Y (1,1) = Y (2,2). Thus, given the symmetry, there is no need to further consider the characteristics of the conductivities Y (1,1) and Y (2,2) for both ports.

A graph (Fig. 5) shows the frequency dependence of the reactance to the angular frequency, with inductance from Eq. (3), for all the structures under consideration. All the presented variants of inductors have a similar inductance pattern up to 2 GHz, corresponding to ≈7 nH (determined by the geometry of the Table 2), after which, due to the proximity of the SRF, a sharp rise in the characteristic occurs, followed by a fall and transition to the capacitive reactance hemisphere.

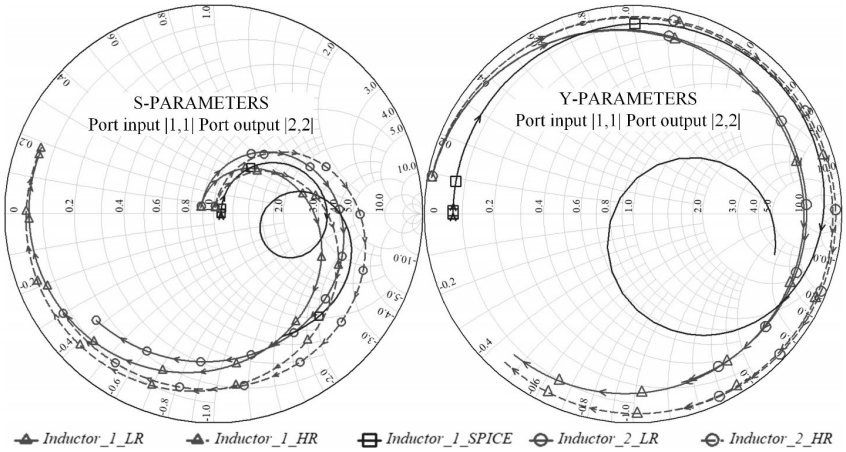

Fig. 4. Smith charts: S-parameters (left) and Y-parameters (right)

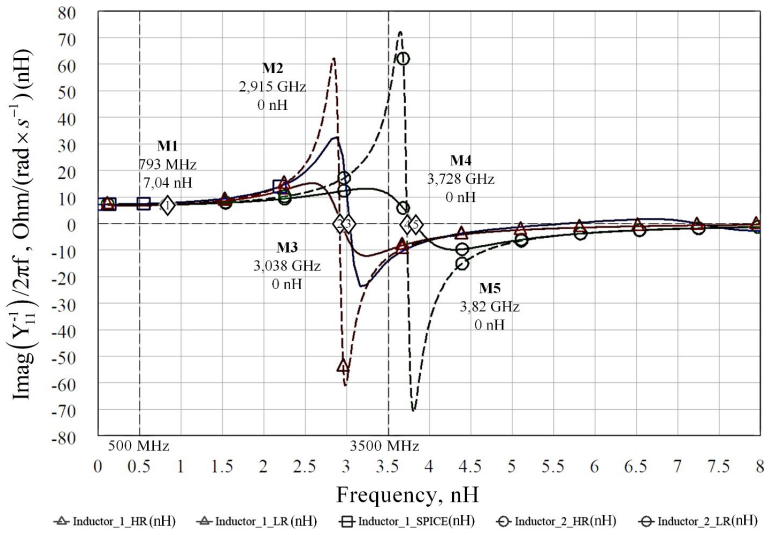

Fig. 5. Frequency dependence of the reactance to the angular frequency (inductance)

Figure 5 shows that the structure with a smaller number of metal layers has high SRF value, while "Inductor_1" has a cutoff of the operating band due to the presence of self-resonance frequencies at ≈2.915 GHz for model simulations with different substrates (HR and LR).

In addition, the frequency dependence of the "Inductor_1" structure with the number of upper metals equal to 7 correlates with the data obtained from the result of SPICE modeling in the range of self-resonance frequencies, which indicates the correctness of the model and development methodology of this device. The difference in peak amplitudes in this case is not so significant and is explained by the difference in the conductivity of the substrate.

Figure 6 illustrates Q-factor versus frequency with coil conductor thicknesses dependence from Eq. (4). According to the model, the Q-factor for a low-resistance substrate does not significantly differ when switching from a three-layer to a five-layer inductor topology, while the thin structure has a high Q-factor characteristic due to the delayed mutual resonance frequency (Fig. 5). The difference becomes much more significant when using a high-resistance (HR) substrate. The Q-factor obviously increases almost twice as much in both structures, while given the removal of the SRF, the thin structure "Inductor_2" has a flatter characteristic along with the operating frequency band (0.5 ... 3.5 GHz) with a higher amplitude of up to 18.03. The SPICE model values for the first inductor generally correlate with the absolute

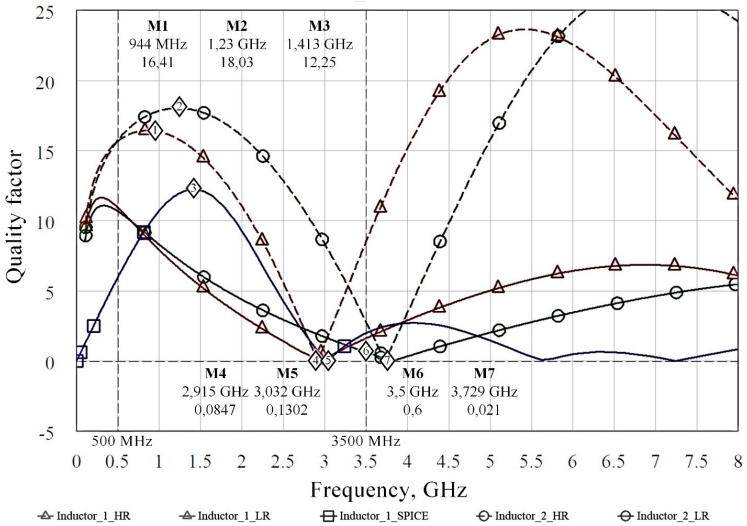

Fig. 6. Quality factor in the frequency domain

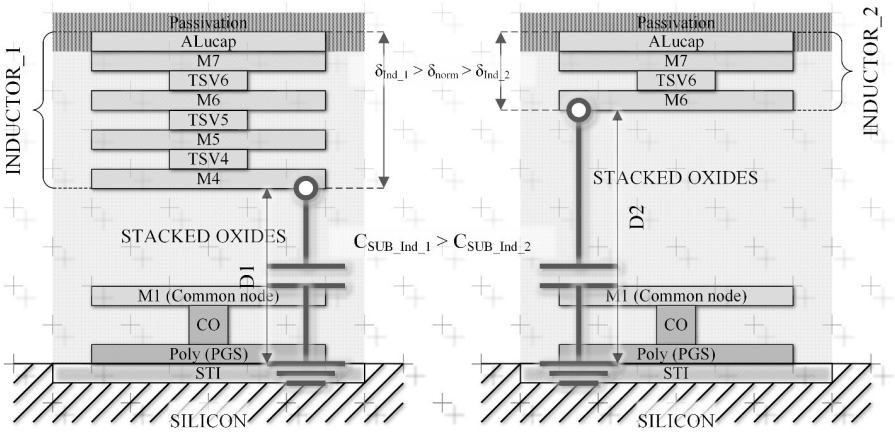

Fig. 7. Inductor models comparison

Q values obtained on the LR substrate but are shifted at the peak towards the low frequencies. In contrast to the results obtained from the EM model, the SPICE model has several self-resonance frequencies outside the operating range in the surveyed area, which explains the difference in Q after the first self-resonance frequency (3.038 GHz).

The results summary of the inductor models using EM FEM simulations is presented in Table 3.

Table 3

Inductor simulation results

Designation	Low resistance substrate (LR)				High resistance substrate (HR)			
	Inductor_1		Inductor_2		Inductor_1		Inductor_2	
Structure thickness (T), μm	4.63		2.1		4.63		2.1	
Frequency (F), GHz	0.5	3.5	0.5	3.5	0.5	3.5	0.5	3.5
Inductance (L), nH	6.81	–	7.01	11.6	6.87	–	7.01	46.57
Quality factor (Q)	10.96	–	10.69	0.63	15.68	–	15.75	2.79

Conclusion

Based on the simulation results, it can be concluded that "Inductor_2" exhibits better parameters in the frequency range with a smaller thickness, and this is despite the fact that at frequencies of about 500 MHz, large skin layer thickness (~3.5 μm) is required. This effect is caused by the fact that the capacitance of the inductor (Fig. 7) to the substrate increases sharply with the use of more metal layers, and, conversely, for a thin inductance coil, the capacitive coupling drops so much that it exceeds the negative effect caused by the thickness of the skin layer.

The use of a high resistance silicon substrate (HR) gives a significant increase in figure of merit in relation to structures based on low resistance (LR) silicon substrates. In this case, the frequencies of the self-resonance point and the point of minimum values of the figure of merit do not strongly depend on the conductivity of the substrate.

Thus, the replication of the inductor layers to the maximum metallization thicknesses in silicon processes can lead to a deterioration in the frequency properties of the device when operating in the LTE bands. A complete picture of coil behavior requires finite element EM modeling.

REFERENCES

1. **P. Suresh P., Daniel J.V., Parthasarathy V., Aswathy R.H.** A state of the art review on the Internet of Things (IoT) history, technology and fields of deployment. *2014 International Conference on Science Engineering and Management Research (ICSEMR)*. Chennai, India, 2014, Pp. 1–8. DOI: 10.1109/ICSEMR.2014.7043637

2. **Chevalier P., Gianesello F., Pallotta A., Goncalves J., Bertrand G., Borrel J., Boissonnet L., Brezza E., Buczko M., Canderle E., et al.** PD-SOI CMOS and SiGe BiCMOS Technologies for 5G and 6G communications. *2020 IEEE International Conference on Electron Devices Meeting (IEDM)*. DOI: 10.1109/IEDM13553.2020.9371954

3. **Krasnikov G.Ya.** *Constructive and technological features of submicron MOSFETs*. Moscow: Technosphere Publ., 2011. 800 p. (rus)

4. **Timoshenkov V.P., Khlybov A.I., Rodionov D.V.** 3-5 GHz two-channel low-noise amplifier for ultra-wideband microwave systems. *Proceedings of the International Scientific and Technical Conference on Electronics*, Moscow, 2015, Pp. 49–50. (rus)

5. **Shashank Tiwari, Venkata Narayana Rao Vanukuru, Jayanta Mukherjee.** Noise figure analysis of 2.5 GHz folded cascode LNA using high-Q layout optimized. *2015 IEEE Asia Pacific Conference on Postgraduate Research in Microelectronics and Electronics (PrimeAsia)*. DOI: 10.1109/PrimeAsia.2015.7450477

6. **Chou H.-T., Chen S.-W., Chiou H.-K.** A low-power wideband dual-feedback LNA exploiting the gate-inductive bandwidth/gain-enhancement technique. *2013 IEEE MTT-S International Microwave Symposium Digest (MTT)*. DOI: 10.1109/mwsym.2013.6697349

7. **Babak L.I., Cherkashin M.V., Sheerman F.I., Dobush I.M., Kokolov A.A., Salnikov A.S., Kalentyev A.A., Garais D.V., Goryainov A.E., Zhabin D.A.** Development of GaAs and SiGe MICROWAVE monolithic integrated circuits, libraries of elements and CAD modules at the Tomsk University of Control Systems and Radioelectronics. *Electronic Engineering. Series Microelectronics, Scientific and Technical Journal*, 2015, Iss. 4 (160), Pp. 4–17. (rus)

8. **Olebogeng Bone Kobe, Joseph Chuma, Rodrigo Jamisola, Matthews Chose.** A review on quality factor enhanced on-chip microwave planar resonators. *Engineering Science and Technology, an International Journal*, 2017, Vol. 20, Iss. 2, Pp. 460–466, https://doi.org/10.1016/j.jestch.2016.09.024

9. **Greenhouse H.** Design of planar rectangular microelectronic inductors. *IEEE Transactions on Parts, Hybrids, and Packaging*, 1974, Vol. 10, No. 2, Pp. 101–109. DOI: 10.1109/TPHP.1974.1134841

10. **Mohan S.S., del Mar Hershenson M., Boyd S.P., Lee T.H.** Simple accurate expressions for planar spiral inductances. *IEEE Journal of Solid-State Circuits*, 1999, Vol. 34(10), Pp. 1419–1424. DOI: 10.1109/4.792620

11. **Johansson T., Samji S.** On the design of a CMOS-integrated load modulated balanced amplifier. *2020 IEEE Nordic Circuits and Systems Conference (NorCAS)*, Oslo, Norway. DOI: 10.1109/NorCAS51424.2020.9264997

12. **Burghartz J.N., Rejaei B.** On the design of RF spiral inductors on silicon. *IEEE Transactions on Electron Devices*, 2003, Vol. 50, No. 3, Pp. 718–729. DOI: 10.1109/TED.2003.810474

13. **Bhaskar A., et al.** Substrate engineering of inductors on SOI for improvement of Q-factor and application in LNA. *IEEE Journal of the Electron Devices Society*, 2020, Vol. 8, Pp. 959–969. DOI: 10.1109/JEDS.2020.3019884

14. **Balachandran Prameela, Daniel Asha.** A novel high Q active inductor design for wireless applications. *Procedia Computer Science*, 2020, 171. DOI: 10.1016/j.procs.2020.04.28

15. **Unigarro Calpa E.U., Florian A.A., Bohorquez Reyes J.C., Ramirez F., Riquelme J.S., Segura-Quijano F.E.** On-chip inductor in 0.18-μm CMOS for low-cost fully integrated contactless powered sensors. *IEEE Microwave and Wireless Components Letters*, 2020, Vol. 30, No. 10, Pp. 989–992. DOI: 10.1109/LMWC.2020.3016573

16. **Ko Jae-Hyeong, Kim Koon-Tae, Byun Jin-Kyu, Kim Hyeong-Seok.** Parameter extraction and optimal design of spiral inductor using evolution strategy and sensitivity. *Magnetics*, IEEE Transactions. on. 46, Pp. 2831–2834. DOI: 10.1109/TMAG.2010.2045114

Received 03.03.2021.

СПИСОК ЛИТЕРАТУРЫ

1. **P. Suresh P., Daniel J.V., Parthasarathy V., Aswathy R.H.** A state of the art review on the Internet of Things (IoT) history, technology and fields of deployment // 2014 Internat. Conf. on Science Engineering and Management Research. Chennai, India, 2014. Pp. 1–8. DOI: 10.1109/ICSEMR.2014.7043637

2. **Chevalier P., Gianesello F., Pallotta A., Goncalves J., Bertrand G., Borrel J., Boissonnet L., Brezza E., Buczko M., Canderle E., et al.** PD-SOI CMOS and SiGe BiCMOS Technologies for 5G and 6G communications // 2020 IEEE Internat. Conf. on Electron Devices Meeting (IEDM). DOI: 10.1109/IEDM13553.2020.9371954

3. **Красников Г.Я.** Конструктивно-технологические особенности субмикронных МОП-транзисторов. Изд. 2-е, испр. М.: Техносфера, 2011. 800 с.

4. **Тимошенков В.П., Хлыбов А.И., Родионов Д.В.** 3-5 ГГц двухканальный малошумящий усилитель для сверхширокополосных СВЧ-систем // Труды Междунар. науч.-техн. конф. Электроника-2015. М., 2015. С. 49–50.

5. **Shashank Tiwari, Venkata Narayana Rao Vanukuru, Jayanta Mukherjee.** Noise figure analysis of 2.5 GHz folded cascode LNA using high-Q layout optimized // 2015 IEEE Asia Pacific Conf. on Postgraduate Research in Microelectronics and Electronics (PrimeAsia). DOI: 10.1109/PrimeAsia.2015.7450477

6. **Chou H.-T., Chen S.-W., Chiou H.-K.** A low-power wideband dual-feedback LNA exploiting the gate-inductive bandwidth/gain-enhancement technique // 2013 IEEE MTT-S International Microwave Symposium Digest (MTT). DOI: 10.1109/mwsym.2013.6697349

7. **Бабак Л.И., Черкашин М.В., Шеерман Ф.И., Добуш И.М., Коколов А.А., Сальников А.С., Калентьев А.А., Гарайс Д.А., Горяинов А.Е., Жабин Д.А.** Разработка GaAS и SiGe СВЧ монолитных интегральных схем, библиотек элементов и модулей САПР в Томском университете систем управления и радиоэлектроники // Электронная техника. Сер. 3. Микроэлектроника. 2015. Вып. 4 (160). С. 4–17.

8. **Olebogeng Bone Kobe, Joseph Chuma, Rodrigo Jamisola, Matthews Chose.** A review on quality factor enhanced on-chip microwave planar resonators // Engineering Science and Technology, an International Journal. 2017. Vol. 20. Iss. 2. Pp. 460–466. URL: https://doi.org/10.1016/j.jestch.2016.09.024

9. Greenhouse H. Design of planar rectangular microelectronic inductors // IEEE Transactions on Parts, Hybrids, and Packaging. 1974. Vol. 10. No. 2. Pp. 101–109. DOI: 10.1109/TPHP.1974.1134841

10. **Mohan S.S., del Mar Hershenson M., Boyd S.P., Lee T.H.** Simple accurate expressions for planar spiral inductances // IEEE Journal of Solid-State Circuits. 1999. Vol. 34(10). Pp. 1419–1424. DOI: 10.1109/4.792620

11. **Johansson T., Samji S.** On the design of a CMOS-integrated load modulated balanced amplifier // 2020 IEEE Nordic Circuits and Systems Conf. (NorCAS), Oslo, Norway. DOI: 10.1109/NorCAS51424.2020.9264997

12. **Burghartz J.N., Rejaei B.** On the design of RF spiral inductors on silicon // IEEE Transactions on Electron Devices. 2003. Vol. 50. No. 3. Pp. 718–729. DOI: 10.1109/TED.2003.810474

13. **Bhaskar A., et al.** Substrate engineering of inductors on SOI for improvement of Q-factor and application in LNA // IEEE Journal of the Electron Devices Society. 2020. Vol. 8. Pp. 959–969. DOI: 10.1109/JEDS.2020.3019884

14. **Balachandran Prameela, Daniel Asha.** A novel high Q active inductor design for wireless applications // Procedia Computer Science. 2020. 171. DOI: 10.1016/j.procs.2020.04.28

15. **Unigarro Calpa E.U., Florian A.A., Bohorquez Reyes J.C., Ramirez F., Riquelme J.S., Segura-Quijano F.E.** On-chip inductor in 0.18-μm CMOS for low-cost fully integrated contactless powered sensors // IEEE Microwave and Wireless Components Letters. 2020. Vol. 30. No. 10. Pp. 989–992. DOI: 10.1109/LMWC.2020.3016573

16. **Ko Jae-Hyeong, Kim Koon-Tae, Byun Jin-Kyu, Kim Hyeong-Seok.** Parameter extraction and optimal design of spiral inductor using evolution strategy and sensitivity // Magnetics, IEEE Transactions. on. 46. Pp. 2831–2834. DOI: 10.1109/TMAG.2010.2045114

Статья поступила в редакцию 03.03.2021.

THE AUTHORS / СВЕДЕНИЯ ОБ АВТОРАХ

Kotlyarov Evgeniy Yu.
Котляров Евгений Юрьевич
E-mail: ekotlyarov86@gmail.com

Mikhailov Viktor Yu.
Михайлов Виктор Юрьевич
E-mail: vmikhaylov@niime.ru

Zubov Igor A.
Зубов Игорь Александрович
E-mail: izubov@niime.ru

Nuikin Andrey V.
Нуйкин Андрей Валерьевич
E-mail: anuykin@niime.ru

Iljin Alexander F.
Ильин Александр Федорович
E-mail: alexiljin0@gmail.com

Putrya Mikhail G.
Путря Михаил Георгиевич
E-mail: mishapmg@gmail.com

DOI: 10.18721/JCSTCS.14103
УДК 621.396

DISADVANTAGES OF THE INSTRUMENTAL ERROR DETERMINING METHOD OF AIRFIELD QUASI-DOPPLER AUTOMATIC DIRECTION FINDERS

G.K. Aslanov[1], R.B. Kazibekov[2], R.R. Musaibov[1]

[1] Dagestan State Technical University, Makhachkala, Russian Federation;

[2] Derbent Scientific Research Institute "Volna", Derbent, Russian Federation

An increase in the aircraft flights intensity leads to the need to improve the efficiency of the airfield radio equipment functioning. One of the ways to improve the accuracy of navigation equipment is to reduce the instrumental error. The article analyzes the methods of checking the instrumental error of the ADF. Is shown that the so-called "electric rotation" of the antenna system (AS) head used in the radio direction finders ADF-80K, ADF-80, ADF-85, "Platan", DF-2000 for checking the instrumental error leads to incorrect results. The authors employed the linearity property of the Fourier transform in the simulation to prove the incorrectness of the method for determining the ADF instrumental error with the "electric rotation" of the AS head. The simulation results showed that in the ADF operating in the quasi-Doppler mode, the failure of the vibrators located along the bearing line to the radio source does not lead to the appearance of bearing error, while the failure of the vibrators located orthogonally to the bearing line can result in a bearing error reaching 3.750. The simulation results confirmed that unlike the ADF that use the AS head "electric rotation", the ADF with mechanical rotation show reliable results of the instrumental error measurement. The paper proposes a new method for checking the instrumental bearing errors using the values of the AS phase non-identities which ensures the reliability of the measurement results.

Keywords: instrumental error, aerodrome automatic direction finders, phase non-identity, antenna system, electric rotation.

Citation: Aslanov G.K., Kazibekov R.B., Musaibov R.R. Disadvantages of the instrumental error determining method of airfield quasi-Doppler automatic direction finders. Computing, Telecommunications and Control, 2021, Vol. 14, No. 1, Pp. 33–42. DOI: 10.18721/JCSTCS.14103

НЕДОСТАТКИ МЕТОДИКИ ОПРЕДЕЛЕНИЯ ИНСТРУМЕНТАЛЬНОЙ ПОГРЕШНОСТИ АЭРОДРОМНЫХ КВАЗИДОПЛЕРОВСКИХ АВТОМАТИЧЕСКИХ РАДИОПЕЛЕНГАТОРОВ

Г.К. Асланов[1], Р.Б. Казибеков[2], Р.Р. Мусаибов[1]

[1] Дагестанский государственный технический университет, г. Махачкала, Российская Федерация;

[2] Дербентский НИИ «Волна», г. Дербент, Российская Федерация

Увеличение интенсивности полетов воздушных судов приводит к необходимости повышения эффективности функционирования аэродромного радиотехнического оборудования. Одним из путей повышения точности навигационного оборудования является

уменьшение инструментальной погрешности. В статье проведен анализ методик проверки инструментальной погрешности АРП. Показано, что используемое в радиопеленгаторах АРП-80К, АРП-80, АРП-85, «Платан», DF-2000 для проверки инструментальной погрешности, так называемое «электрическое вращение» головки антенной системы (АС), приводит к получению не соответствующих действительности результатов. При моделировании, для доказательства некорректности методики определения инструментальной погрешности АРП, с «электрическим вращением» головки антенной системы использовано свойство линейности преобразования Фурье. Результаты моделирования показали, что в АРП, работающем в квазидоплеровском режиме, выход из строя вибраторов, расположенных вдоль линии пеленга на источник радиоизлучения, не приводит к появлению ошибки пеленгования, а выход из строя вибраторов, расположенных ортогонально к линии пеленга, приводит к появлению ошибки пеленгования, которая может достигать 3,750. Результаты моделирования подтвердили, что в отличие от АРП, использующих «электрическое вращение» головки АС, в АРП, использующих механическое вращение, результаты замеров инструментальной погрешности являются достоверными. Предложена новая методика проверки инструментальной погрешности пеленгования с использованием значений фазовых неидентичностей АС, обеспечивающая достоверность результатов измерений.

Ключевые слова: инструментальная погрешность, аэродромные автоматические радиопеленгаторы, фазовая неидентичность, антенная система, электрическое вращение.

Ссылка при цитировании: Aslanov G.K., Kazibekov R.B., Musaibov R.R. Disadvantages of the instrumental error determining method of airfield quasi-Doppler automatic direction finders // Computing, Telecommunications and Control. 2021. Vol. 14. No. 1. Pp. 33–42. DOI: 10.18721/JCSTCS.14103

Introduction

Qualitative and quantitative changes in aviation equipment lead to an increase in the intensity of flights, as a result of which there is a need to improve the efficiency of the functioning of airfield radio equipment.

One of the means of radio engineering support for flights are automatic and radio direction finders systems (ADF and RDF).

The use of radio direction finders for air traffic control raised requirements to their bearing accuracy of the ADF, which are due to economic and safety considerations [13]. This explains the appearance in recent years of a large number of publications on improving the accuracy of direction finding of RDFs [3–9, 11, 12, 14–17].

As you know, in order to prevent dangerous approaches, there should be a protective space around each aircraft (AC), within which the presence of another AC is not allowed.

A calculation confirmed that an alignment of such routes as Moscow-St. Petersburg and Moscow-Khabarovsk leads to a saving of flight time by 3-7 minutes per hour of flight, which corresponds to an annual saving of 100 to 200 hours per aircraft [1, 2, 13].

One of the ways to improve the accuracy of navigation equipment is to reduce the instrumental error.

Analysis of methods for measuring the instrumental error in airfield ADF

In the radio direction finders operated in the Air Force (ADF-11, ADF-11M2, ADF-AS), the measurement of the instrumental error of the ADF is performed using a control and test generator by rotating the head of the antenna system (AS).

However, this method is inconvenient and the testing requires a lot of effort. In this regard, such RDF as ADF-80K, ADF-80, ADF-85, “Platan”, DF-2000, operated in civil aviation, use the “electric rotation” of the AS head: instead of rotating the AS head the reference signal is discretely shifted as to display the relative bearing to the radio source.

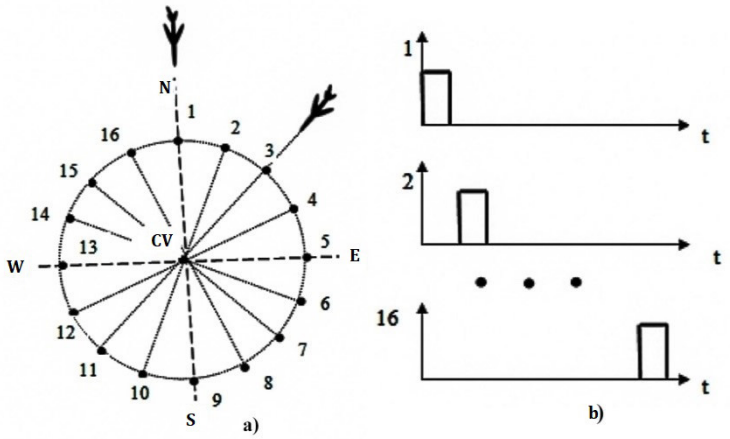

Fig. 1. Explanation of the principle of determining the instrumental error of the ADF by rotating the AS head

However, in practice, there is no "electric rotation" of the antenna head, and the measurements obtained in this way are unreliable.

To explain this, let us consider the principle of the ADF [13].

Figure 1a shows an ADF AS consisting of a central vibrator (CV) and sixteen ring vibrators (RV) arranged in a circle. AS RVs are driven by switching pulses (Fig. 1b).

The first vibrator is directed to the north and is activated by the first switching pulse. The reference signal, relative to which the bearing to the radio source is determined, is shifted 90^0 forward (to the left) relative to the first one.

In civil aviation, sixteen-vibrator wide-base antennas with a diameter of 3.2 m are used.

Figure 2 shows a sample of the phase differences between the RV and CV of the AS when the aircraft is flying towards vibrator 1, which are determined in accordance with the expression [2]:

$$\phi_i = \frac{2\pi R}{\lambda}\cos\beta\cos\left(\theta - \frac{2\pi(i-1)}{N}\right), \quad I = 1, ..., N, \tag{1}$$

where R – the AS radius; N – number of elements of the AS; λ – wavelength of the direction-finding signal; β – aircraft elevation angle; θ – bearing from the aircraft.

Figure 3 shows a sample of the phase differences between the RV and CV of the AC while taking the bearings of an on-board radio station operating at a frequency of 125 MHz, with bearing of 45^0 and elevation angle of 0^0 (the aircraft flies towards vibrator 3).

With the "electric rotation" of the AS, instead of the mechanical rotation of the antenna head, a discrete offset of the reference signal is made relative to the sample of the phase differences of the CV and RV of the AS.

However, the results obtained in this way are unreliable, since the instrumental error is checked only for one of the points, and for the remaining points, the error of forming the phase shift of the reference voltage is added to this error. This is explained in Fig. 4.

In Fig. 4a, the step curve corresponds to a sample of the phase differences of the antenna array signals, with the bearing and the angle of location equal to 0^0.

The sinusoid 1 corresponds to the first harmonic of the envelope sample of the phase differences of the vibrators of the antenna array.

Let the first vibrator be faulty in AS (i.e. the phase difference between the first and the central vibrator is zero).

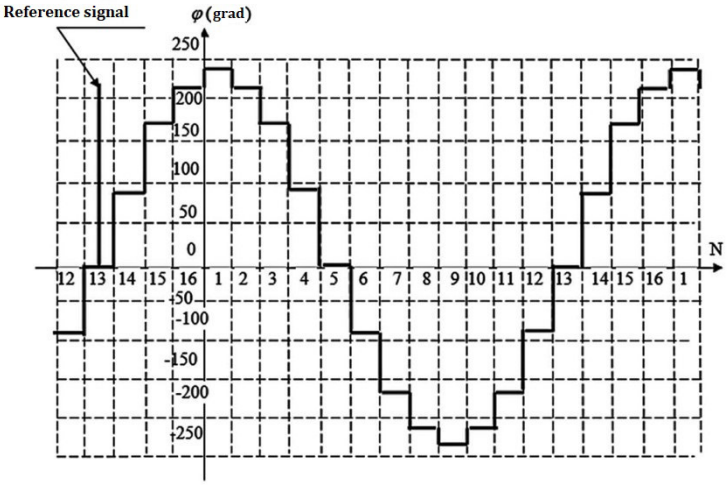

Fig. 2. Sample of phase differences between RV and CV of the AS while taking the bearings of an on-board radio station operating at a frequency of 125 MHz, with bearing of 0^0 and elevation angle of 0^0

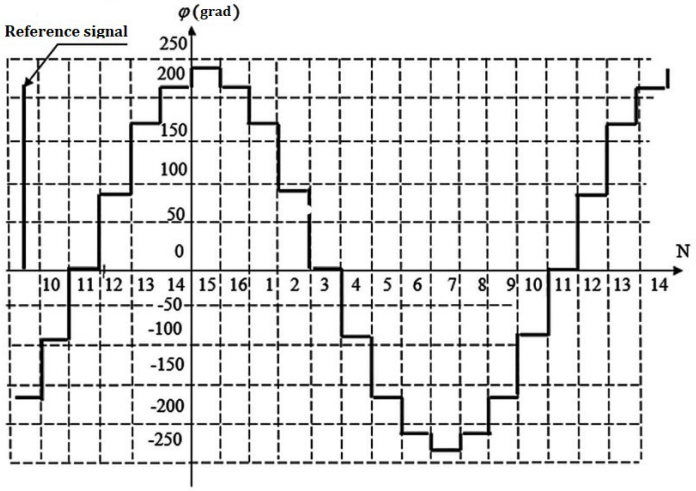

Fig. 3. Sample of the phase differences between the RV and CV of the AC while taking the bearings of an on-board radio station operating at a frequency of 125 MHz, with bearing of 45^0 and elevation angle of 0^0

This can be simulated as the appearance of a phase difference between the central and first ring vibrators of interference, opposite in phase to the signal from the onboard radio station.

Pulse 2 corresponds to the phase difference between the central and first ring vibrators in the presence of only interference.

Sinusoid 3 corresponds to the first harmonic of the phase difference of the interference component between the first and central vibrators.

As you can see from the Figure, sinusoids 1 and 2 are shifted relative to each other by 180^0. In this regard, the sum of sinusoids 1 and 2 give sinusoid 4 coinciding with sinusoid 1 in phase, but with a lower amplitude. Thus, the failure of the vibrator located on the line passing through the aircraft and the central vibrator of the antenna system does not lead to a bearing error.

This is explained by the vector diagram shown in Fig. 4c. Here, vectors 1, 3, 4 correspond to the amplitudes of sinusoids 1, 3, 4 of Fig. 4a. Vector 4 is superimposed on vector 1, so, for ease of perception, vector 4 is slightly shifted to the right.

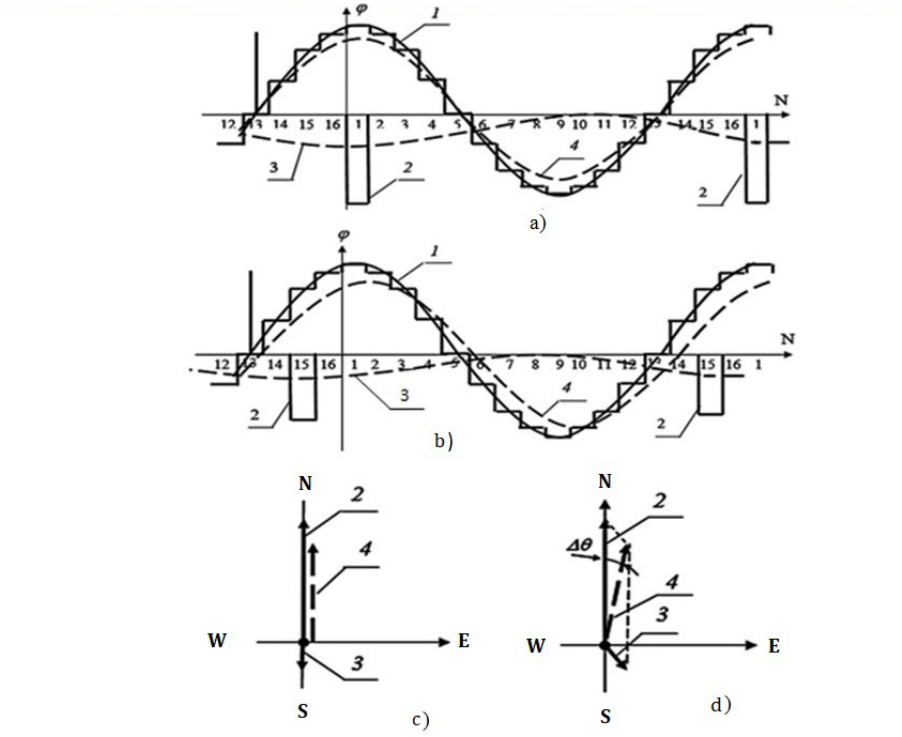

Fig. 4. Time and vector diagrams of the ADF AS operation

Figure 4b shows the case when the fifteenth vibrator of the antenna system is faulty. Here, as in Fig. 4a, sinusoid 1 corresponds to the first harmonic of the envelope of the sample of the phase differences of the antenna array vibrators.

Pulse 2 corresponds to the phase difference between the central and the fifteenth ring vibrators, if there is only interference.

Sinusoid 3 corresponds to the first harmonic of the pulse 2.

As you can see from the Figure, sinusoids 1 and 3 are shifted relative to each other by 135^0. In this regard, the sum of sinusoids 1 and 2 give sinusoid 4, which does not coincide with sinusoid 1 in phase, i.e. there is a bearing error equal to $\Delta\theta$.

This is explained by a vector diagram shown in Fig. 4d.

When the head of the antenna system is mechanically rotated, for example, when it is rotated by 315^0, vibrator 1 takes the position that vibrator 15 occupied before the rotation, which leads to a bearing error. Thus, when the antenna head is rotated mechanically, there is a complete simulation of the control and test generator (aircraft) moving around the antenna.

With the electric rotation of the antenna head, due to the fact that instead of moving the control and test generator or rotating the antenna head, the reference signal is discretely moved, relative to which the bearing is measured, the bearing error caused by the failure of the first vibrator will always be zero.

Calculation of the instrumental error caused by the failure of the AS vibrators

Let us determine the bearing error caused by the failure of the antenna system vibrator, depending on its position relative to the radio source. To do this, we use the linearity of the Fourier transform, according to which the first harmonic of the sample of the phase envelope of the antenna system is equal to the sum of the first harmonics of its components [10].

Let us assume the switching pulse duration of the antenna system vibrators equals τ (for modern domestic ADF, $\tau = 0.00144$ s), and the scanning period of the AS is T (for domestic ADF, $T = 0.023$ s).

Then, the first harmonic of the Fourier series expansion of the first phase sampling pulse will be equal to:

$$S_{11} = \frac{2\phi_1}{\pi} sin\left(\frac{\pi\tau}{T}\right) cos\omega t. \tag{2}$$

The first harmonic of the i^{th} pulse is determined by the formula,

$$S_{1i} = \frac{2\phi_i}{\pi} sin\left(\frac{\pi\tau}{T}\right) cos\left(\frac{(i-1)\pi}{8}\right) cos\omega t + \frac{2\phi_i}{\pi} sin\left(\frac{\pi\tau}{T}\right) sin\left(\frac{(i-1)\pi}{8}\right) sin\omega t. \tag{3}$$

The coefficients of the Fourier series for the ith pulse are determined by the expressions:

$$a_{i1} = \frac{2\phi_i}{\pi} sin\left(\frac{\pi\tau}{T}\right) cos\left(\frac{(i-1)\pi}{8}\right), \tag{4}$$

$$в_{i1} = \frac{2\phi_i}{\pi} sin\left(\frac{\pi\tau}{T}\right) sin\left(\frac{(i-1)\pi}{8}\right). \tag{5}$$

The sum of the first harmonics that make up the samples of the phase differences of the signals will be determined by the expression:

$$S_{\Sigma} = \sum_{i=1}^{N}\left(\frac{2\phi_i}{\pi} sin\left(\frac{\pi\tau}{T}\right) cos\left(\frac{(i-1)\pi}{8}\right) cos\omega t + \frac{2\phi_i}{\pi} sin\left(\frac{\pi\tau}{T}\right) sin\left(\frac{(i-1)\pi}{8}\right) sin\omega t\right). \tag{6}$$

In order to determine the dependence of the bearing error on the relative position of the faulty vibrator and the bearing on the radio source, a computer experiment was conducted.

The simulation results showed that in quasi-Doppler ADF operating in the meter wave range, a line drawn through the faulty and central vibrators of the antenna system coinciding with the bearing to the radio source does not lead to a bearing error. The failure of the vibrator, located perpendicular to the bearing, leads to an error reaching 3.75^0.

When the ADF operates in the differential-phase mode, a malfunction of the vibrator located orthogonally to the bearing does not lead to a bearing error, but a location along the bearing leads to a maximum error.

It should be noted that the incorrect operation of the ADF due to the failure of the AS vibrator can be detected when checking the phase non-identity of the ADF AS.

Suggestions for ensuring the accuracy of ADF instrumental error measurements

One of the suggestions to ensure the accuracy of the ADF instrumental error measurements is to return to the mechanical rotation of the antenna system head, which, as noted above, is a time-consuming operation.

The instrumental error of the ADF mainly depends on the phase non-identity of the vibrators of the AS.

To determine the phase non-identity of the vibrators, an antenna monitoring generator is connected to the central vibrator of the AS, and the phase differences of the signals between the RV and CV are determined, from which the calculated values of the phase differences are subtracted.

In the ADF that have been put into operation in civil aviation in the last 20 years, the direction-finding information is processed in a channel micro-computer, which allows software to eliminate the drawback in determining the instrumental error.

For example, for a frequency of 125 MHz, for a bearing and a position angle equal to 0^0, phase samples between CV and RV are calculated (Fig. 2). The values of the phase non-identities of the vibrators of the antenna system are added to the phase samples. Based on the obtained values, the bearing is determined taking into account the instrumental error.

The ideal phase samples are calculated for another azimuth, for example, 45^0. The phase non-identity values of the corresponding vibrators are added to the new values of the phase samples. Based on the obtained sample, the bearing is calculated taking into account the instrumental error.

The differences between the specified bearing values and the calculated path found will be the instrumental errors of the ADF for the corresponding azimuths.

Results analysis

In radio direction finders operated in the Air Force (ADF-11, ADF-11M2, ADF-AS), the measurement of the instrumental error of the ADF is performed using a control and test generator by rotating the head of the antenna system. Due to the fact that this method is inconvenient and labor intensive, such RDFs as ADF-80K, ADF-80, ADF-85, "Platan", DF-2000, intended for operation in civil aviation, use the so-called "electric rotation" of the antenna system head, according to which, instead of rotating the AS head the reference signal is discretely shifted as to display the relative bearing to the radio source. The paper shows that this method gives unreliable measurement results. With this method, the instrumental bearing error is determined by one of the points and the error of forming the reference signal is added to it.

By modeling, it is shown that the failure of any AS vibrator leads to the appearance of an instrumental error, which can reach 3.75^0.

A method for eliminating the disadvantage of determining the instrumental error by a software method using the results of measuring the phase non-identity of the vibrators of the antenna system of the radio direction finder is proposed.

Conclusion

The paper shows that the method of determining the instrumental error based on the so-called "electric rotation" of the antenna system used in the radio direction finders ADF-80K, ADF-80, ADF-85, "Platan", DF-2000 does not give reliable results.

A method is proposed to eliminate the disadvantage by a software method using the results of measuring the phase non-identity of the antenna system of the radio direction finder.

REFERENCES

1. **Aslanov G.K., Gasanov O.I.** Analiz prichin vozniknoveniya anomalnykh oshibok v kvazidoplerovskikh avtomaticheskikh radiopelengatorakh [Analysis of the anomalous errors causes in quasi-Doppler automatic radio direction finders]. *Nauchno-tekhnicheskiye vedomosti SPbGPU. Informatika, telekommunikatsii, upravleniye*. 2009, No. 2 (76), Pp. 87–93. (rus)

2. **Aslanov G.K., Mamedov L.K., Magomedov K.M.** Matematicheskiye modeli protsessa vychisleniya pelenga v aerodromnykh kvazidoplerovskikh avtomaticheskikh radiopelengatorakh. [Mathematical models of the bearing calculation process in aerodrome quasi-Doppler automatic direction finders]. *Nauchno-tekhnicheskiye vedomosti SPbGPU. Informatika, telekommunikatsii, upravleniye*, 2008, No. 2 (54), Pp. 267–272. (rus).

3. **Botnev V.A., Ustinov S.M.** Distance finding method between a point and a segment in navigation. *St. Petersburg State Polytechnical University Journal. Computer Science. Telecommunications and Control Systems*, 2019, Vol. 12, No. 2, Pp. 68–79. (rus). DOI: 10.18721/JCSTCS.12206

4. **Vasin A.A., Ponomarev L.I., Cheremisin O.P.** Vysokotochnoye pelengovaniye proizvolno korrelirovannykh mnogoluchevykh signalov s ispolzovaniyem tsifrovykh antennykh reshetok [High-precision direction finding of arbitrarily correlated multipath signals using digital antenna arrays]. *Radiotekhnika i elektronika*, 2015, No. 12 (60), Pp. 1237–1247. (rus)

5. **Dubrovin A.V.** Otsenka srednekvadraticheskoy oshibki izmereniya pelenga putem vychisleniya nevyazok faz [Estimation of bearing measurement root-mean-square error by phase residuals calculating]. *Radiotekhnika i elektronika*, 2019, No. 8 (64), Pp. 796–799. (rus)

6. **Ivanov A.V., Surkov V.O., Komarov D.V.** Kvazioptimalnyye algoritmy obnaruzheniya, identifikatsii i adaptivnogo otsenivaniya dlya obrabotki informatsii v navigatsionnykh sistemakh nazemnykh podvizhnykh obyektov na osnove sputnikovykh radionavigatsionnykh sistem [Quasi-optimal algorithms for detection, identification and adaptive evaluation for information processing in ground-based mobile objects navigation systems based on satellite radio navigation systems]. *Radiotekhnika i elektronika*, 2020, No. 6 (65), Pp. 568–577. (rus)

7. **Ivanov N.M.** Adaptivnyye metody obnaruzheniya i pelengovaniya signalov [Adaptive methods for the signals detection and direction finding]. *Radiotekhnika i elektronika*, 2016, No. 10 (61), Pp. 979–983. (rus)

8. **Kovalev F.N.** Opredeleniye koordinat tseli po doplerovskoy chastote i uglovoy skorosti v prosvetnoy radiolokatsionnoy sisteme. [Determination of target coordinates by Doppler frequency and angular velocity in the lumen radar system]. *Radiotekhnika i elektronika*, 2015, No. 12 (60), Pp. 1248–1250. (rus)

9. **Kurochkin L.M., Kurochkin M.A., Popov S.G., Popov M.V.** Results of experimental studies of positioning accuracy using various satellite navigation systems. *St. Petersburg State Polytechnical University Journal. Computer Science. Telecommunications and Control Systems*, 2017, Vol. 10, No. 4, Pp. 79–88. (rus). DOI: 10.18721/JCSTCS.10407

10. **Maks Zh.** *Metody i tekhnika obrabotki signalov pri fizicheskikh izmereniyakh* [*Methods and techniques of signal processing in physical measurements*]. In 2 Vol. Moscow: Mir Publ., 1983. 312+256 p. (rus)

11. **Melikhova A.P., Tsikin I.A.** Angle of Arrival Method for Global Navigation Satellite Systems Integrity Monitoring. *St. Petersburg State Polytechnical University Journal. Computer Science. Telecommunications and Control Systems*, 2015, No. 1(212), Pp. 37–48. (rus). DOI: 10.5862/JCSTCS.212.4

12. **Muzychenko N.Yu.** Metod sovmestnogo priyema i monoimpulsnogo pelengovaniya signalov radioizluchayushchikh dinamicheskikh obyektov [Method of joint reception and monopulse direction finding of radio-emitting dynamic objects signals]. *Radiotekhnika i elektronika*, 2020, No. 8 (65), Pp. 809–812. (rus)

13. **Saidov A.S., Tagilayev A.R., Aliyev N.M., Aslanov G.K.** *Proyektirovaniye fazovykh avtomaticheskikh radiopelengatorov* [*Design of phase automatic direction finders*]. Moscow: Radio i Svyaz Publ., 1997. (rus)

14. **Nikolskiy V.I., Sirota A.A.** Algoritmy vosstanovleniya prostranstvenno-chastotnogo raspredeleniya sistematicheskoy oshibki radiopelengovaniya v khode naturnykh ispytaniy [Algorithms for restoring the spatial-frequency distribution of radio direction finding systematic error during full-scale tests]. *Radiotekhnika*, 2009, No. 4 (143), Pp. 4–10. (rus)

15. **Rozenberg I.N., Sokolov S.V., Bayandurova A.A.** Povysheniye tochnosti pozitsionirovaniya letatelnogo apparata pri yego dvizhenii po zadannoy linii trayektorii [Aircraft positioning accuracy improving during its movement along a given trajectory line]. *Izvestiya vysshikh uchebnykh zavedeniy. Aviatsionnaya tekhnika*, 2018, No. 2, Pp. 64–70. (rus)

16. **Shevchenko M.Ye., Malyshev V.N., Sokolov S.S., Gorovoy A.V., Solovyev C.N., Stenyukov N.C.** Intervalnoye i tochechnoye pelengovaniye istochnikov radioizlucheniya pri shirokopolosnom radiomonitoringe [Interval and point direction finding of radio sources during broadband radio monitoring]. *Izvestiya vuzov. Radioelektronika*, 2020, No. 6 (23), Pp. 28–42. (rus)

17. **Yudin V.N., Volkov A.M.** Oshibki raznostno-fazovogo pelengovaniya izluchateley, obladayushchikh fazouglovoy zavisimostyu [Errors of difference-phase direction finding of emitters with phase-angle dependence]. *Radiosvyaz i raditekhnika*, 2020, No. 12, Pp. 50–53. (rus)

Received 24.02.2021.

СПИСОК ЛИТЕРАТУРЫ

1. **Асланов Г.К., Гасанов О.И.** Анализ причин возникновения аномальных ошибок в квазидоплеровских автоматических радиопеленгаторах // Научно-технические ведомости СПбГПУ. Информатика, телекоммуникации, управление. 2009. № 2 (76). С. 87–93.

2. **Асланов Г.К., Мамедов Л.К., Магомедов К.М.** Математические модели процесса вычисления пеленга в аэродромных квазидоплеровских автоматических радиопеленгаторах // Научно-технические ведомости СПбГПУ. Информатика, телекоммуникации, управление. 2008. № 2 (54). С. 267–272.

3. **Ботнев В.А., Устинов С.М.** Методика определения расстояния от точки до отрезка в задачах навигации // Научно-технические ведомости СПбГПУ. Информатика. Телекоммуникации. Управление. 2019. Т. 12. № 2. С. 68–79. DOI: 10.18721/JCSTCS.12206

4. **Васин А.А., Пономарев Л.И., Черемисин О.П.** Высокоточное пеленгование произвольно коррелированных многолучевых сигналов с использованием цифровых антенных решеток // Радиотехника и электроника. 2015. № 12 (60). С. 1237–1247.

5. **Дубровин А.В.** Оценка среднеквадратической ошибки измерения пеленга путем вычисления невязок фаз // Радиотехника и электроника. 2019. № 8 (64). С. 796–799.

6. **Иванов А.В., Сурков В.О., Комаров Д.В.** Квазиоптимальные алгоритмы обнаружения, идентификации и адаптивного оценивания для обработки информации в навигационных системах наземных подвижных объектов на основе спутниковых радионавигационных систем // Радиотехника и электроника. 2020. № 6 (65). С. 568–577.

7. **Иванов Н.М.** Адаптивные методы обнаружения и пеленгования сигналов // Радиотехника и электроника. 2016. № 10 (61). С. 979–983.

8. **Ковалев Ф.Н.** Определение координат цели по доплеровской частоте и угловой скорости в просветной радиолокационной системе // Радиотехника и электроника. 2015. № 12 (60). С. 1248–1250.

9. **Курочкин Л.М., Курочкин М.А., Попов С.Г., Попов М.В.** Результаты экспериментальных исследований точности позиционирования при использовании различных систем спутниковой навигации // Научно-технические ведомости СПбГПУ. Информатика. Телекоммуникации. Управление. 2017. Т. 10. № 4. С. 79–88. DOI: 10.18721/JCSTCS.10407

10. **Макс Ж.** Методы и техника обработки сигналов при физических измерениях: В 2-х т. Пер. с франц. М.: Мир, 1983. 312+256 с.

11. **Мелихова А.П., Цикин И.А.** Пеленгационный метод контроля целостности поля глобальных навигационных спутниковых систем // Научно-технические ведомости СПбГПУ. Информатика, телекоммуникации, управление. 2015. № 1 (212). С. 37–48. DOI: 10.5862/JCSTCS.212.4

12. **Музыченко Н.Ю.** Метод совместного приема и моноимпульсного пеленгования сигналов радиоизлучающих динамических объектов // Радиотехника и электроника. 2020. № 8 (65). С. 809–812.

13. **Саидов А.С., Тагилаев А.Р., Алиев Н.М., Асланов Г.К.** Проектирование фазовых автоматических радиопеленгаторов. М.: Радио и связь, 1997.

14. **Никольский В.И., Сирота А.А.** Алгоритмы восстановления пространственно-частотного распределения систематической ошибки радиопеленгования в ходе натурных испытаний // Радиотехника. 2009. № 4 (143). С. 4–10.

15. **Розенберг И.Н., Соколов С.В., Баяндурова А.А.** Повышение точности позиционирования летательного аппарата при его движении по заданной линии траектории // Известия высших учебных заведений. Авиационная техника. 2018. № 2. С. 64–70.

16. **Шевченко М.Е., Малышев В.Н., Соколов С.С., Горовой А.В., Соловьев С.Н., Стенюков Н.С.** Интервальное и точечное пеленгование источников радиоизлучения при широкополосном радиомониторинге // Известия вузов. Радиоэлектроника. 2020. № 6 (23). С. 28–42.

17. **Юдин В.Н., Волков А.М.** Ошибки разностно-фазового пеленгования излучателей, обладающих фазоугловой зависимостью // Радиосвязь и радиотехника. 2020. № 12. С. 50–53.

Статья поступила в редакцию 24.02.2021.

THE AUTHORS / СВЕДЕНИЯ ОБ АВТОРАХ

Aslanov Gajdarbek K.
Асланов Гайдарбек Кадырбекович
E-mail: uits@dstu.ru

Kazibekov Rustam B.
Казибеков Рустам Бидирханович
E-mail: kazibrus11@mail.ru

Musaibov Rashid R.
Мусаибов Рашид Рагимханович
E-mail: rashid_musaibov@mail.ru

DOI: 10.18721/JCSTCS.14104
УДК 621.396.4

HIGH PRECISION PASSIVE RADAR ALGORITHM

V.A. Vargauzin, D.I. Nikolaev

Peter the Great St. Petersburg Polytechnic University,
St. Petersburg, Russian Federation

The work is devoted to the study of the location determination algorithm for an arbitrary number of receiving stations using the differential-rangefinder method. The algorithm uses all possible Time Differences of Arrival (TDOAs) of the signal from the radio emission source to the receiving stations. In this case, the concept of a "reference" receiving station is excluded, relative to which the range differences are estimated in the classical method, and the signal TDOAs from the source between all possible pairs of receiving stations are used. It is shown that for a given number of receiving stations, the transition from the algorithm with one "reference" station to the proposed algorithm can significantly increase the accuracy of determining the location. Moreover, with an increase in the number of receiving stations, the efficiency of such a transition increases. In addition, for both methods, it has been demonstrated that adding a new receiving station improves positioning accuracy, but the gain decreases with the increasing number of stations. The work can find application in various monitoring systems, since it can significantly increase the accuracy of location determination only through algorithmic solutions, without costly replacement of equipment.

Keywords: determination of object location, receiving station, time difference of arrival, radio emission source, positioning accuracy.

Citation: Vargauzin V.A., Nikolaev D.I. High precision passive radar algorithm. Computing, Telecommunications and Control, 2021, Vol. 14, No. 1, Pp. 43–49. DOI: 10.18721/JCSTCS.14104

АЛГОРИТМ ПАССИВНОЙ РАДИОЛОКАЦИИ ПОВЫШЕННОЙ ТОЧНОСТИ

В.А. Варгаузин, Д.И. Николаев

Санкт-Петербургский политехнический университет Петра Великого,
Санкт-Петербург, Российская Федерация

Работа посвящена исследованию алгоритма определения местоположения (ОМП) для произвольного числа приемных станций (ПС) разностно-дальномерным методом (РДМ). Алгоритм использует все возможные разности времени прихода сигнала от источника радиоизлучения (ИРИ) до ПС. При этом исключается понятие «опорная» ПС, относительно которой в классическом РДМ оцениваются разности дальностей, и используются разности времен прихода сигнала от ИРИ между всеми возможными парами ПС. Продемонстрировано, что при заданном числе ПС переход от алгоритма с одной «опорной» ПС к предлагаемому алгоритму позволяет существенно повысить точность ОМП. При этом с ростом числа ПС эффективность такого перехода возрастает. Кроме того, для обоих методов продемонстрировано, что добавление новой ПС повышает точность ОПМ, однако с ростом числа ПС выигрыш уменьшается. Работа может найти применение в различных системах мониторинга, поскольку позволяет существенно повысить точность ОМП лишь за счет алгоритмических решений, без дорогостоящей замены оборудования.

Ключевые слова: определение местоположения объекта, приемная станция, разность времен прихода, источник радиоизлучения, точность позиционирования.

Ссылка при цитировании: Vargauzin V.A., Nikolaev D.I. High precision passive radar algorithm // Computing, Telecommunications and Control. 2021. Vol. 14. No. 1. Pp. 43–49. DOI: 10.18721/JCSTCS.14104

Introduction

Classical methods of location determination (LD) of a radio emission source (RES) are based on the use of minimal necessary number of time differences of the signal arrival (TDoA) from the RES to various receiving stations (RSs). At the same time, it is possible to improve the LD by means of using a redundant number of TDOAs.

Let us consider a passive system that employs the differential-rangefinder method (RDM) for the LD. With a classical approach, there are 3 RSs and one signal processing point used a in such a system for the LD in a plane [1]. One RS is a reference one relative to which the TDOAs are computed. Using the TDOAs obtained, we can construct lines of position with their junction point applied to estimate the location determination. Increasing the number of the RS facilitates formation of new TDOAs, and as a consequence induces the appearance of new information on the positioning. The use of such information can essentially lead to an improvement of the RES LD. However, either a possibility of increasing the number of RSs, as a rule, is not considered at all [1, 2], or a method of an arbitrary number of RSs is considered which is based on calculating TDOAs relative to one reference RS [3, 6, 8–10, 12–14]. Publications [4, 5] consider a method with a greater number of RS based on splitting a set of RS into 3 RSs for each of which, however, there is a reference RS assigned.

Paper [11] is devoted to the application of RDM in maritime navigation and considers a possibility of using 3–4 mobile RSs. I presents a method which evaluates the influence of the mutual positioning of the RSs on the precision of the LD.

Articles [15, 16] consider a possibility of combining RDM with the angle-of-arrival (AOA) method to obtain more accurate results. The proposed method uses 3 RSs.

Works [17–21] generalized an RDM algorithm for the three-dimensional space. For this purpose, the 4th RS was added to the system. One of the RSs is chosen as the reference receiving station.

The above listed methods do not take into account all available TDOAs which makes the algorithm insufficiently complete. These papers present no study of the possibility of increasing the number of the RSs.

The purpose of the paper consists in the development and research of the LD method for an arbitrary number of RSs which employs all possible TDoAs from RES to RS.

Algorithm

The proposed method is a generalization of the method considered in publications [3, 6]. According to this method, in addition to the use of a set $[\tau_{12}, \tau_{13}, ..., \tau_{1k}]$ (where k is the number of RSs) from $n = k - 1$ (method 1) TDOAs between the reference station (which is denoted by number 1) and the rest of the stations, we also account for the TDOAs between any two stations, i.e. the τ_{ij} TDOAs. The additional TDOAs are obtained as a result of a cross-correlation analysis of the realizations of input signals of the respective RSs. However, "mirror" τ_{ij} TDOAs are not taken into account. As a result, we obtain a vector of the TDOA measurements the elements of which include the measurements between all possible combinations of the RS pairs, excluding the "mirror" pairs. The number of the elements not excluding the "mirror" pairs is obviously equal to the number of the combinations from k by 2. Therefore, the measurements vector has $n = k\,(k - 1) / 2$ elements (method 2). By multiplying this vector by the radiation (light) speed, we obtain a measurement vector of the range difference R.

Let us construct an LD algorithm. For this, consider a hypothesis that a RES has coordinates x, y. Introduce a conditional range vector (column) $R_{hip}(x, y)$, provided that the hypothesis that the RES has coordinates x, y is true, in the plane:

$$R_{hip}\left(x,y\right)=\left[R_{12}\left(x,y\right),R_{13}\left(x,y\right),...,R_{ij}\left(x,y\right),...R_{(k-1)k}\left(x,y\right)\right]^{T}, \quad (1)$$

where $R_{ij}\left(x,y\right)=\sqrt{\left(x_i-x\right)^2+\left(y_i-y\right)^2}-\sqrt{\left(x_j-x\right)^2+\left(y_j-y\right)^2}$ is the range difference from a point with the x, y to the RSs with the numbers i and j. Then, in compliance with the criterion of the minimum sum of disparity squares [5, 6] between the vectors R_{hip} and R, we clearly need to minimize the following function:

$$F\left(x,y\right)=\left(R_{hip}\left(x,y\right)-R\right)^{T}\left(R_{hip}\left(x,y\right)-R\right). \quad (2)$$

With this, the estimation of the RES LD lies in the coordinates $\left(\hat{x},\hat{y}\right)$ which satisfy an equation

$$F\left(\hat{x},\hat{y}\right)=\min_{(x,y)}\left(F\left(x,y\right)\right). \quad (3)$$

We need to highlight that both for the proposed algorithm and the algorithm with one reference RS [3, 6], one and the same function (2) and Eq. (3) are applied. The difference consists in the n number of vectors R_{hip} and R.

We can find a solution to nonlinear Eq. (3) via various approaches. One of them would obviously be a brute-force search of all possible values within the projected area of the RES location which however is very complex computationally. We could employ the simplex Nelder – Mead method of finding the minimum as a more efficient approach [7].

Modeling

Let us note that the measurement results of the TDOAs (range differences) are not independent random variables, which with other conditions being equal impairs the LD effectiveness. Thus, to verify the initial assumptions of the effectiveness of the proposed algorithm we constructed a model, the purpose of which essentially consists in a demonstration of weak influence of the correlation and, consequently, a significant increase in the LD effectiveness when using additional $k\,(k-1)/2-(k-1)$ TDOAs in the algorithm at a fixed k number of RSs.

Assuming that the signal-to-noise ratio (SNR) at the RS output does not depend on the serial number of the RS (although, in practice individual RSs can have a SNR that differs from all others), we evaluate a relation $\frac{\sigma_{LD}}{\sigma_r}$ between the LD root-mean-square error (RMSE) σ_{LD} and the range difference RMSE σ_r. Since the range difference RMSE σ_r is defined by the SNR, it does not depend on the serial number of the RS as well.

At the fixed number of the RS, we employed the modeling method to study the $\frac{\sigma_{LD}}{\sigma_r}$ in the center of a circle of a unit radius. The RSs were located on the circle with their polar coordinates described in the following way:

$$\begin{cases} R_i=1 \\ \varphi_i=\dfrac{2\pi}{k}, \end{cases} \qquad i=0,1,...,k-1.$$

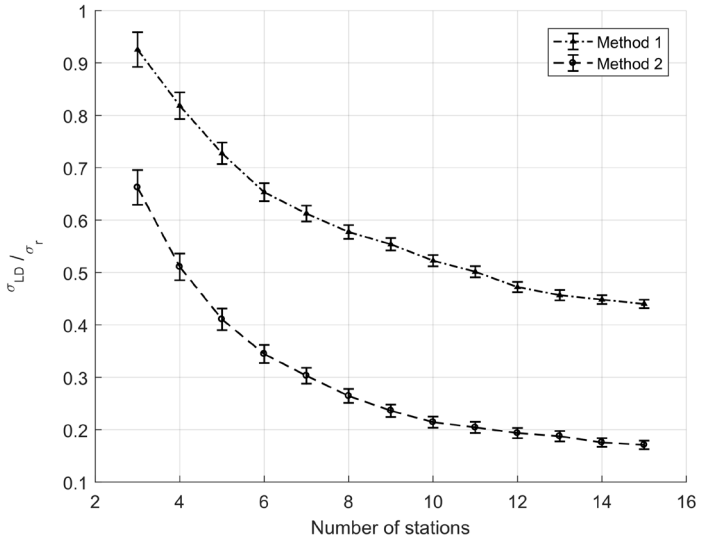

Fig. 1. Dependence of $\frac{\sigma_{LD}}{\sigma_r}$ on the number of RSs for Method 1 and Method 2

The RS input signals were modeled in several steps. First, in the observation interval, we generated a RES signal of a given duration and form. Then, for each RS, we formed a signal delayed for the time equal to the time of propagation of the signal from the RES to the respective RS. Then we added noise to the delayed signals. The obtained signals present the result of modeling the realizations of the RS input signals.

After that, we calculated the cross-correlations between the input signals of each pair of the RSs (excluding the "mirror" pairs). Maximum arguments of the obtained cross-correlations are the estimates of the TDOAs to the RSs. We multiplied them by the speed of light and obtained vector R. This vector is further used in the RES LD algorithm and estimation of σ_{LD}.

After multiple statistical tests we obtained an estimate of the $\frac{\sigma_{LD}}{\sigma_r}$ relation for the RES located in the center of the circle. The modeling results are presented in Fig. 1.

It follows from the Figure, that Method 2 using $k\,(k-1)\,/\,2$ TDOAs leads to a considerable reduction of the $\frac{\sigma_{LD}}{\sigma_r}$ value in comparison with the use of $k-1$ TDOAs relative to one reference RS. For example, with 8 RS $\frac{\sigma_{LD}}{\sigma_r}$ decreases by more than 50%. We can also see that with the growth of the number of RS, a transition from Method 1 to Method 2 becomes more and more feasible.

Let us additionally note that for both methods, adding a new RS reduces the $\frac{\sigma_{LD}}{\sigma_r}$ value. However, with the increase in the number of RS, the gain decreases.

Conclusion

An algorithm using $n = k - 1$ TDOAs relative to one reference station is much less efficient than the one that uses all available $n = k\,(k-1)\,/\,2$ TDOAs. In this respect, we can consider the algorithm with $n = k\,(k-1)\,/\,2$ TDOAs to be a high precision passive radar algorithm.

REFERENCES

1. **Grishin Yu.P., Ipatov V.P., Kazarinov Yu.M. et al.** Radiotekhnicheskiye sistemy: ucheb. dlya vuzov [*Radio engineering systems: textbook for universities*]. M.: Vyssh. shk. [High School], 1990. 496 p. (rus)

2. **Konovalov A.A.** *Osnovy trayektornoy obrabotki radiolokatsionnoy informatsii* [*Fundamentals of trajectory processing of radar information*], SPb.: Izd-vo SPbGETU "LETI", 2013. Vol. 1. 164 p. (rus)

3. **Al-Odkhari A.Kh., Fokin G.A., Fedorenko I.V., Ryabenko D.S., Lavrov S.V.** Issledovaniye vliyaniya geometricheskogo raspredeleniya punktov priyema i istochnika radioizlucheniya na tochnost pozitsionirovaniya [Investigation of the influence of the geometric distribution of the receiving points and the radio emission source on the positioning accuracy]. *Vestnik Polotskogo gosudarstvennogo universiteta. Seriya C, Fundamentalnyye nauki*. 2017. No. 4. Pp. 2–7. (rus)

4. **Vargauzin V.A., Nikolayev D.I.** Razrabotka algoritma opredeleniya mestopolozheniya istochnika radioizlucheniya raznostno-dalnomernym metodom s ispolzovaniyem 4-kh priyemnykh ustroystv [Development of an algorithm for determining the location of a radio emission source by the difference-ranging method using 4 receiving devices]. *SPBSPU Science Week: proceedings of the scientific conference with international participation, November 19–24, 2018. Institute of Physics of Nanotechnology and Telecommunications*. St. Petersburg: Polytech-Press Publishing House, 2018. Pp. 3–5. (rus)

5. **Rachitskiy D.V., Nikolayev D.I., Vargauzin V.A.** Algoritm vzveshennykh otsenok opredeleniya koordinat istochnika radioizlucheniya raznostno-dalnomernym passivnym metodom dlya proizvolnogo chisla stantsiy [Algorithm of weighted estimates for determining the coordinates of the radio emission source by the differential-range-finding passive method for an arbitrary number of stations]. *SPbPU Science Week: proceedings of the scientific conference with international participation, November 18–23, 2019 Institute of Physics, Nanotechnology and Telecommunications*. St. Petersburg: Polytech-Press, 2019. Pp. 20–23. (rus)

6. **Bezuverov G.V., Gerasimov O.I.** Algoritmy passivnoy lokatsii v raspredelennoy seti datchikov po raznostno-dalnomernomu metodu [Algorithms of passive location in a distributed network of sensors using the difference-ranging method], *Informatsionno-izmeritelnyye upravlyayushchiye sistemy*, 2008, Vol. 6, No. 5, Pp. 12–14. (rus)

7. **Vargauzin V.A., Potapichev V.N.** Primeneniye optimizatsionnogo algoritma Nedlera – Mida pri reshenii sputnikovoy geolokatsionnoy zadachi raznostno-dalnomernym metodom [Application of the Nedler-Mead optimization algorithm when solving a satellite geolocation problem using the differential-rangefinder method]. *SPBSPU Science Week: materials of a scientific conference with international participation. Institute of Physics, Nanotechnology and Telecommunications*. St. Petersburg: Polytech Publishing House, 2017, Pp. 8–10. (rus)

8. **Rui L., Ho K.C.** Elliptic localization: performance study and optimum receiver placement. *Department of Electrical and Computer Engineering, University of Missouri, Columbia,* 2020, Vol. 20, Pp. 4673–4688.

9. **Sanaa S.A. Al-Samahi, Yang Zhang, Dominic Ho.** Elliptic and Hyperbolic Localizations Using Minimum Measurement Solutions. *Signal Processing*, 2019, P. 107273.

10. **Kuptsov V., Badenko V., Ivanov S., Fedotov A.** Method for Remote Determination of Object Coordinates in Space Based on Exact Analytical Solution of Hyperbolic Equations. *Sensors*, 2020, Vol. 20, Pp. 5472.

11. **Du H.-J., Lee P.Y.** Passive Geolocation Using TDOA Method from UAVs and Ship/Land-Based Platforms for Maritime and Littoral Area Surveillance. *Ottawa, Canada: Technical Memorandum*, 2004, Pp. 38.

12. **Fletcher F., Ristic B., Musicki D.** Recursive estimation of emitter location using TDOA measurements from two UAVs. *10th International Conference on Information Fusion. Quebec*, 2007, Pp. 1–8.

13. **Okello N., Fletcher F., Musicki D., Ristic B.** Comparison of Recursive Algorithms for Emitter Localisation using TDOA Measurements from a Pair of UAVs. *IEEE Transactions on Aerospace and Electronic Systems*, 2011, Vol. 47 (3), Pp. 1723–1732.

14. **Fokin G.A., Alodhari A.H.** TDOA measurement processing for positioning using unmanned aerial vehicles. *T-Comm* (*Media Publisher*), 2018, Vol. 12 (7), Pp. 52–58.

15. **Yin J., Wan Q., Yang S., Ho K.C.** A Simple and Accurate TDOA-AOA Localization Method Using Two Stations. *IEEE Signal Processing Letters*, 2016, Vol. 23 (1), Pp. 144–148.

16. **Giacometti R., Baussard A., Jahan D., Cornu C., Khenchaf A., Quellec J.** Localization of radar emitters from a single sensor using multipath and TDOAAOA measurements in a naval context. *24th European Signal Processing Conference* (*EUSIPCO*). Budapest, 2016, pp. 692–696.

17. **Tie-Nan Zhang, Xing-Peng Mao, Chun-Lei Zhao, Xiao-Zhuan Long.** Optimal and fast sensor geometry design method for TDOA localisation systems with placement constraints. *IET Signal Processing*, 2019, Vol. 13, P. 708.

18. **Augusto Aubry, Vincenzo Carotenuto, Antonio De Maio, Luca Pallotta.** Joint Exploitation of TDOA and PCL Techniques for Two-Dimensional Target Localization. *Aerospace and Electronic Systems IEEE Transactions* on, 2020, Vol. 56, No. 1, Pp. 597–609.

19. **Weijia Wang, Peng Bai, Xiaolong Liang, Yubing Wang, Jiaqiang Zhang.** Optimal deployment of sensor–emitter geometries for hybrid localisation using TDOA and AOA measurements. *Science Measurement & Technology IET*, 2019, Vol. 13, No. 5, Pp. 622–631.

20. **Ali Noroozi, Mohammad Ali Sebt.** Algebraic solution for three-dimensional TDOA/AOA localisation in multiple-input–multiple-output passive radar. *Radar Sonar & Navigation IET*, 2018, Vol. 12, No. 1, Pp. 21–29.

21. **Ali Noroozi, Mohammad Ali Sebt.** Weighted least squares target location estimation in multi-transmitter multi-receiver passive radar using bistatic range measurements. *Radar Sonar & Navigation IET*, 2016, Vol. 10, No. 6, Pp. 1088–1097.

Received 03.03.2021.

СПИСОК ЛИТЕРАТУРЫ

1. **Гришин Ю.П.** Радиотехнические системы: учеб. для вузов / Ю.П. Гришин, В.П. Ипатов, Ю.М. Казаринов и др. М.: Высш. шк., 1990. 496 с.

2. **Коновалов, А.А.** Основы траекторной обработки радиолокационной информации: в 2 ч. / А.А. Коновалов. СПб.: Изд-во СПбГЭТУ "ЛЭТИ", 2013. Ч. 1. 164 с.

3. **Аль-Одхари А.Х., Фокин Г.А., Федоренко И.В., Рябенко Д.С., Лавров С.В.** Исследование влияния геометрического распределения пунктов приема и источника радиоизлучения на точность позиционирования // Вестник Полоцкого государственного университета. Серия С, Фундаментальные науки. 2017. № 4. С. 2–7.

4. **Варгаузин В.А., Николаев Д.И.** Разработка алгоритма определения местоположения источника радиоизлучения разностно-дальномерным методом с использованием 4-х приемных устройств. Неделя науки СПбПУ: материалы научной конференции с международным участием, 19–24 ноября 2018г. Институт физики нанотехнологий и телекоммуникаций. СПб.: Изд-во Политех-Пресс, 2018. С. 3–5.

5. **Рачицкий Д.В., Николаев Д.И., Варгаузин В.А.** Алгоритм взвешенных оценок определения координат источника радиоизлучения разностно-дальномерным пассивным методом для произвольного числа станций. Неделя науки СПбПУ: материалы научной конференции с международным участием, 18–23 ноября 2019 г. Институт физики, нанотехнологий и телекоммуникаций. СПб.: Политех-Пресс, 2019. С. 20–23.

6. **Безуверов Г.В., Герасимов О.И.** Алгоритмы пассивной локации в распределённой сети датчиков по разностно-дальномерному методу // Информационно-измерительные управляющие системы. 2008. Т. 6. №5. С. 12–14.

7. **Варгаузин В.А., Потапичев В.Н.** Применение оптимизационного алгоритма Недлера – Мида при решении спутниковой геолокационной задачи разностно-дальномерным методом. Неделя науки СПбПУ: материалы научной конференции с международным участием. Институт физики, нанотехнологий и телекоммуникаций. СПб.: Изд-во Политехн. ун-та, 2017. С. 8–10.

8. **Rui L., Ho K.C.** Elliptic localization: performance study and optimum receiver placement. Department of Electrical and Computer Engineering, University of Missouri, Columbia, 2020, Vol. 20, Pp. 4673–4688.

9. **Sanaa S.A. Al-Samahi, Yang Zhang, Dominic Ho.** Elliptic and Hyperbolic Localizations Using Minimum Measurement Solutions, Signal Processing, 2019. P. 107273.

10. **Kuptsov V., Badenko V., Ivanov S., Fedotov A.** Method for Remote Determination of Object Coordinates in Space Based on Exact Analytical Solution of Hyperbolic Equations, Sensors. 2020. Vol. 20. P. 5472.

11. **Du H.-J., Lee P.Y.** Passive Geolocation Using TDOA Method from UAVs and Ship/Land-Based Platforms for Maritime and Littoral Area Surveillance. Ottawa, Canada: Technical Memorandum. 2004. P. 38.

12. **Fletcher F., Ristic B., Musicki D.** Recursive estimation of emitter location using TDOA measurements from two UAVs // 10th International Conference on Information Fusion, Quebec. 2007. Pp. 1–8.

13. **Okello N., Fletcher F., Musicki D., Ristic B.** Comparison of Recursive Algorithms for Emitter Localisation using TDOA Measurements from a Pair of UAVs // IEEE Transactions on Aerospace and Electronic Systems. 2011. Vol. 47 (3). Pp. 1723–1732.

14. **Fokin G.A., Alodhari A.H.** TDOA measurement processing for positioning using unmanned aerial vehicles // T-Comm (Media Publisher). 2018. Vol. 12 (7). Pp. 52–58.

15. **Yin J., Wan Q., Yang S., Ho K.C.** A Simple and Accurate TDOA-AOA Localization Method Using Two Stations // IEEE Signal Processing Letters. 2016. Vol. 23 (1). Pp. 144–148.

16. **Giacometti R., Baussard A., Jahan D., Cornu C., Khenchaf A., Quellec J.** Localization of radar emitters from a single sensor using multipath and TDOAAOA measurements in a naval context // 24th European Signal Processing Conference (EUSIPCO), Budapest. 2016. Pp. 692–696.

17. **Tie-Nan Zhang, Xing-Peng Mao, Chun-Lei Zhao, Xiao-Zhuan Long.** Optimal and fast sensor geometry design method for TDOA localisation systems with placement constraints // IET Signal Processing. 2019. Vol. 13. P. 708.

18. **Augusto Aubry, Vincenzo Carotenuto, Antonio De Maio, Luca Pallotta.** Joint Exploitation of TDOA and PCL Techniques for Two-Dimensional Target Localization // Aerospace and Electronic Systems IEEE Transactions on. 2020. Vol. 56. No. 1. Pp. 597–609.

19. **Weijia Wang, Peng Bai, Xiaolong Liang, Yubing Wang, Jiaqiang Zhang.** Optimal deployment of sensor–emitter geometries for hybrid localisation using TDOA and AOA measurements // Science Measurement & Technology IET. 2019. Vol. 13. No. 5. Pp. 622–631.

20. **Ali Noroozi, Mohammad Ali Sebt.** Algebraic solution for three-dimensional TDOA/AOA localisation in multiple-input–multiple-output passive radar // Radar Sonar & Navigation IET. 2018. Vol. 12. No. 1. Pp. 21–29.

21. **Ali Noroozi, Mohammad Ali Sebt.** Weighted least squares target location estimation in multi-transmitter multi-receiver passive radar using bistatic range measurements // Radar Sonar & Navigation IET. 2016. Vol. 10. No. 6. Pp. 1088–1097.

Статья поступила в редакцию 03.03.2021.

THE AUTHORS / СВЕДЕНИЯ ОБ АВТОРАХ

Vargauzin Victor A.
Варгаузин Виктор Анатольевич
E-mail: var@mail.spbstu.ru

Nikolaev Denis I.
Николаев Денис Игоревич
E-mail: nikolaev.d.i@yandex.ru

DOI: 10.18721/JCSTCS.14105
УДК 004.72

ON PROGRAMMING AN APPLICATION TO MITIGATE DOS ATTACK USING OPENDAYLIGHT CONTROLLER IN SOFTWARE-DEFINED NETWORKING

C.D. Cajas Guijarro, D.O. Budanov

Peter the Great St. Petersburg Polytechnic University,
St. Petersburg, Russian Federation

Denial of Service (DoS) attacks try to deplete system resources by consuming bandwidth. In this paper the application using Software-Defined Networking (SDN) principles for DoS attack mitigation based on traffic monitoring in a network is proposed. The most important details about the programming aspects of the application using OpenDaylight (ODL) are explained. The application generates both proactive and reactive rules that should be installed in the network devices. Therefore, it is possible to have statistics of the flows and track possible anomalies such as an unexpected increase of the throughput in one or more of the flows. This allows to detect a DoS attack and mitigate it, installing the appropriate rules. Simulation results obtained with the application when using virtual switches in a network with a linear topology are presented.

Keywords: DoS attack, software-defined networking, OpenDaylight, controller, proactive rules, reactive rules, throughput.

Citation: Cajas Guijarro C.D., Budanov D.O. On programming an application to mitigate DoS attack using OpenDaylight controller in software-defined networking. Computing, Telecommunications and Control, 2021, Vol. 14, No. 1, Pp. 50–59. DOI: 10.18721/JCST-CS.14105

ПРОГРАММИРОВАНИЕ ПРИЛОЖЕНИЯ ДЛЯ СНИЖЕНИЯ ВЛИЯНИЯ АТАКИ ТИПА ОТКАЗ В ОБСЛУЖИВАНИИ С ИСПОЛЬЗОВАНИЕМ КОНТРОЛЛЕРА OPENDAYLIGHT В ПРОГРАММНО-ОПРЕДЕЛЯЕМЫХ СЕТЯХ

К.Д. Кахас Гихарро, Д.О. Буданов

Санкт-Петербургский политехнический университет Петра Великого,
Санкт-Петербург, Российская Федерация

Атаки типа «отказ в обслуживании» (Denial of Service, DoS) нацелены на истощение системных ресурсов за счет генерации большого количества запросов. В данной работе представлено приложение, использующее принципы программно-определяемых сетей для снижения влияния DoS-атаки, основанное на мониторинге трафика в сети. Приведено объяснение наиболее важных аспектов программирования приложения с использованием платформы OpenDaylight. Предлагаемое в работе приложение создает как проактивные, так и реактивные правила, которые могут быть установлены в сетевых устройствах. Это позволяет реализовать сбор статистики о потоках в сети и отслеживание аномалий, таких, например, как неожиданное увеличение трафика в одном или нескольких потоках. Таким образом, становится возможным обнаружить DoS-атаку и снизить ее влияние на функционирование сети, установив соответствующие правила. Результаты моделиро-

вания разработанного приложения при использовании виртуальных коммутаторов представлены для сети с линейной топологией.

Ключевые слова: DoS атака, программно-определяемые сети, OpenDaylight, контроллер, проактивные правила, реактивные правила, пропускная способность.

Ссылка при цитировании: Cajas Guijarro C.D., Budanov D.O. On programming an application to mitigate DoS attack using OpenDaylight controller in software-defined networking // Computing, Telecommunications and Control. 2021. Vol. 14. No. 1. Pp. 50–59. DOI: 10.18721/JCSTCS.14105

Introduction

Software-Defined Networking (SDN) is a recent networking paradigm that has modified the way to work and study networks [1]. SDN implementsthe decoupling of the data and control planes. The forwarding decisions are taken by a centralized controller instead of the switches in traditional networks. Due to the switches do not perform the intelligence of the network, they can be cheaper and on the side of the controller this centralization allows to make better network decisions [2].

Despite the main SDNs advantages, there are still security attacks in this kind of network. One of the most popular kinds of such attacks is Denial of Service (DoS) [3]. This paper presents the steps of programming an application that can detect and mitigate DoS attack exploiting ICMP drop using the OpenDaylight controller.

There are several ideas developed below to mitigate DoS attacks in SDN. In the paper [3] B.H. Lawal and A.T. Nuray proposed an SDN application that collects information using sFlow software system, so that the controller handles the network decisions according to this software. In the case of adaptability, the controller must not depend on other network software to make decisions (or at least has minimal dependence), an exception to the OpenFlow switches. So, the idea is that the own controller can estimate the throughput of the traffic flows of the network. Another implementation is presented in [4] by R. Kandoi and M. Antikainen. They proposed a configuration and tuning of parameters of the rules such as the timeout value. This idea will help to defend against the DoS attack. But if the attack can vary or be carried out from different sources, the bandwidth can still be compromised and overwhelmed. Also, this solution may require to repeatedly request rules for previously known flows adding overflow in the communication between the controller and the switches.

We propose a solution based only on the use of controller capabilities. The basic idea is to track flows in the SDN network and estimate the throughput of each flow, installing rules that help make such estimation. If a flow is higher than a threshold, the application detects that and mitigates this possible DoS attack. The basic notions of the application and tests of its functionality are described in [5]. This paper focuses on the key aspects of programming the application and tests the refreshing time that it takes to estimate the throughputs of the flows and detect a possible DoS attack.

Software-Defined Networking

As mentioned before, SDN is a networking architecture that makes the split of the control and switching planes [1]. The switches and routers must be extremely efficient at switching and must reduce their intelligence to a minimum. The management of the control plane is done in a device called controller (Fig. 1).

The controller executes software modules and bundles that establish the network's functionality and assemble the rules that must be installed on them. The controller uses protocols (e.g. OpenFlow) to communicate with the switches.

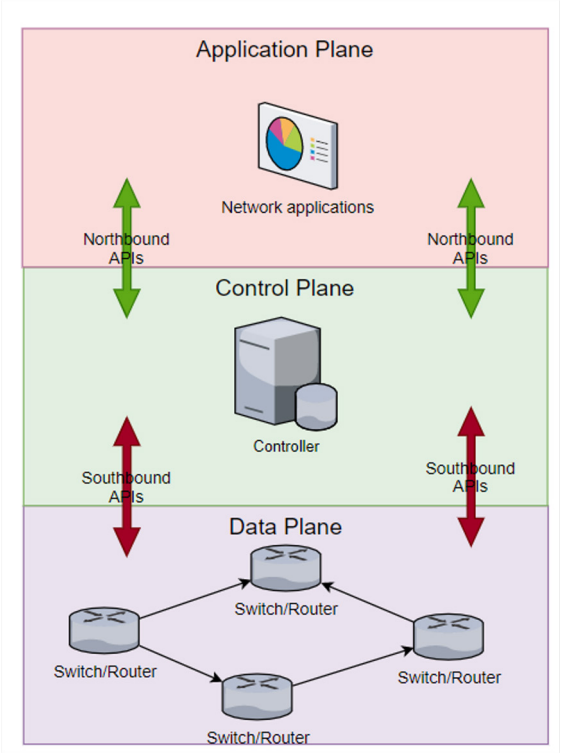

Fig. 1. SDN architecture

OpenDaylight

OpenDaylight (ODL) is a modular open-source platform that customizes and automates networks of any size and scale [6]. One of the most common uses of ODL is software-defined networking. The main layers of the OpenDaylight architecture are the Controller Platform Layer and the Service Abstraction Layer (SAL) that are shown in Fig. 2. As shown in Fig. 2, southbound (SB) plugins communicate with network devices and northbound (NB) plugins allow communication with applications that use the controller.

Controller Platform Layer contains the modules that provide essential functionalities. The modules of this layer define the operation of a network according to which of they are selected by the controller. Our application to mitigate the DoS attack resides in this layer.

Model Driven Service Abstraction Layer (MD-SAL) uses the idea of data providers and data consumers in the modules. MD-SAL connects consumers to providers and supports data adaptation between them. This allows modules to communicate with each other without minding which protocols are being used by the controller and network devices [7]. OpenDaylight uses OGSI system architecture which uses the MD-SAL [8]. MD-SAL is a shared layer for the northbound and the southbound APIs and the data structures used in different modules and components of an SDN controller. MD-SAL achieves the communication between different plugins from different modules regardless of the layer (NB or SB) due to a common layer [9]. The data structures and the creation of plugins implemented in applications are modeled using Yang language [10]. The generation of the module API is carried out after the compilation of the Yang models. MD-SAL ensures the framework to support:

- Subscriptions to publish and listen notifications. Service that is generated in providers when data in the data store is changed.

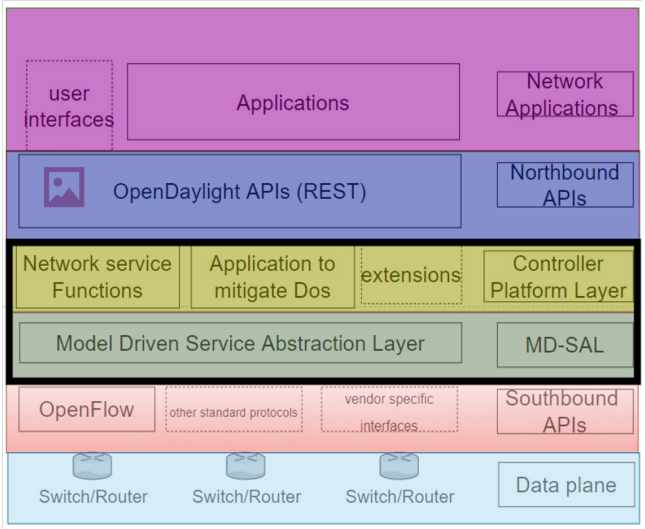

Fig. 2. OpenDaylight architecture

• Datastore. The providers and consumers use the data store of the MD-SAL to store data. This storing enables the exchange of data between providers and consumers. This data store can be split into clusters [11].

• Remote Procedure Call (RPC). It is a procedure that is used when a consumer receives notifications to get data from providers.

The proposed application to mitigate the DoS uses the DataBrokerService, so a simple Yang model was developed to interact with the data store using reading and writing transactions, and the following notification services:

• PacketProcessingService: used to process arriving packets at the controller.
• Ipv4PacketListener: used to process and decode the arriving IP packets at the controller.
• OpenDaylightInventoryListener: used to get related information about the OpenFlow switches.

Programming the application

The proposed application is deployed as an ODL plugin that sends a set of rules to the OpenFlow switches [12] so that they forward every IP packet to the controller and the destination port. The installation of both proactive and reactive rules is carried out to monitoring the flows that are in the network. A rule in SDN is a primitive that establishes how a packet that ingress to the switch is handled. A rule has a key that is used as an identifier. Besides, the rule saves information about how many packets (or bytes) have matched the rule. So, with the information of the key and the number of bytes, it is possible to estimate the throughput of each flow at a certain time. The proactive rules are generated when the controller populates them in the flow table before any packets arrived. These rules are usually installed when the notification about the connection between the controller and the switches is established. The switches do not know the location of the hosts at the beginning of the communication. So it is necessary to install these proactive rules at the beginning to avoid the loss of the first packets. These proactive rules will make flooding considering the functionality of a switch. On the other hand, the reactive rules are installed when the first packets arrive to the switch. The firsts packets in the controller allow knowing the location of the hosts with their respective IP address and input port. Therefore, it is possible to install a reactive rule to make forwarding of data without generating flood and sending data only to the respective output port.

The following classes from the SDN Hub Project [13] were reused while implementing the application:

• **InventoryUtils:** This class possesses methods to decode the headers of the packets received at the controller. Also, this class allows getting values relative to the information of the packets such as Datapath ID, input ports and output ports.

• **GenericTransactionUtils:** This class has methods to interact with the data store using reading and writing transactions.

There were additional files added to the base project [13]. After that Maven was used [14]. To add services such as RPC, access to the datastore and subscription to notifications several pom.xml files were modified. Files added to the project:

• PacketParsingUtils.java: This file contains the classes with methods for extracting information from the packet headers such as the value of source or destination IP addresses.

• rules.java: In this file, the actions corresponding to establish the proactive and reactive rules are implemented.

• application.java: In this file, the proposed application to detect and mitigate DoS is deployed, besides, the rules to drop flows that are attacking the network.

Key ideas to generate reactive and proactive rules. Both proactive and reactive rules are generated according to [6]. The basis is to use the same ideas that both rules allow the forwarding of the data in the network considering the functionalities of the two-layer switch. Once the application starts, it registers itself to receive notifications. The *OnNodeUpdated* notification is invoked when every switch registers to the controller. This notification has information about the switch that is registered to the controller, e.g. ID of the switch, ports, etc. With the information of this notification, the *install_proactive_rules* method is invoked. The idea is to make flooding for, as discussed previously, hosts' identification in a network. The matching conditions of the proactive rules are established considering only input forwarding ports and the IP protocol. In the output actions the method *install_proactive_rules* takes each forwarding port as input and the other forwarding ports as output for every port of the switches in every switch, e.g. if the switch has five forwarding ports, the method *install_proactive_rules* will install five proactive rules.

The idea of reactive rules is to track the flows of the network and reduce the overhead that flooding implies. These rules are generated when the firsts IP packets arrive at the controller. The idea is to save the input port and the source IP address in a map called *IP_table*. When other packets arrive at the controller, the input port and the source IP address are matched for every element of the *IP_table*. If there is no coincidence, these elements are saved in the *IP_table*. Considering the destination IP address of the packet, this element is searched in the map *IP_table*. If the element is found, it is possible to know the output port and the reactive rule can be created. The matching fields will be the IP protocol, input port, source IP address, destination IP address. The output actions are to send the packet to the corresponding output port. It is necessary to consider that the reactive rules will have higher priority than the proactive rules.

Key ideas to detect and mitigate DoS attacks. The idea to detect a DoS attack is considering the scenario where both proactive and reactive rules are installed in every switch. Once the application is initialized, an object *time* of the class *Timer* is created. The method *schedule* is configured in the object *time*. This method has the following prototype: *public void schedule*(*TimerTask task*, *long delay*, *long period*), where the argument *task* is the process to detect and mitigate DoS attack, the *delay* will be set to 0 and the *period* is initialized with the value of the variable *refreshing_time*. It means that this process will be executed every *refreshing_time* seconds. After, that object *data* is created. This object is an instance created by the method *Runtime.getRunTime().exec*(*"sudo ovs-ofctl dump-flows -OOpenFlow13 S1"*) execution. The object *data* allows writing the command *sudo ovs-ofctl dump-flows -OOpenFlow13 S1* in the controller. This command allows getting all the rules installed in the switch S1. Where:

ovs-ofctl: Command line to monitor OpenFlow switches
dump-flows: Print of all rules of the switch
-OOpenFlow13: Protocol OpenFlow 1.3
S1: Switch ID S1

```
 cookie=0x2c00000000000000, duration=1145.979s, table=0, n_packets=
477, n_bytes=709842, priority=5000,ip,in_port=2,nw_src=10.0.0.4,nw_
dst=10.0.0.1 actions=output:1
```

Fig. 3. Example of a rule

An example of the results of the following command is presented in Fig. 3.

Where:

cookie: Identifier of the rule

duration: Time that the rule has been installed

table: Identifier of the table where the rules are saved

n_packets: Number of packets that were matched the rule

n_bytes: Number of bytes that were matched the rule

priority: Value that shows the urgency to apply a rule. Higher values imply more priority

ip: Match field –IP protocol

in_port: Match field – input port

nw_src: Match field – source IP address

nw_dst: Match field – destination IP address

actions: Forwarding the packets to the output.

The idea is to save in every switch the values of the cookie to know if the rules belong to the developed application (reactive rules). The fields of *in_port*, *nw_src*, *nw_dst* are gotten from the object *data* and saved in an object called *identifier*. This object is useful to know the kind of flow. Besides, the value *n_bytes* can be gotten from the object *data*. This value is necessary to know the current number of bytes that matching the packets. The values of *identifier* and *n_bytes* are saved as a tuple. This process is done for every rule in the list of the application reactive rules in every switch. The *n_bytes* is updated according the expression $n\_bytes = n\_bytes - n\_bytesi$, where *n_bytesi* is the number of bytes of the previously saved tuple.

Therefore, the value of *n_bytes/refreshing_time* is the throughput of each flow. All these values are saved in an array called *rules_number_bytes*. Then every element of the array is compared to the value of the variable *threshold* (value that can be set by the programmer). If the value is higher than the *threshold*, the method *install_drop_rules* is invoked.

Key ideas to generate drop rules. The basis of these rules is to drop the packets that belong to flows whose throughput is higher than the threshold. The matching fields of the drop rules are the input port, the source IP address, destination IP address and the IP protocol. The output actions are to drop the packets.

The flow diagram of the whole application is shown in Fig. 4.

Experimental Results

The network shown in Fig. 5 was tested in Mininet emulator [15]. Functionality tests of the application are presented in [5]. The results provided in this section are the performance of the application while changing one of its critical value, the *refreshing_time*. The bandwidth of each link is 1 Mbps and the threshold was set to 500 Kbps. The idea is to change the refresh time in different scenarios to check performance values such as throughput, time to establish an optimal threshold that can detect a DoS attack. The attacker will be the host *00:00:00:00:04*, and it will attack the host *00:00:00:00:03*. The results of the values were calculated in the switch *openflow:3*.

As can be seen from the Table 1, the maximum value of the threshold is close to the value of the *refreshing_time*. This is explained by the fact the application checks the value of the throughput of each flow at each time interval, set by the value of *refreshing_time*. So, the maximum time to detect a DoS attack will be when the DoS attack begins as soon as the interval of *refreshing_time* begins.The throughput during the

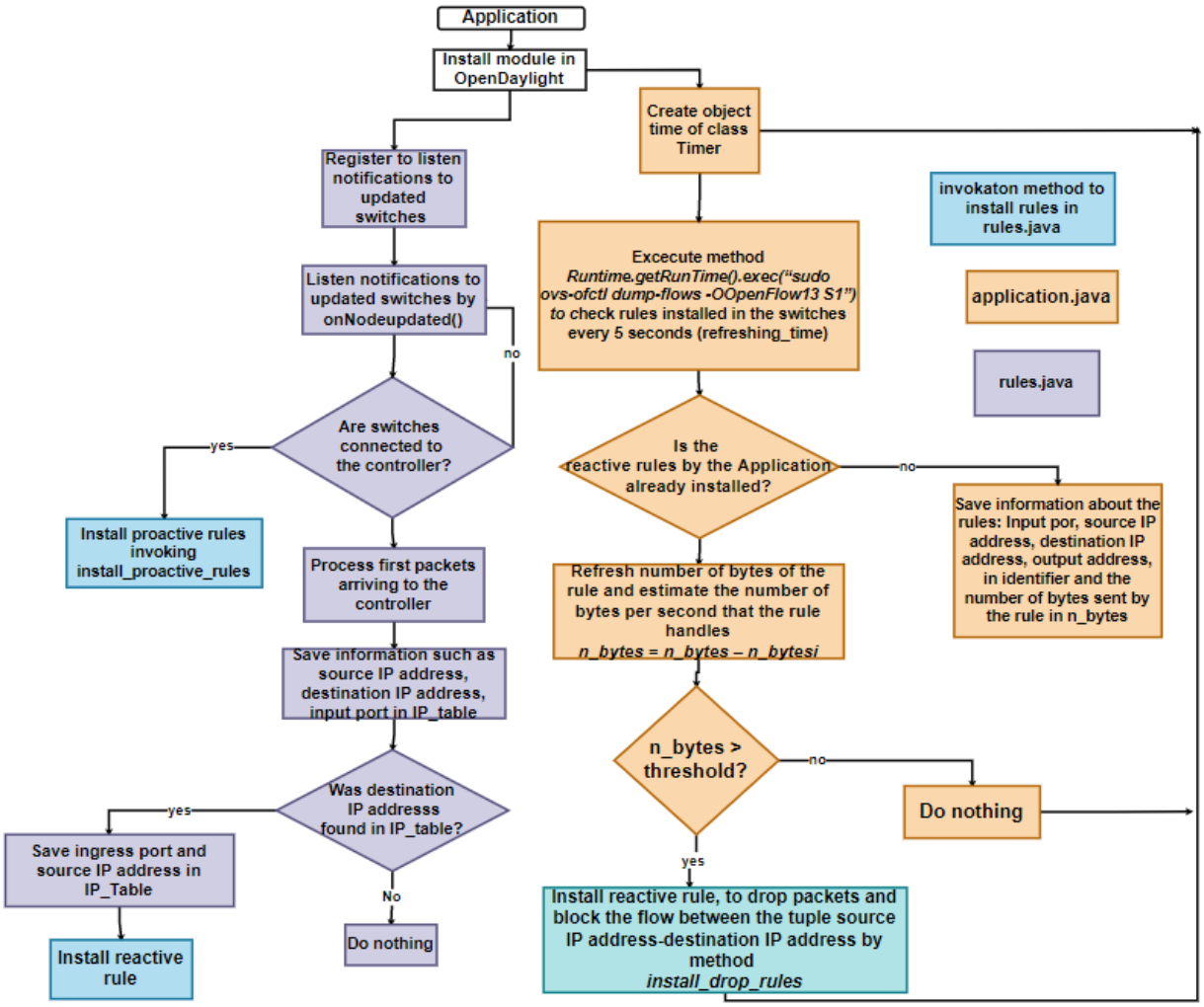

Fig. 4. Flow diagram of the whole application

Table 1

Performance changes owing to refreshing time variations

Refreshing time, s	Throughput during the DoS attack, Kbps	Average time of processing ICMP packets, ms	Average time of processing ICMP packets, ms
1	900.6	405.5	1.8
2	910.5	276.1	2.4
5	925.4	268.4	4.8
8	940.3	211.1	7.8
15	967.5	181.1	14.7
30	980.4	130.0	29.6

DoS attack is quite uniform, there is not a high difference and it has sense because this value is the maximum capacity of each link of the network.

It is possible to see the difference in the average time of processing ICMP packets. This occurs because with the small values of the *refreshing_time* a complete saturation is achieved due to the DoS

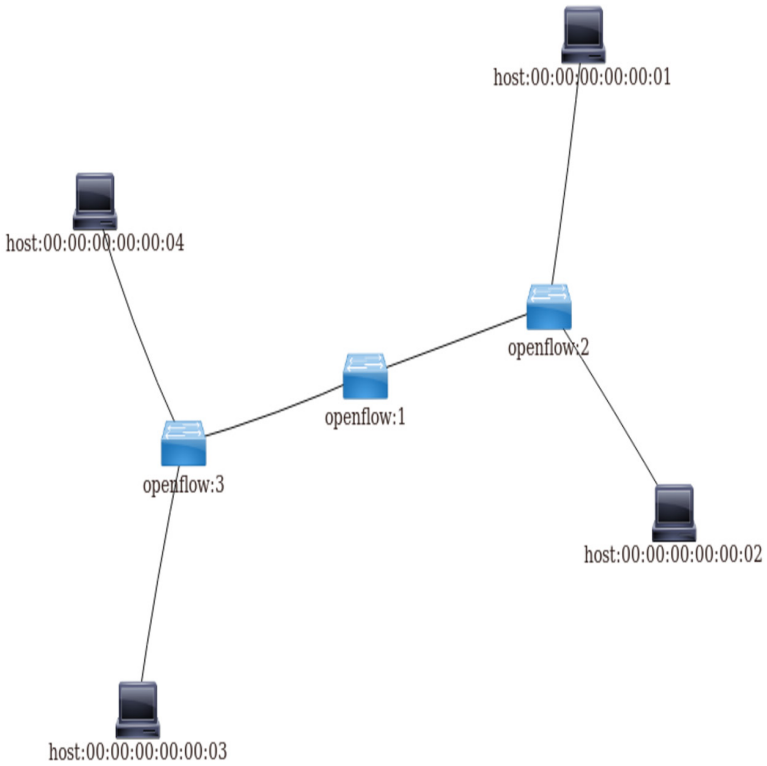

Fig. 5. Network topology tested in mininet

attack. At higher values of *refreshing_time*, due to some ICMP packets are discharged, the average time is reduced.

Conclusion

In this article, the approach to program an application that can detect and mitigate the DoS flood attack has been proposed. The application was emulated on the SDN network using the OpenDaylight controller. The main ideas about the programming were to implement classes which describe and install proactive and reactive rules. These rules give the application an ability to function as a two-layer switch, track each flow and save statistics of each flow such as the number of bytes. This information will be used at each time interval to estimate the throughput and compare it to a threshold value to decide if there is a DoS attack. If an attack is detected the rules installation is performed to drop the flows whose throughputs are higher than the threshold. Tests to collect information about the performance changes due to the variation of refreshing time interval to detect a DoS attack were carried out.

REFERENCES

1. **Kreutz D., Ramos F.M.V., Veríssimo P.E., Rothenberg C.E., Azodolmolky S., Uhlig S.** Software-Defined Networking: A Comprehensive Survey. *Proceedings of the IEEE*, 2015, Vol. 103, No. 1, Pp. 14–76.

2. **Antikainen M., Aura T., Sarel M.** Attacking an SDN with a Compromised OpenFlow Switch. *Proceedings of the 19th Conference on Secure IT Systems*, 2014, Pp. 233–243

3. **Lawal B.H., Nuray A.T.** Real-time detection and mitigation of distributed denial of service (DDoS) attacks in software defined networking (SDN). *Proceedings of 26th Signal Processing and Communications Applications Conference*, 2018, Pp. 1–4.

4. **Kandoi R., Antikainen M.** Denial-of-Service Attacks in OpenFlow SDN Networks. *Proceedings of the International Symposium on Integrated Network Management* (*INM*), 2015, Pp. 1322–1326.

5. **Cajas C., Budanov D.** Mitigation of Denial of Services Attacks Using OpenDaylight Application in Software-Defined Networking. *Proceedings of the 2021 IEEE Conference of Russian Young Researchers in Electrical and Electronic Engineering* (*EIConRus 2021*), 2021, Pp. 260–265.

6. **Cajas C., Valdivieso C., Mejía D., Bernal I.** On programming an MP-TCP analyzer plugin using OpenDayLight Beryllium as the SDN controller. *Proceedings of the 2017 IEEE Second Ecuador Technical Chapters Meeting* (*ETCM*), 2017, Vol. 2, Issue 19, Pp. 1–6.

7. **Paliwal M., Shrimankar D., Tembhurne O.** Controllers in SDN: A Review Report. *IEEE Access*, 2018, Vol. 6, Pp. 36256–36270.

8. **Khattak Z. K., Awais M., Iqbal A.** Performance evaluation of OpenDaylight SDN controller. *Proceedings of the 20th IEEE International Conference on Parallel and Distributed Systems* (*ICPADS*), 2014, Pp. 671–676.

9. **Becerra F., Mejía D., Bernal I.** Solving MP-TCP's Shared Bottlenecks Using a SDN with OpenDayLight as the Controller. *Proceedings of the 2018 IEEE ANDESCON*, 2018, Pp. 1–6.

10. **Vilalta R., Via S., Mira F., Sanabria L., Martinez R., Casellas R., Munoz R., Alonso-Zarate J.** Control and management of a connected car using YANG/RESTCONF and cloud computing. *Proceedings of the 8th International Conference on the Network of the Future* (*NOF*), 2017, Pp. 120–122.

11. **Kim T., Myung J., Yoo S.** Load Balancing of Distributed Datastore in OpenDaylight Controller Cluster. *The IEEE Transactions on Network and Service Management*, 2019, Vol. 16, Issue 1, Pp. 72–83.

12. **Alsaeedi M., Mohamad M.M., Al-Roubaiey A.A.** Toward Adaptive and Scalable OpenFlow-SDN Flow Control. *IEEE Access*, 2019, Vol. 7, Pp. 107346–107379.

13. **Seetharaman S., Ramachandran A., Natarajan S.** SDNHub Opendaylight Tutorial, 2014.

14. **Xiong Z.-H., Yang Y.-Z.** Automatic updating method based on Maven. *Proceedings of the 9th International Conference on Computer Science & Education*, 2014, Pp. 1074–1077.

15. Mininet, Available: *http://mininet.org/* (Accessed: 07.03.2021).

Received 10.03.2021.

СПИСОК ЛИТЕРАТУРЫ

1. **Kreutz D., Ramos F.M.V., Veríssimo P.E., Rothenberg C.E., Azodolmolky S., Uhlig S.** Software-Defined Networking: A Comprehensive Survey. Proceedings of the IEEE, 2015, Vol. 103, No. 1, Pp. 14–76.

2. **Antikainen M., Aura T., Sarel M.** Attacking an SDN with a Compromised OpenFlow Switch. Proceedings of the 19th Conference on Secure IT Systems, 2014, Pp. 233–243

3. **Lawal B.H., Nuray A.T.** Real-time detection and mitigation of distributed denial of service (DDoS) attacks in software defined networking (SDN). Proceedings of 26th Signal Processing and Communications Applications Conference, 2018, Pp. 1–4.

4. **Kandoi R., Antikainen M.** Denial-of-Service Attacks in OpenFlow SDN Networks. Proceedings of the International Symposium on Integrated Network Management (INM), 2015, Pp. 1322–1326.

5. **Cajas C., Budanov D.** Mitigation of Denial of Services Attacks Using OpenDaylight Application in Software-Defined Networking. Proceedings of the 2021 IEEE Conference of Russian Young Researchers in Electrical and Electronic Engineering (EIConRus 2021), 2021, Pp. 260–265.

6. **Cajas C., Valdivieso C., Mejía D., Bernal I.** On programming an MP-TCP analyzer plugin using OpenDayLight Beryllium as the SDN controller. Proceedings of the 2017 IEEE Second Ecuador Technical Chapters Meeting (ETCM), 2017, Vol. 2, Issue 19, Pp. 1–6.

7. **Paliwal M., Shrimankar D., Tembhurne O.** Controllers in SDN: A Review Report. IEEE Access, 2018, Vol. 6, Pp. 36256–36270.

8. **Khattak Z.K., Awais M., Iqbal A.** Performance evaluation of OpenDaylight SDN controller. Proceedings of the 20th IEEE International Conference on Parallel and Distributed Systems (ICPADS), 2014, Pp. 671–676.

9. **Becerra F., Mejía D., Bernal I.** Solving MP-TCP's Shared Bottlenecks Using a SDN with OpenDayLight as the Controller. Proceedings of the 2018 IEEE ANDESCON, 2018, Pp. 1–6.

10. **Vilalta R., Via S., Mira F., Sanabria L., Martinez R., Casellas R., Munoz R., Alonso-Zarate J.** Control and management of a connected car using YANG/RESTCONF and cloud computing. Proceedings of the 8th International Conference on the Network of the Future (NOF), 2017, Pp. 120–122.

11. **Kim T., Myung J., Yoo S.** Load Balancing of Distributed Datastore in OpenDaylight Controller Cluster. The IEEE Transactions on Network and Service Management, 2019, Vol. 16, Issue 1, Pp. 72–83.

12. **Alsaeedi M., Mohamad M.M., Al-Roubaiey A.A.** Toward Adaptive and Scalable OpenFlow-SDN Flow Control. IEEE Access, 2019, Vol. 7, Pp. 107346–107379.

13. **Seetharaman S., Ramachandran A., Natarajan S.** SDNHub Opendaylight Tutorial, 2014.

14. **Xiong Z.-H., Yang Y.-Z.** Automatic updating method based on Maven. Proceedings of the 9th International Conference on Computer Science & Education, 2014, Pp. 1074–1077.

15. Mininet [электронный ресурс] URL: http://mininet.org/ (дата обращения: 07.03.2021).

Статья поступила в редакцию 10.03.2021.

THE AUTHORS / СВЕДЕНИЯ ОБ АВТОРАХ

Кахас Гихарро Карлос Давид
Cajas Guijarro C.D
E-mail: cajasgcarlos@hotmail.com

Буданов Дмитрий Олегович
Budanov Dmitry O.
E-mail: budanov_do@spbstu.ru

DOI: 10.18721/JCSTCS.14106
УДК 004

REINFORCEMENT LEARNING FOR INDUSTRIAL MANUFACTURING CONTROL SYSTEM

M.Ya. Hanafi, V.P. Shkodyrev

Peter the Great St. Petersburg Polytechnic University,
St. Petersburg, Russian Federation

The problem posed is a very general case of optimal control of a dynamic, potentially stochastic, and partially observable system for which a model is not necessarily available. We analyze the disadvantages of classical approaches of the control theory and present a new modified numerical reinforcement learning rule of machine learning algorithm. Control theory is a field that has been studied for a very long time and which deals with the behavior of dynamic systems and how to influence it. Among the best-known examples are LQG (Linear Quadratic Gaussian) or PID (Proportional Integral Derivative) controllers. Most of the existing approaches presuppose (analytical) knowledge of the dynamic system, and one of the constraints is the need to be able to free oneself from a priori models. We focus on modified reinforcement learning approach to adaptive control policy as perspective area of control of complex dynamical system under uncertainty.

Keywords: reinforcement learning, multi agent system, oil manufacturing, Bellman equations, dynamic programming.

Citation: Hanafi M.Ya., Shkodyrev V.P. Reinforcement learning for industrial manufacturing control system. Computing, Telecommunications and Control, 2021, Vol. 14, No. 1, Pp. 60–69. DOI: 10.18721/JCSTCS.14106

УСИЛЕНИЕ ОБУЧЕНИЯ ДЛЯ СИСТЕМЫ УПРАВЛЕНИЯ ПРОМЫШЛЕННЫМ ПРОИЗВОДСТВОМ

Я.М. Ханафи, В.П. Шкодырев

Санкт-Петербургский политехнический университет Петра Великого,
Санкт-Петербург, Российская Федерация

Поставленная задача представляет общий случай оптимального управления динамической, потенциально стохастической и частично наблюдаемой системой, для которой модель не обязательно доступна. В статье представлен анализ недостатков классических подходов теории управления и предлагается новый модифицированный алгоритм машинного обучения с подкреплением. Теория управления – область, которая изучалась очень долгое время и которая касается поведения динамических систем и того, как на нее влиять. Среди наиболее известных примеров – LQG (Линейно-квадратичное гауссовское управление) или ПИД-контроллеры. Большинство существующих подходов предполагают (аналитическое) знание динамической системы, и одним из ограничений является необходимость иметь возможность освободиться от априорных моделей. Мы концентрируем внимание на преимуществах использования моделей машинного обучения с подкреплением как перспективной стратегии управления сложными динамическими системами в условиях неопределенности.

Ключевые слова: усиление обучения, мультиагентная система, нефтепереработка, уравнения Беллмана, динамическое программирование.

Ссылка при цитировании: Hanafi M.Ya., Shkodyrev V.P. Reinforcement learning for industrial manufacturing control system // Computing, Telecommunications and Control. 2021. Vol. 14. No. 1. Pp. 60–69. DOI: 10.18721/JCSTCS.14106

Introduction

Reinforcement learning is the digital learning environment's solution to the problem of optimal control. In this paradigm, IT agents learn to control an environment by interacting with it [1, 2]. They regularly receive local information about the quality of the control carried out in the form of a digital reward (or reinforcement signal), and their objective is to maximize a cumulative function of these rewards over the long term, generally modelled by a so-called value "reward function". The choice of actions applied to the environment according to its configuration is called a policy, and the value function therefore quantifies the quality of that policy [3]. Generally speaking, the agent does not have a model (neither physical nor statistical for example) of its environment, nor of the reward function that defines the optimality of the control [4, 5]. However, a common assumption we make is that the environment is Markovian, i.e., the effect of the application of an action depends only on the current configuration of the environment, not on the path taken to reach it [6]. This standard is very general and makes it possible to focus on a large number of applications. However, its practical application can be difficult. First of all, when the description of the environment to be controlled is too large, an accurate representation of the value (or policy) function is not possible [7]. In this case, the problem of generalization arises (or function approximation): on the one hand, it is necessary to design algorithms whose algorithmic complexity is not too great, and on the other hand they should be capable of inferring the behavior to be followed for an unknown environment configuration when similar situations have already been experienced. Another problem lies in the fact that, in the most general case, the agent learns to control the environment while at the same time controlling it [8]. This often results in successive phases of quality assessment of a policy and its improvement. From a learning perspective, this induces non-stationarity (we evaluate the quality of a policy that is constantly modified), a problem rarely addressed in the literature as such. This interweaving of learning and control also causes a problem known as the dilemma between exploration and exploitation. For each action it chooses, the agent must decide between an action it considers optimal in relation to his imperfect knowledge of the world and another action, considered sub-optimal, aimed at improving this knowledge. To deal with this problem effectively, it should be possible to estimate confidence that the agents have in their estimates. If these different difficulties are known, the methods of the literature generally treat them separately. Thus, a thought-out method for dealing with the dilemma between exploration and exploitation will not necessarily adapt to the problem of generalization, and vice versa.

Background

There are several approaches to deal with the reinforcement learning paradigm. However, an important part of the literature is based on dynamic programming and it is with this view that we approach it.

Dynamic programming. Dynamic programming can be defined in a very general way as a set of algorithmic techniques whose principle is to determine the optimal solution of a problem from an optimal solution of a sub-problem. In our context, these are all the methods that allow the exact (or approximate) solution of the Bellman equation, without any learning component [9].

Bellman equations. The objective of dynamic programming is to discover one of the policies whose value function is maximal for the set of states [10]. Noting $\left(S \to \mathbb{R}\right) \subset \mathbb{R}^{|S|}$ where $\left|S\right|$ is the cardinal of the state space, or in other words that the value function can be seen as a vector with as many components as there are states, it is possible to equip the value functions with a partial order relation [11]:

$$V_1 \le V_2 \Leftrightarrow \forall s \in S, V(s) \le V_2(s). \quad (1)$$

A partial order can be defined based on the policies, via the associated value functions:

$$\pi_1 \le \pi_2 \Leftrightarrow V^{\pi_1} \le V^{\pi_2}. \quad (2)$$

The objective is therefore to determine the optimal policy π^* defined by:

$$\pi^* = \arg\max_{\pi} V^{\pi}. \quad (3)$$

However, it is possible to define the value function recursively:

$$\begin{aligned} V^{\pi}(s) &= E\left[\sum_{i=0}^{\infty} \gamma^i R(S_i, \pi(S_i), S_{i+1}) \middle| S_0 = s, \pi\right]; \\ &= E_{s'|s,\pi(s)}\left[R(s, \pi(s), s') + \gamma V^{\pi}(s')\right]; \\ &= \sum_{s' \in S} p(s'|s, \pi(s))\left(R(s, \pi(s), s') + \gamma V^{\pi}(s')\right). \end{aligned} \quad (4)$$

The value of a state is therefore the average (according to the transition probabilities) of the sum of the reward obtained following the application of the action specified by the policy we wish to evaluate and the value of the state towards which the system transits, weighted by the discount factor [12]. This equation, called the Bellman evaluation equation, defines a linear system of $|S|$ equations with $|S|$ unknowns to determine the value function of a given policy and thus quantify its quality [13].

Another equation, this one being non-linear, allows us to directly determine the function of optimal value $V^* = V^{\pi^*}$. Given the state s, assume the optimal value function known in the states s' to which the system can transit. The optimal value function in state s' maximizes (weighted by the transition probabilities) the immediate reward plus the optimal value in state s' to which the system transits, weighted by the discount factor. This is the Bellman optimality equation [11, 13]:

$$V^*(s) = \max_{a \in A} \sum_{s' \in S} p(s'|s, a)\left(R(s, a, s') + \gamma V^*(s')\right). \quad (5)$$

This defines a non-linear system with $|S|$ equations and $|S|$ unknowns. If the optimal value function is known, it is easy to deduce the optimal policy, which is greedy with respect to the latter, i.e., it verifies:

$$\pi^*(s) = \arg\max_{a \in A} \sum_{s' \in S} p(s'|s, a)\left(R(s, a, s') + \gamma V^*(s')\right). \quad (6)$$

We summarize these important equations for the following, defining in passing the corresponding operators T^{π} and T^*.

Bellman's evaluation equation is used to determine the value function of a given policy π:

$$\forall s \in S, V^{\pi}(s) = \sum_{s' \in S} p(s'|s, a)\left(R(s, a, s') + \gamma V^*(s')\right) \Leftrightarrow V^{\pi} = T^{\pi} V^{\pi}. \quad (7)$$

The Bellman optimality equation is used to determine the optimal value function V^*:

$$\forall s \in S, V^*(s) = \max_{a \in A} \sum_{s' \in S} p(s'|s,a)\left(R(s,a,s') + \gamma V^*(s')\right) \Leftrightarrow V^* = T^* V^*. \quad (8)$$

Moreover, the Bellman operators T^π and T^* are infinite norm contractions.

Method Notation

We focus on two methods whose ideas are used extensively in reinforcement learning, namely the policy iteration and value iteration algorithms.

Policy Iteration. The first approach we present is policy iteration. The algorithm (see Listing 1) is initialized with any policy. Its principle is to evaluate the value function of the current policy (which we call policy evaluation), and then improve this policy by considering the greedy policy with respect to the previously calculated value function. In other words, in a given state, the action chosen is the one that leads (on average) to the greatest accumulation of rewards. It is important to note that this is not necessarily the action chosen by the policy, unless the policy is optimal [10–12, 14]. More formally, if at iteration i the policy π_i is evaluated, the improved policy π_{i+1} is defined by:

$$\forall s \in S, \pi_{i+1}(s) = \arg\max_{a \in A} \sum_{s' \in S} p(s'|s,a)\left(R(s,a,s') + \gamma V^{\pi_i}(s')\right). \quad (9)$$

With this improvement scheme, it can be shown that there is policy improvement, i.e. $\pi_{i+1} \geq \pi_i$. If one has equality, then Bellman's optimality equation is verified, and the algorithm has converged. Moreover, since the number of policies is finite, this algorithm converges in a finite number of iterations (this number of iterations being empirically much smaller than the cardinal of the policy space). It should be noted that the evaluation of the policy is equivalent to solving a linear system, the complexity of this evaluation is therefore in $O\left(|S|^3\right)$. The existence of a solution to this system is guaranteed by the Banach fixed point theorem (V_i is the fixed point of the contraction T^{π_i}). The computation of the associated greedy policy is in $O\left(|S|^2 |A|\right)$. The complexity of this algorithm is therefore in $O\left(|S|^2 |A| + |S|^3\right)$ per iteration. The ideas of this algorithm, i.e., evaluation of a policy followed by improvement, are widely used in the ideas of this algorithm, i.e., policy evaluation followed by improvement, are widely used in reinforcement learning algorithms [14, 15].

Value Iteration. The second approach we present, based on Bellman's optimality equation, aims at directly determining the optimal value function V^*. Since the Bellman operator T^* is a contraction and V^* is its unique fixed point, the *Algorithm 02* has a finite number of iterations, which is why a stopping criterion

Listing 1. Algorithm 1: Policy Iteration

Algorithm 1: **Policy Iteration**

Initialization
Policy π_i
i=0
While π_{i+1} != π_i do
    Evaluation of the policy;
    Solve $V_i = T^{\pi i} V_i$
    Improvement of the policy
    For ALL $s \in S$
        $\pi_{i+1}(s) = \arg\max_{a \in A} \sum_{s' \in S} p(s'|s,a)\left(R(s,a,s') + \gamma V^{\pi_i}(s')\right)$
    i++

Listing 2. Algorithm 2: Value Iteration

Algorithm 2: **Value Iteration**

Initialization
Value function V_0
i=0
While $\|V_{i+1} - V_i\|_\infty \geq \varepsilon$ **do**
    Iterating the value;
    $V_{i+1} = T^* V_i$
    i++

is introduced. This allows the error to be limited. Indeed, it can be shown that if the stopping criterion is verified at iteration i, then $\|V_i - V^*\| \leq \frac{2\gamma}{1-\gamma}\varepsilon$. However, this bound does not guarantee the quality of the associated greedy policy (see Listing 2).

Case studies and experimental results

Our case studies are based on real oil manufacturing production data. Oil manufacturing production is a complex process that has a hierarchy structure and many complex sub-systems.

Every manufacturing is based on a sequence of processes, each of those processes has its inputs and outputs. Depending on its structure, each process can have one or more outputs, which in turn become the inputs of the next process or the final products. Each process can be controlled by a set of factors, that can interfere with the outputs. Each of those processes can be composed by a sub-process so at the end of the structure of the factories we will have a hierarchy structure the base of this structure is the key to optimal control of the manufacturing system. We describe objective control of a complex technical system as a network of interest in a manufacturing subsystem. Every manufacture aims for high profit from its prod-

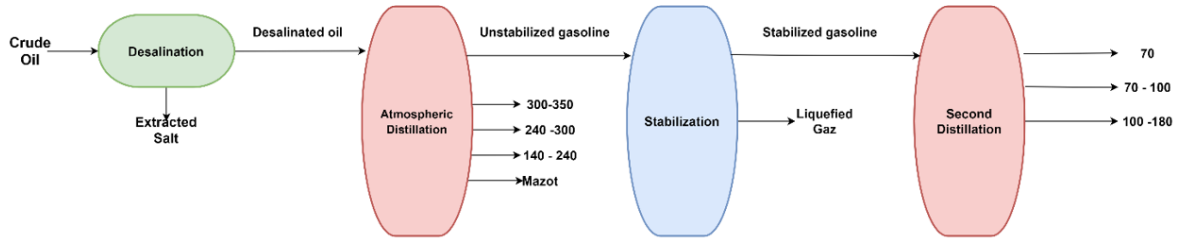

Fig. 1. Technological process of oil manufacturing

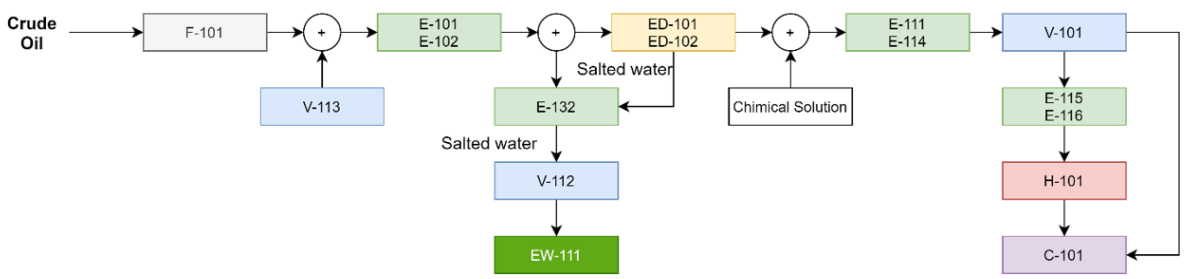

Fig. 2. Technological process of a desalination unit in oil manufacturing

ucts, and the oil manufacturing is not different. It is critical for oil manufacturing to have good quality of their production and that will be the top objective of the manufacturing alongside with the quantity of the production which is the second objective of the manufacturing to highly benefits from the production. The quality and the productivity are mostly the top objective on every manufacturing alongside other objective depends on the type of the manufacturing. So generally, there are always two or more objectives which makes us categorize this problem as a multi objective problem [16, 17].

Multi Objective Optimization: is an area of multiple criteria decisions making, that is concerned with mathematical optimization problems involving more than one objective function to be optimized simultaneously.

$$\begin{cases} \dfrac{\max}{\min} f_m(x) \quad m = 1, 2, .., M; \\ g_i(x) \geq 0 \quad j = 1, 2, .., J; \\ h_k(x) \geq 0 \quad k = 1, 2, ..., K; \\ x_i^{(L)} \leq x_i \leq x_i^{(U)} \quad i = 1, 2, ..., n. \end{cases} \tag{10}$$

The vector x is a vector of n decision variables $x = (x_1, x_2, ..., x_n)^T$.$x_i^{(L)}$ and $x_i^{(U)}$ is the lower and upper bounds of variable x_i, respectively. These variables define decision space or research space D. Generally, an element of the research space is called a possible or potential solution. The terms $g_j(x)$ and $h_k(x)$ are the constrained functions. Inequality constraints are treated as "superior or equal" type constraints since "inferior or equal" type constraints can be treated as duality. A solution x that does not satisfy all $(J + K)$ constraints is said to be an unfeasible solution. The set of feasible solutions constitutes a feasible region. The vector $f(x) = (f_1(x), f_2(x), ..., f_M(x))^T$ is the objective vector. Each of the M objective functions is either maximizing or minimizing which depends on the problem addressed. Using the principle of duality, a problem of maximization can be reduced to a problem of minimization by multiplying the objective function by -1 [18, 19].

Multi agent parallelization system. The oil manufacturing environment has a distributed and complex hierarchy. For that, we need to use a multi agent parallelization system as it deals with a large control process that controls multiple components.

As the Approximate Policy iterates with Value and Policy Networks, the standards scheme for approximation space value E involves using a cost function approximation $\tilde{J}$ of J (the optimal cost function). At a given state x that will minimize (or maximize) the approximation E, which forms as an expected value involved in the cost of the first stage $g(x, u, w)$ and the future costs which sufficiently reduced, in that we can note this as the approximate $\tilde{Q}$ factor corresponding to a pair (x, u), that minimizing the Q factors overall and that gives you a control that it used in state X [20].

$$\text{At } x: \min_{u \in U(x)} E\left\{ g(x,u,w) + \alpha \tilde{J}\left(f(x,u,w) \right) \right\}, \tag{11}$$

where E is the approximation, $g(x, u, w)$ is the first stage, $\alpha \tilde{J}\left(f(x,u,w) \right)$ is the optimal cost approximation (future stage).

One of the issues emerging is how to approximate the policies. The solution of that is to introduce a family of policies $\mu(x, r)$, a parametric family that depends on a parameter r [21].

Figures 3 and 4 show that each sub-system is a system environment having its own agent that controls it depending on the state of the environment itself. By applying the reinforcement learning to our system, we can describe its characteristics as:

• *Environment*: the process itself is the environment of the agent, which has every value that the agents need to take actions.

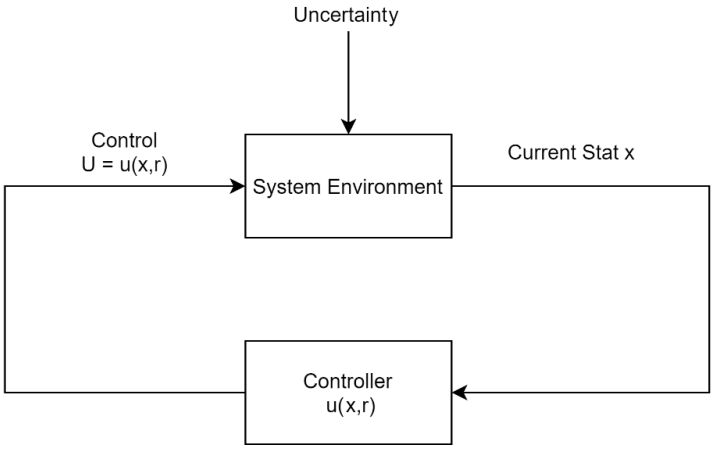

Fig. 3. Optimization and training over parametric family of policies

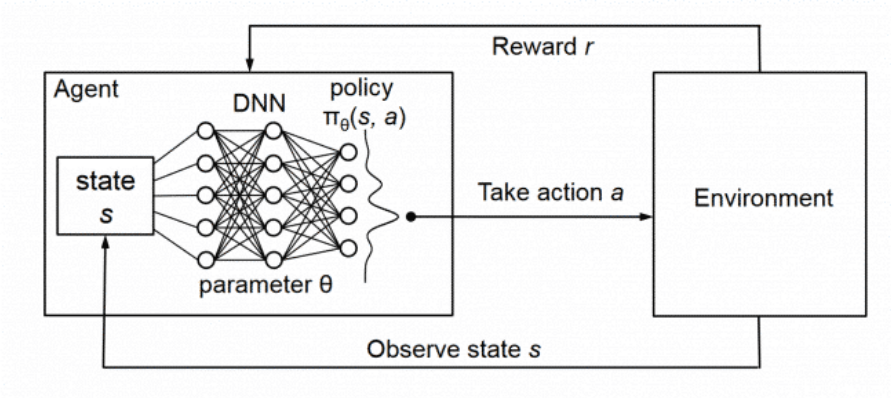

Fig. 4. Reinforcement Learning Loop

• *State*: is it the actual situation for the agent, which it retains if the result is satisfactory and there are no problems, or there are no changes in the environment or task from other agents.

• *Reward*: the agent's reward depends on the output goals, in the start of the learning the reward can be a failure, but over time, it learns the best configuration that can be used.

• *Discount Factor*: as the process advances, the agents put new goals to follow (increasing the productivity and the quality).

• *Policy*: our agents use dynamic policy to achieve the optimal goals, after a certain time of learning the agents stick to a certain policy that gives the best results.

• *Value*: as those processes have limitation, an agent calculates a future value (best value to obtain) and tries to achieve it; if it achieves it over time, the agent determines a new value for future achievement.

• *Q-Value*: the agents take extra action in case of unknown configuration, in case a configuration exceeds a limit, or a hazard is detected.

• *Action*: depending on all the above parameters, the agents act by changing the control values of the process.

Figure 5 presents the sequence of an agent process control by updating its own value and policy leading to optimal control.

As the agent has an objective to maximize quality and productivity, Fig. 5 (1–6) shows that each time it developed a new policy and determined a new value to reach the objective depending on the environment.

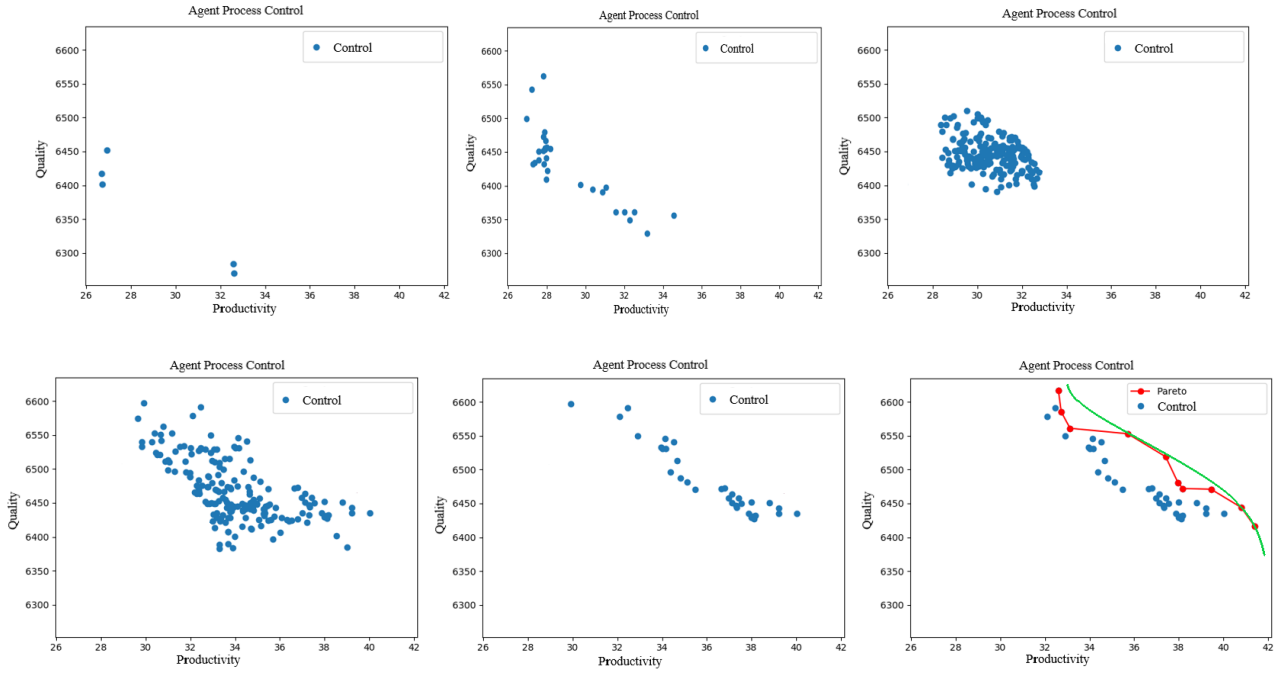

Fig. 5. Agent's policy and value updating results

The red line represents the agent's optimal value that it reaches (Pareto values), and the green line is the new value that the agent is trying to reach (The Pareto Front).

Conclusion

The field of reinforcement learning has exploded in recent years. Ever since the impressive breakthrough on the ImageNet classification challenge in 2012, the successes of supervised deep learning have continued to pile up and people from many different backgrounds have started using deep neural networks to solve a wide range of new tasks including the ways of learning intelligent behavior in complex dynamic environments. In this article, we took the advantage of the reinforcement learning, which consists in the fact that the agent can adapt to its environment by updating the policy it is using and the value it determines to reach an optimal control. The results obtained in this article not only show an optimal configuration, but can also prevent an error leading to enormous risks and losses as the agent can understand the limitation of the environment, take an extra action depending on an unknown configuration, and prevent the human errors in the manufacturing.

REFERENCES

1. **Singh S., Lewis R., Barto A., Sorg J.** Intrinsically motivated reinforcement learning: An evolutionary perspective. *Autonomous Mental Development, IEEE Transactions on*, 2010, Vol. 2, Pp. 70–82. DOI: 10.1109/TAMD.2010.2051031

2. **Sundas A., Bhatia A., Saggi M., Ashta J.** *Reinforcement Learning*, 2020, P. 281.

3. **Matignon L., Laurent G.J., Le Fort-Piat N.** Reward function and initial values: Better choices for accelerated goal-directed reinforcement learning. *Artificial Neural Networks – ICANN 2006*, Berlin, Heidelberg, 2006, Pp. 840–849. DOI: 10.1007/11840817_87

4. **Macal C.M., North M.J.** Tutorial on agent-based modelling and simulation. *Journal Simulation*, 2010, Vol. 4, No. 3, Pp. 151–162. DOI: 10.1057/jos.2010.3

5. **van Gog T., Rummel N.** Example-based learning: Integrating cognitive and social-cognitive research perspectives. *Educ Psychol Rev.*, 2010, Vol. 22, No. 2, Pp. 155–174. DOI: 10.1007/s10648-010-9134-7

6. **Hadoux E.** *Markovian sequential decision-making in non-stationary environments: application to argumentative debates*, Nov. 2015, P. 117.

7. **Arulkumaran K., Deisenroth M.P., BrundageM., Bharath A.A.** A brief survey of deep reinforcement learning. *IEEE Signal Process. Mag.*, 2017, Vol. 34, No. 6, Pp. 26–38. DOI: 10.1109/MSP.2017.2743240

8. **Lillicrap T.P., et al.** Continuous control with deep reinforcement learning. arXiv:1509.02971 [cs. LG], Sept. 2015. Available: *http://arxiv.org/abs/1509.02971* (Accessed: 07.03.2021).

9. **Helman P.** The principle of optimality in the design of efficient algorithms. *Journal of Mathematical Analysis and Applications*, 1986, Vol. 119, No. 1–2, Pp. 97–127. DOI: 10.1016/0022-247X(86)90147-2

10. **Puterman M.L., Patrick J.** Dynamic programming. *Encyclopedia of Machine Learning*. Boston, MA: Springer US, 2010, Pp. 298–308.

11. **Feng Y., Li L., Liu Q.** A Kernel Loss for Solving the Bellman Equation. arXiv:1905.10506v3 [cs. LG], 8 Jan. 2020. Available: *http://arxiv.org/abs/1905.10506* (Accessed: 07.03.2021).

12. **Geist M., Pietquin O.** Kalman temporal differences. *Journal of Artificial Intelligence Research (JAIR)*, 2010, Vol. 39, Pp. 483–532. DOI: 10.1613/jair.3077

13. **Aguilar C.O., Krener A.J.** Numerical solutions to the Bellman equation of optimal control. *J. Optim Theory Appl*, 2014, Vol. 160, No. 2, Pp. 527–552. DOI: 10.1007/s10957-013-0403-8

14. **Otterlo M., Wiering M.** Reinforcement learning and Markov decision processes. *Reinforcement Learning: State of the Art*, 2012, Pp. 3–42. DOI: 10.1007/978-3-642-27645-3_1

15. **Beitelspacher J., Fager J., Henriques G., Mcgovern A.** *Policy Gradient vs. Value Function Approximation: A Reinforcement Learning Shootout*, March 2006.

16. **Yassine H.M., Shkodyrev V.P.** Optimal production manufacturing based on intelligent control system. *Technological Transformation: A New Role for Human, Machines and Management*, Cham, 2021, Pp. 210–220. DOI: 10.1007/978-3-030-64430-7_18

17. **Yassine H.M., Shkodyrev V.P.** The intelligent control system of optimal oil manufacturing production. *The 3rd International Conference on Computational Intelligence and Intelligent Systems*, New York, NY, USA, Nov. 2020, Pp. 131–135. DOI: 10.1145/3440840.3440848

18. **Gunantara N.** A review of multi-objective optimization: Methods and its applications. *Cogent Engineering*, 2018, Vol. 5. DOI: 10.1080/23311916.2018.1502242

19. **Deb K.** Multi-objective optimization. *Search Methodologies*. Berlin: Springer, 2014, Pp. 403–449.

20. **Nissim R., Brafman R.** *Multi-agent A* for parallel and distributed systems*. 2012, P. 1266.

21. **Rousset A., Herrmann B., Lang C., Philippe L.** A survey on parallel and distributed multi-agent systems for high performance computing simulations. *Computer Science Review*, 2016, Vol. 22. DOI: 10.1016/j.cosrev.2016.08.001

Received 07.03.2021.

СПИСОК ЛИТЕРАТУРЫ

1. **Singh S., Lewis R., Barto A., Sorg J.** Intrinsically motivated reinforcement learning: An evolutionary perspective // Autonomous Mental Development, IEEE Transactions on. 2010. Vol. 2. Pp. 70–82. DOI: 10.1109/TAMD.2010.2051031

2. **Sundas A., Bhatia A., Saggi M., Ashta J.** Reinforcement Learning. 2020. P. 281.

3. **Matignon L., Laurent G.J., Le Fort-Piat N.** Reward function and initial values: Better choices for accelerated goal-directed reinforcement learning // Artificial Neural Networks – ICANN 2006. Berlin: Heidelberg, 2006. Pp. 840–849. DOI: 10.1007/11840817_87

4. **Macal C.M., North M.J.** Tutorial on agent-based modelling and simulation // J. Simulation. 2010. Vol. 4. No. 3. Pp. 151–162. DOI: 10.1057/jos.2010.3

5. **van Gog T., Rummel N.** Example-based learning: Integrating cognitive and social-cognitive research perspectives // Educ Psychol Rev. 2010. Vol. 22. No. 2. Pp. 155–174. DOI: 10.1007/s10648-010-9134-7

6. **Hadoux E.** Markovian sequential decision-making in non-stationary environments: Application to argumentative debates. Nov. 2015. P. 117.

7. **Arulkumaran K., Deisenroth M.P., BrundageM., Bharath A.A.** A brief survey of deep reinforcement learning // IEEE Signal Process. Mag. 2017. Vol. 34. No. 6. Pp. 26–38. DOI: 10.1109/MSP.2017.2743240

8. **Lillicrap T.P., et al.** Continuous control with deep reinforcement learning // arXiv:1509.02971 [cs. LG], Sept. 2015 // URL: http://arxiv.org/abs/1509.02971 (Дата обращения: 07.03.2021).

9. **Helman P.** The principle of optimality in the design of efficient algorithms // J. of Mathematical Analysis and Applications. 1986. Vol. 119. No. 1–2. Pp. 97–127. DOI: 10.1016/0022-247X(86)90147-2

10. **Puterman M.L., Patrick J.** Dynamic programming // Encyclopedia of Machine Learning. Boston, MA: Springer US, 2010, Pp. 298–308.

11. **Feng Y., Li L., Liu Q.** A Kernel Loss for solving the Bellman equation // arXiv:1905.10506v3 [cs. LG], 8 Jan. 2020 // URL: http://arxiv.org/abs/1905.10506 (Дата обращения: 07.03.2021).

12. **Geist M., Pietquin O.** Kalman temporal differences // J. of Artificial Intelligence Research (JAIR). 2010. Vol. 39. Pp. 483–532. DOI: 10.1613/jair.3077

13. **Aguilar C.O., Krener A.J.** Numerical solutions to the Bellman equation of optimal control // J. Optim Theory Appl. 2014. Vol. 160. No. 2. Pp. 527–552. DOI: 10.1007/s10957-013-0403-8

14. **Otterlo M., Wiering M.** Reinforcement learning and Markov decision processes // Reinforcement Learning: State of the Art. 2012. Pp. 3–42. DOI: 10.1007/978-3-642-27645-3_1

15. **Beitelspacher J., Fager J., Henriques G., Mcgovern A.** Policy Gradient vs. Value Function Approximation: A Reinforcement Learning Shootout. March 2006.

16. **Yassine H.M., Shkodyrev V.P.** Optimal production manufacturing based on intelligent control system // Technological Transformation: A New Role for Human, Machines and Management. Cham, 2021. Pp. 210–220. DOI: 10.1007/978-3-030-64430-7_18

17. **Yassine H.M., Shkodyrev V.P.** The intelligent control system of optimal oil manufacturing production // The 3rd Internat. Conf. on Computational Intelligence and Intelligent Systems. NY, USA, Nov. 2020. Pp. 131–135. DOI: 10.1145/3440840.3440848

18. **Gunantara N.** A review of multi-objective optimization: Methods and its applications // Cogent Engineering. 2018. Vol. 5. DOI: 10.1080/23311916.2018.1502242

19. **Deb K.** Multi-objective optimization // Search Methodologies. Berlin: Springer, 2014. Pp. 403–449.

20. **Nissim R., Brafman R.** Multi-agent A* for parallel and distributed systems. 2012. P. 1266.

21. **Rousset A., Herrmann B., Lang C., Philippe L.** A survey on parallel and distributed multi-agent systems for high performance computing simulations // Computer Science Review. 2016. Vol. 22. DOI: 10.1016/j.cosrev.2016.08.001

Статья поступила в редакцию 07.03.2021.

THE AUTHORS / СВЕДЕНИЯ ОБ АВТОРАХ

Ханафи Яссин Мохамед
Hanafi Mohamed Yassine
E-mail: hanafi.med.yassine@gmail.com

Шкодырев Вячеслав Петрович
Shkodyrev Viacheslav P.
E-mail: shkodyrev@spbstu.ru

ИНФОРМАТИКА, ТЕЛЕКОММУНИКАЦИИ И УПРАВЛЕНИЕ

COMPUTING, TELECOMMUNICATIONS AND CONTROL

Том 14, № 1, 2021

Учредитель — Федеральное государственное бюджетное образовательное учреждение высшего профессионального образования «Санкт-Петербургский государственный политехнический университет»

Журнал зарегистрирован Федеральной службой по надзору в сфере информационных технологий и массовых коммуникаций (Роскомнадзор). Свидетельство о регистрации ЭЛ № ФС77-77378 от 25.12.2019 г.

Телефон редакции (812)552-62-16

E-mail: infocom@spbstu.ru

Компьютерная верстка *А.А. Кононова*

Перевод на английский язык *Д.Ю. Алексеева*

Лицензия ЛР № 020593 от 07.08.97

Дата выхода 31.03.2021. Формат 60×84 1/8

Санкт-Петербургский политехнический университет Петра Великого
Адрес университета и редакции: 195251, Санкт-Петербург, ул. Политехническая, д. 29.